UNIVERSITA' DELLA CALABRIA
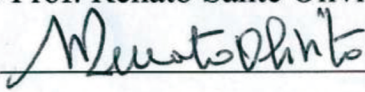
Dipartimento di Ingegneria Meccanica, Energetica e Gestionale - DIMEG

Scuola di Dottorato "Pitagora" in Scienze Ingegneristiche
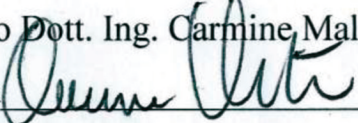
CICLO XXVII

Dottorato di Ricerca in Ingegneria dei Materiali e delle Strutture

INNOVATIVE METHODOLOGIES FOR CONCEPT MODELLING OF VEHICLE BODY STRUCTURES

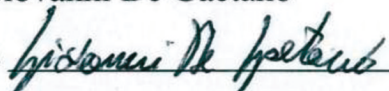**Settore Scientifico Disciplinare ING-IND/13 Meccanica Applicata alle Macchine**

Coordinatore: Ch.mo Prof. Renato Sante Olivito

Firma ~~Renato Olivito~~

Supervisori: Ch.mo Prof. Domenico Mundo

Firma ~~_____~~

Ch.mo Dott. Ing. Carmine Maletta

Firma ~~_____~~

Dottorando: Ing. Giovanni De Gaetano

Firma ~~Giovanni De Gaetano~~

Academic year 2013/2014

A mio zio Carlo,
fonte di ispirazione ed esempio di vita

Acknowledgments

Table of Contents

Chapter 3: A Dedicated MPC Element for Beam-Joint Connection

Chapter 4: Industrial Applications

List of Figures

List of Tables

8

Prefazione

Il termine "*Concept Modelling*" si riferisce ad una serie di tecniche di modellazione, utilizzate durante le primissime fasi del processo di sviluppo di un prodotto. Il loro obiettivo consiste nel ridurre il tempo di immissione sul mercato e nell'ottimizzare le varie prestazioni funzionali di un nuovo prodotto, già in fase di progettazione concettuale.

In particolare, in campo automobilistico, tali prestazioni sono relative a rumore e vibrazioni, dinamica, sicurezza, emissioni ed efficienza energetica del veicolo. Ciascuno di questi attributi risulta però difficile da migliorare durante le ultime fasi del processo di sviluppo, senza evitare di arrecare conflitto con gli altri parametri progettuali. Per tale ragione, molti ricercatori hanno ultimamente sviluppato varie tecniche CAE (*Computer-Aided Engineering*), che possono essere utilizzate già nelle fasi iniziali per esplorare maggiori alternative di progettazione del veicolo e contribuire così alla scelta del miglior progetto.

Benché le applicazioni delle tecniche di modellazione concettuale siano significativamente aumentate, alcuni limiti e difficoltà di utilizzo sono tuttora presenti.

Scopo di tale dissertazione è quello di sviluppare nuove metodologie e di migliorare gli approcci concettuali già esistenti, finalizzati alla riduzione di modelli dettagliati agli Elementi Finiti di telai automobilistici.

Il primo capitolo della tesi fornirà una descrizione generale del processo di sviluppo del veicolo, affrontando, in particolare, la fase di progettazione concettuale. Quest'ultima è la fase in cui il progetto non è ancora ben determinato e le modifiche da applicare possono essere effettuate in modo rapido ed efficace, a condizione che siano a disposizione dei progettisti adeguati strumenti predittivi per l'analisi dei diversi casi applicativi e per la risoluzione dei problemi decisionali.

Inoltre, verrà anche presentata una descrizione dello stato dell'arte riguardante i metodi concettuali CAE, insieme ad un'analisi delle principali categorie nelle quali tali metodi vengono suddivisi.

Il secondo capitolo si concentrerà sulla formulazione di una nuova metodologia concettuale, basata sul modello dinamico lineare delle strutture travi-formi ed in grado di prevedere con precisione il comportamento statico e dinamico dei membri longilinei di un veicolo. Il modello analitico utilizzato trae spunto dal modello di Timoshenko, descrivente le vibrazioni flessionali e torsionali delle travi prismatiche attraverso equazioni differenziali relative alle funzioni di ampiezza modale.

Infatti, partendo da un modello modale coerente, le proprietà di rigidezza del modello 1D concettuale equivalente possono essere stimate attraverso l'utilizzo di valori di riferimento per le frequenze naturali, calcolate antecedentemente attraverso analisi numeriche agli Elementi Finiti o test sperimentali.

Il capitolo illustrerà anche un'applicazione dello stesso metodo dinamico, relativa alla riduzione di strutture travi-formi ultraleggere, come quelle sandwich con all'interno configurazioni a nido d'ape. Tali strutture innovative si stanno oggigiorno rivelando altamente promettenti in varie applicazioni industriali, grazie alle loro proprietà di leggerezza, alta rigidezza a flessione e resistenza a carichi distribuiti, in aggiunta alla loro ottima capacità di assorbimento di energia.

Un tipico pannello sandwich è formato da due rigide lamiere sottili e da una struttura a nido d'ape racchiusa tra loro, avente minore densità, rigidezza e resistenza. Variando spessori e tipologia di materiale per entrambe le parti, è possibile ottenere diverse proprietà e desiderate prestazioni.

Tali ragioni suggeriscono un loro probabile utilizzo anche in campo automobilistico, in vista di ulteriori miglioramenti delle prestazioni statiche e dinamiche di diverse componenti, una su tutte, il telaio.

Tuttavia, per uno sviluppo coerente della ricerca, le loro caratteristiche non possono essere trascurate in fase di analisi concettuale. Per tale ragione, verrà eseguito, in fase preliminare, uno studio della caratterizzazione sperimentale e della modellazione numerica di tali particolari strutture, al fine di poter validare la nuova metodologia concettuale anche su questi particolari modelli.

Il terzo capitolo sarà relativo invece alla descrizione di una nuova dedicata tipologia di collegamento, utile a correlare elementi *beam* 1D (sostituenti i corrispettivi modelli travi-formi dettagliati) con elementi *shell* appartenenti ai modelli 3D dei giunti.

Utilizzando un approccio statico, tale tipologia di connessione sarà in grado di restituire una correlazione molto accurata tra il moto dei nodi relativi alla sezione periferica del giunto ed il moto del nodo centrale appartenente all'elemento beam 1D. Necessaria sarà, però, un'approfondita ricerca sugli approcci e le logiche relative agli elementi di connessione di elementi ibridi, al fine di trovare un giusto punto di partenza per la suddetta ricerca, verso una migliore modellazione dell'interfaccia 1D/3D.

Infine, il quarto capitolo illustrerà un caso di applicazione industriale, in cui il nuovo elemento di connessione verrà convalidato, attraverso un'applicazione su un modello parzialmente concettualizzato di telaio automobilistico. Le analisi modali dimostreranno che l'elemento proposto è in grado di superare i limiti relativi agli elementi di connessione attualmente più utilizzati in fase di modellazione, restituendo così un modello concettuale con caratteristiche molto simili a quelle del corrispettivo modello dettagliato di telaio.

Verrà inoltre presentato, in seguito, un particolare caso di ottimizzazione strutturale, in cui i parametri geometrici degli elementi concettuali beam 1D saranno utilizzati come variabili di progetto. L'obiettivo consisterà nell'ottenere, in tempi molto brevi, una struttura ottimale avente peso minimo, nonché le stesse prestazioni dinamiche del modello originale di telaio.

Introduction

In the contest of development process of complex products, design engineers have to face the challenging problem to fulfil several and sometimes conflicting design criteria, for highly competitive markets that require more and more increasing reductions of the time-to-market.

Particularly for the automotive field, performances related to Noise, Vibration and Harshness (NVH), dynamics, safety, emissions and energy efficiency of the vehicle, are hard to improve in the last steps of the development process, without raising conflicts with each other. Traditional Computer-Aided Design (CAD) software tools are limited, because they can be applied only when detailed geometric data of the vehicle are available. Furthermore, it is not possible to apply fast and easy parameterizations of models, since they are based, typically, on the traditional definition of geometry via points, lines and surfaces. Therefore, the experience of engineers is a very important factor at the beginning of the design process, in order to examine the most appropriate structural concepts.

For such a reason, many researchers have developed various predictive Computer-Aided Engineering (CAE) tools, known as *Concept Modelling Techniques*, in order to reduce the time-to-market in manufacturing industry and improve various functional performance attributes of products, already in the earliest stages of the product development process. These methodologies can be used to quickly explore more design alternatives and contribute to the choice of a better initial design.

Although in the last years the application of concept modelling for vehicle design has significantly increased, some difficulties are still encountered. The goal of this dissertation is to develop new methodologies and improve existing concept approaches, for a more accurate and efficient reduction of detailed Finite Element (FE) vehicle body models, already defined in predecessor design processes, towards a more accurate estimation of the vehicle structural dynamics.

The first chapter of the thesis provides a general description of the vehicle development cycle. This is a complex chain that can be described as a multi-level process, where a two-ways transition from the physical to the virtual level is performed. At the beginning of the process, a functional analysis translates the views of the customers and legislative requirements into design targets and constraints. This is the starting point of the design process, which consists of three phases: concept design, detailed engineering and refinement engineering.

Each of these three phases leads to the creation of virtual prototypes, passing through the intermediate steps of 1D and 3D component model generation. In particular, the *1D modelling* is based on the definition of simulation models of functional systems, representing the physical behaviour of various subsystems in an analytical or numerical formulation, without the need for a detailed geometry representation. Instead, in the *3D modelling* step, detailed simulation models are used, built from a detailed geometry base. Examples for the latter case are Multi-Body Simulation (MBS) models and flexible FE models.

Finally, on the way from the virtual subsystem level back to the physical level, some validation ensures that the virtual and the physical prototypes are in agreement with the design requirements and targets, i.e., with the market and legislative demands respectively.

The research presented in this dissertation mainly focuses the attention in the first of the three design phases. i.e. the concept phase, during which the design is not yet fixed and modifications can be done in a fast and effective way, provided that predictive CAE tools are available to analyse what-if cases and address multiple-attribute balancing and decision-making problems.

Usually, the concept CAE methods are classified into three main categories: methods *based on predecessor FE models*, methods *from scratch*, and methods *concurrent with CAD*. The first category is used to design a variant or incremental improvement of an existing vehicle model. By using a predecessor FE model, early CAE predictions can be performed to identify issues and to include possible countermeasures, already in the initial CAD design. On the contrary, methods "from scratch" are used to support the design process when new vehicle concepts must be designed, assisting the designer to establish a functional layout for the different

vehicle body components. Finally, methods concurrent with CAD aim at integrating CAD and CAE tools, in order to get simulation results as soon as component-level CAD models are available, while vehicle-level models are not yet frozen [1].

The second chapter focuses on formulating a new FE-based method for beam concept modelling, able to accurately predict the static and dynamic behaviours of the vehicle beam-like members. This method is based on the linear dynamic model of beam-like structures, which describes flexural and torsional vibrations of prismatic beams through differential equations related to mode amplitude functions [2]. Indeed, starting from a consistent modal model, the stiffness properties of the equivalent 1D concept model could be estimated, using targeted values of natural frequencies as computed through a numerical FE modal analysis or by experimental testing.

Moreover, the same chapter shows an application of the same dynamic FE-based method to reduce lightweight members, such as honeycomb sandwich beam structures. These innovative structures are appearing as a promising technology in various industrial applications, due to their lightweight properties, high specific bending stiffness and strength under distributed loads, in addition to their good energy-absorbing capacity [3]. A typical honeycomb-core sandwich panel is formed by adhering two high-rigidity thin-face sheets with a low-density honeycomb core, with lower strength and stiffness. By varying thickness and material of core and face sheets, it is possible to obtain various properties and desired performances [4]. These reasons suggest a possible use of such materials in the automotive field, in order to improve performances of the vehicle body. However, for a successful vehicle development, their characteristics cannot be neglected in the conceptual analysis phase. A study of the experimental characterization and numerical modelling of these beams is performed as preliminary step, in order to validate the new concept modelling technique for such components.

The third chapter is related to the description of a new interface Multi-Point Constraint (MPC) connection element, between concept 1D beam elements and 2D shell elements of detailed joints (where three or more beams are connected).

This necessity arises because, for vehicle body structures, the type of used connection at interface cross-sections between concept beams and detailed joints

strongly influence the accuracy of the full vehicle model. Furthermore, the same connection elements are crucial for the accuracy of the reduction of joints into *super-elements*, which are defined by reduced stiffness and mass matrices between boundary nodes of each beam/joint interface. Then, first of all, a thorough research on the most used implementation methods for these transition elements is necessary, in order to find an appropriate starting point of research, towards a consistent 1D/3D interface modelling.

Nowadays, the most common commercial FE software already provide in their libraries some standard connection elements. Furthermore, different mathematical approaches reported in the literature can be used to define new ones.

The approach taken as reference is dedicated for only 2D connection cases and it is based on static "*load continuity*" considerations [5]. The basic idea is to obtain a transformation matrix, defining the relationship between the total forces ideally applied at the central node of the beam/joint interface and the nodal loads over the cross-section. For this purpose, theoretical stress fields resulting from the Saint-Venant assumptions with respect to axial, bending and shear load-cases for a beam-like structure [6] are considered. In linear elastic field, this loads correlation can be inverted, returning kinematic relationships between the motion of peripheral cross-section nodes related to the detailed joint model and the motion of the central node, belonging to the concept beam.

This approach is here extended for the 3D case (thus including the torsion load) and validated for typical automotive beam and joint structures. Dynamic results related to a case study, consisting of three spot-welded thin-walled beams connected with a joint, show a good accuracy of the concept structure, in terms of natural frequency values and modal displacements and rotations of beam middle lines.

Finally, the fourth chapter illustrates an industrial case study concerning a partially conceptualized vehicle body model, through which the MPC connection element is validated. Six connection elements are applied, for each pair of A-, B- and C-pillars interface cross-sections, that divide the concept and the detailed part of the body. The analysed typologies regard open, single-connected and multi-connected cross-sections; then, static relationships between loads applied to the central node and stresses induced at the peripheral nodes of interfaces must be adapted for each of

these types. Dynamic modal analyses show that the proposed element is able to overcome limitations of the most commonly used connection elements, returning a concept model with dynamic characteristics that are very similar to the detailed one.

Subsequently, a size optimization case is also presented, in which geometric parameters of concept 1D beam elements, forming the upper part of the model, are used as design variables. The design space defines geometrical constraints, while the first five natural frequencies are used as targets. The objective is to achieve in a very short time an optimal structure with a minimum weight, having similar dynamic functional performances of the original detailed vehicle body model.

Such an optimization problem is solved by using a Gradient-Based (GB) mathematical programming algorithm, which is among the most common methods used in structural optimization problems. Then, the optimized solution is found step-by-step in direction of the steepest descent, identified by evaluating the sensitivity of the objective function, with respect to all design variables.

This application case shows that concept modelling approaches combined with a size optimization process are fundamental tools for product development, in order to quickly analyse potential problems and weaknesses of projects and improve these aspects, thus drastically reducing the time-to-market.

Chapter 1: The Industrial Vehicle Design Process

1.1. Overview

The development process of a generic complex industrial product needs to be dealt with a systems engineering approach, in order to satisfy complex and often conflicting design criteria. In the automotive field, the Vehicle Development Process (VDP) is a very complex chain of activities, that need costly and time-consuming iterative loops, with significant amount of resources and times for any design phase, as showed in figure 1.1.

Three main design phases can be distinguished, which mainly differ from each other for the amount and level of detail of information available [7-8]:

- *Concept Design*: in this phase, the detailed geometric data are yet not available, but the degrees of freedom (DOFs) for decisions are high and important design modifications can be made. Usually, the engineering experience or the use of concept Computer Aided Engineering (CAE) techniques support the establishment of a principle structure, on which changes can be applied;

- *Detailed Engineering*: in this phase, the detailed vehicle CAD model is developed and validated with CAE simulations. While the model complexity increases, the design space becomes smaller.

- *Refinement Engineering*: this phase regards the design validation, after detailed CAD data were fixed. Only slight modifications are allowed, with the aim of improving the already existing project.

Each of the three steps terminates only when the gap between predicted and expected performances is acceptable.
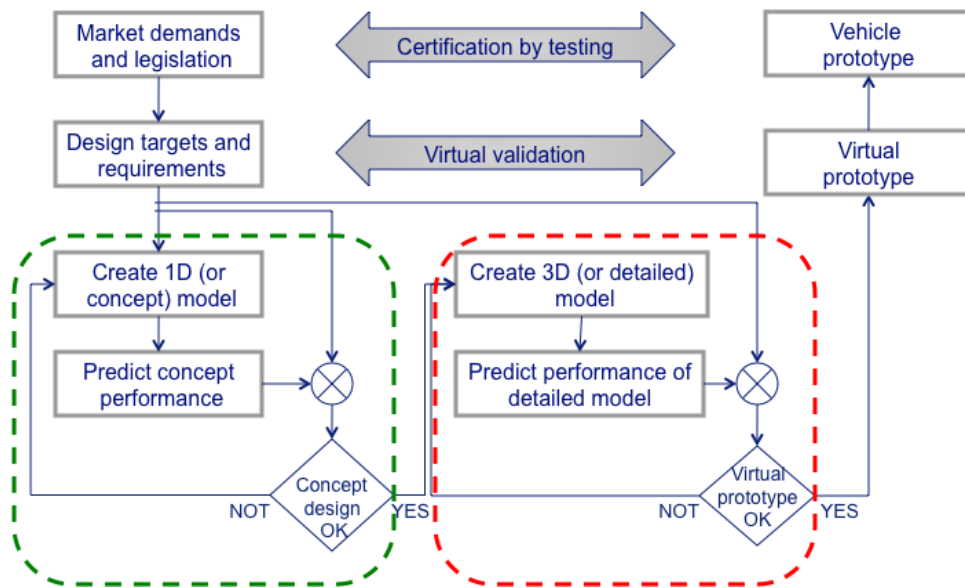
Figure 1.1: Design stages in the vehicle development process.

For every physical level, it is necessary that customer demands and requirements provided by legislations and regulatory bodies are collected and translated into a set of design constraints and targets. Such functional analysis involves primarily the identification of "system-level functions", defining interactions between the vehicle and the external world (driver and passengers, road and environment, market, regulatory bodies,…), and then derives design requirements for each constituent subsystem (vehicle body, chassis and suspension, tire, powertrain,…).

This functional flow-down, from vehicle to subsystems and after to components, is useful to describe how different parts work together, in order to achieve a given function. In a second phase, physical and virtual validations are performed in a

reverse hierarchical order, from components to subsystems and finally to the full vehicle. For this reason, the VDP is also called V-cycle, because can be represented as a V-shape process (figure 1.2).
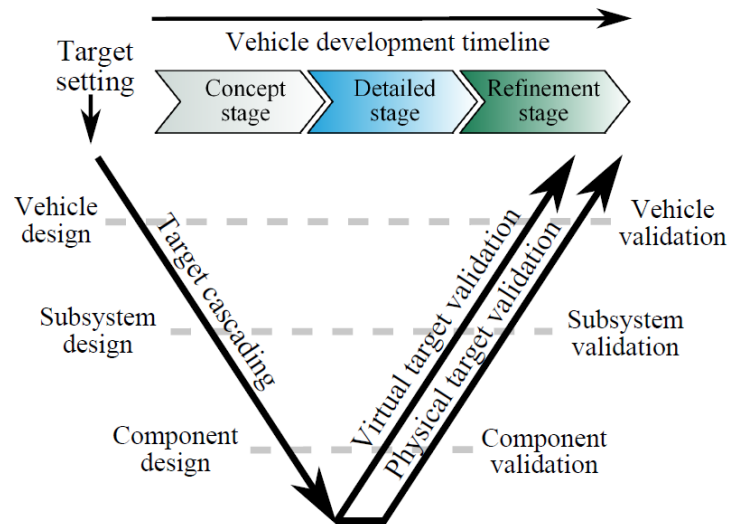
Figure 1.2: The vehicle development V-cycle.

1.2. Functional Analysis

As already mentioned, the design of a complex product such as a vehicle requires firstly the definition of targets for the entire system; then, with a flow-down, these goals are translated for various sub-systems and finally for each single component. This process is achieved with a functional analysis, in which the vehicle is represented as a system interacting with several external entities (figure 1.3). For any of those entities, the vehicle system is expected to serve different functions, while meeting requirements and targeting goals that are often conflicting with each other [9].
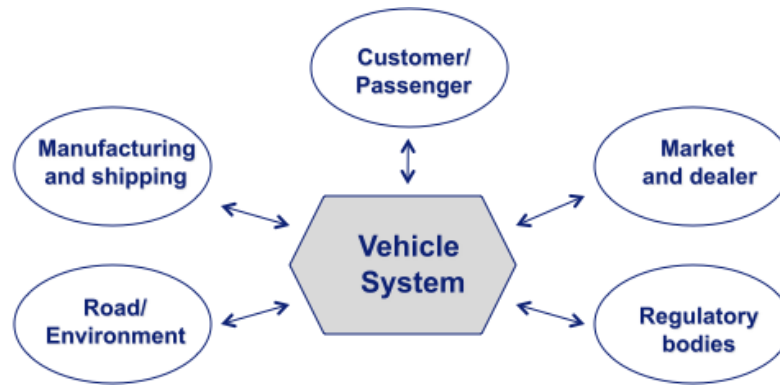
Figure 1.3: The vehicle system: interactions with external entities.

Regarding its interaction with the customer, a vehicle system must not only carry out the simple function of transportation means, but also ensure various performances, such as safety, comfort, good acceleration and roadworthiness, fuel economy, reasonable price and ownership cost. The vehicle should also reflect the commercial strategy of the Original Equipment Manufacturing (OEM), regarding, for example, competitiveness and segment leadership, brand value, attractive styling, with respect to the realistic logistics chain conformity to existing manufacturing plans. Finally, another important aspect, which is recently becoming more and more important, is the satisfaction of the constantly increasing requirements posed by regulatory bodies, which mainly concern the safety and the security standards for driver, occupants and pedestrians, as well as the environmental and ecological impact.

In the next step, design engineers have to set target and identify requirements for each sub-system. This complex process can be divided in four steps:

1. Identify the functions that the vehicle must satisfy, and then specify the performance requirements for the system;

2. Analyse how the subsystems and vehicle components interact or "work together", to provide this function;

3. Analyse the level of involvement and the specific role that each subsystem plays in the achievement of that function, and identify performance targets on the subsystem level so that the vehicle system-level targets will be met;

4. Flow-down the overall vehicle requirements to targets and constraints on each subsystem.

Table 1.1 summarizes, for the most relevant *vehicle performance*, the attributes that designers have to consider while defining each *function strategy*, the external entities that are involved and the core subsystems of a vehicle (tire, chassis and suspensions, vehicle body and powertrain) playing a role in their achievement [9-10].

Performance domains	Performance Attributes	External entities	Subsystems
Ride and handling	Ride isolation Drivability Steering and Cornering Braking	Customer/passenger Road/Environment	Tire Chassis and suspensions Powertrain
Noise and vibration	Quietness Sound quality Squeaks and rattle noise	Customer/passenger Road/Environment Regulatory bodies	Chassis and suspensions Vehicle body Tire Powertrain
Safety and security	Crash avoidance Crashworthiness Durability Pedestrian safety Vehicle visibility	Customer/passenger Road/Environment Regulatory bodies	Chassis and suspensions Vehicle body Tire
Styling	Appealing interior space Attractive exterior look	Customer/passenger Market/dealer	Vehicle body
Economic value	Price Cost to own (maintenance, fuel consumption, taxes)	Customer/passenger Market/dealer Manufacturing/ shipping	Vehicle body Powertrain
Energy use	Acceleration and velocity Fuel economy Aerodynamic drag	Customer/passenger Road/Environment Regulatory bodies	Tire Vehicle body Powertrain
Human satisfaction	Passenger comfort Ease of entrance/egress Accessibility of commands	Customer/passenger Market/dealer	Vehicle body

Table 1.1: List of main vehicle system functions and related attributes.

As it can be seen, the design process focuses on a complex set of functional performance attributes, such as horizontal and lateral vehicle dynamics (handling), vertical vehicle dynamics (ride and comfort), structural durability, noise and vibration, crashworthiness, etc. In order to take into account all relevant vehicle functions, the vehicle system can be considered as an integration of four main subsystem: vehicle body, chassis, suspensions and tire.

Especially in the initial phases of the vehicle development process, the powertrain can be treated as a design constraint rather than a targeted subsystem, since it is typically designed to be used in a wide family of vehicles, and then its engineering process is typically decoupled from the development of the rest of the vehicle.

1.3. The Vehicle Structure

The vehicle structure is one of the fundamental automobile subsystems, which contributes significantly to its development and manufacturing cost [11]. Its main role is obviously to maintain the vehicle shape and to hold the various parts together (suspensions, powertrain, steering system, seats, commands, doors,…). And more than that, very important functions concern the support of various static and dynamic loads applied to it, and the optimization of the NVH behaviour of the full vehicle [9]. Finally, the body must have high reliability, low cost, and high recyclability of materials is required.

The vehicle structure consists of chassis frame and body shell, typically formed by several steel or aluminium metal stampings, assembled in one spatial structure that consists of different thin-walled elements (such as beams, joints and panels), fixed together by spot welds.

Several different vehicle body configurations are distinguished. The main types are:

- *Space-frame configuration*: the spatial structure of the vehicle is composed of interlocking substructures, i.e. beams, in a geometric pattern, connected to each other at interface joints (figure 1.4-a);

- *Body-on-frame configuration*: a separate vehicle body, consisting of beams and panels in a typical shell configuration, is mounted to a rigid frame, supporting the drivetrain and the suspensions (figure 1.4-b);

- *Monocoque configuration*: an integral structure, composed by beams, joints and exterior panels, provides the main structural support, withstanding all major loads coming from the powertrain and suspensions (figure 1.4-c).

The first type of body structure has the advantage of low production costs and its use is currently limited to lower-volume vehicle productions. Instead, the body-on-frame configuration was quite common in passenger cars up to 30 years ago, and it is still leading the segment of light truck.

For its excellent mass-efficiency property, nowadays the monocoque body is the most commonly used configuration for passenger cars. For this reason, most of the structural requirements discussed below refer to monocoque body, but similar considerations apply to all types of vehicle structures.

a)   b)   c)
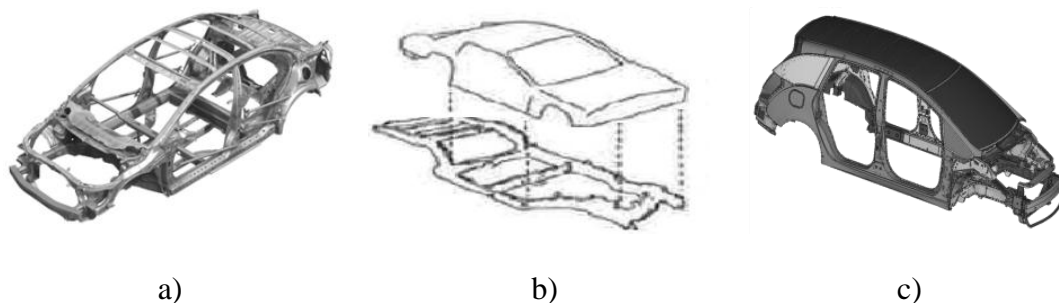
Figure 1.4: Different vehicle body configurations: space-frame (a), body-on-frame (b) and monocoque configuration (c).

Often, when the vehicle body refers to an assembly of the frame and panels (after the welding of its sheet metal components), it is named by the term *Body-In-White* (BIW). In other words, the BIW contains only the parts giving a significant contribution to the structural stiffness, while excluding the others. Figure 1.5 shows a typical vehicle BIW, with some commonly used terms.
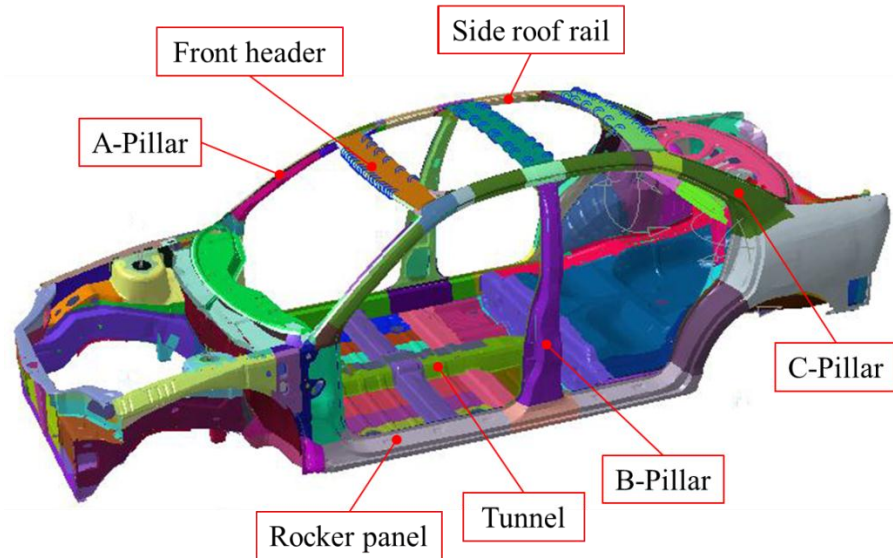
Figure 1.5: Main components of a typical vehicle BIW.

1.3.1. Main performance attributes

The vehicle structure must be able to endure the loads exchanged with the other components (powertrain, suspensions, passenger compartment, …) in a wide range of operational modes (static, steady-state dynamic, transient dynamic conditions, including crash). At the same time, the structural integrity should remain intact and the vehicle deformations must be kept within the proper levels. From these considerations, three classes of structural requirements can be identified, based on the amount of deformation allowed or requested for the achievement of a given function:

- **Stiffness requirements**: namely, the extent to which the structure resists deformation, in response to both static and dynamic loading conditions; up to the elastic limit state, the structure resumes the original undeformed shape, when loads are removed.

- **Strength requirements**: the vehicle structure must have an appropriate yield strength; i. e., only elastic deformations are allowed. Two types of loads must be assessed and monitored in the VDP, being potentially able to cause plastic

25

deformations: instantaneous overloads (due to extreme load cases) and fatigue phenomena.

- **Energy absorption requirements**: in crushing performances, the structure must absorb the big amounts of energy in external parts, while ensuring minimal impact for the passenger compartment and then the safety for human bodies. However, this very important criterion will be not treated hereby, being away from the purposes of this dissertation.

These structural requirements belonging to the three categories listed above have to be identified for all operational modes (or modes of use) of the vehicle, such as cornering, single or double lane changing, ride on bump, braking, frontal, lateral or rear impacts, rollover, etc.

In this way, it is possible to choose between different structural concepts, under the additional constraints of mass, cost, method of production, product application and other.

➢ **Requirements for body bending**

The global bending stiffness is an important design attribute in vehicle design: it indicates if the vehicle structure is strong enough to withstand static and dynamic bending loads, without structural failures.

Static bending loads are mainly due to the weight of the supported vehicle components and subsystems. The main contribution is provided by the engine, the passengers and, in some vehicle segments, the cargo weight, together with the distributed load due to the weight of the body structure itself. In dynamic modes of use, the stress field along the vehicle body is much more severe than in static conditions, since inertial forces are exerted on the structure in addition to gravitational bending loads. In such cases, the global bending loads can be estimated by multiplying static loads by an acceleration factor, whose value is based on the experience of company designers on successful projects.

The targets for K_b (defined as the ratio between applied load and maximum deflection) are considered reasonable in the wide range from 3000 N/m to 10000 N/m [12], with the higher values used as design requirement for vehicles with long wheelbase and/or high masses.

The global bending test, known as *H Point Bending* Test, replicates these static loads due to passengers, luggage and vertical accelerations [13]. As shown in figure 1.6, the structure is constrained at the front and rear shock towers, while vertical loads are applied in one (single point test) or two (two point test) transversal planes that are close to the central pillar-to-rocker joint [14].
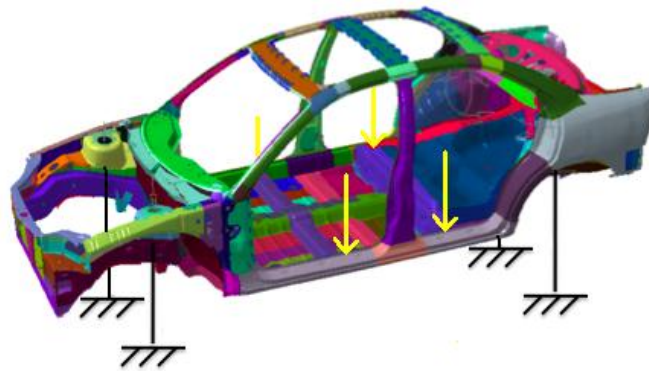
Figure 1.6: H Point Bending Test.

Another aspect to take into account is related to a subjective feeling of the vehicle solidness, perceived by the driver and passengers. The vehicle structure is perceived as solid, if it owns an appropriate stiffness, so that the bending vibrations induced by the road roughness remain below a certain threshold, above which a feeling of "shaky" behaviour is triggered.

To avoid such an uncomfortable sensation, the fundamental bending natural frequency falls in a range where significant excitation sources are not expected. Typically, for common passenger cars, a frequency range of 22-25 Hz is recommended, which is also a range where the sensitivity of the human body to vibratory excitations is low.

From the frequency equations for flexural vibrations of beams in free-free conditions, the required stiffness for the vehicle body, can be derived from the value of the targeted fundamental frequency.

As regarding the bending strength, the test consists in a series of loading and unloading cycles with an increment of the force amplitude, until the obtained permanent deformation causes important loss of vehicle functions.

Fatigue life estimation requires detailed stress analysis and considerable knowledge at component level, unavailable in the concept phase. For this reason, in this phase it is only assumed that the structure can withstand to the worst possible load condition, assuming that in this case the fatigue life is more or less satisfied. Given their variability and unpredictability, the instantaneous loads are taken into account by considering in the test also the extreme loading condition cases, like the towing or jacking modes of use.

➤ **Requirements for body torsion**

During its operation, the vehicle body is subjected to torque excitation in various modes of use, such as the twist ditch maneuverer, where one wheel is disconnected from the road due to abrupt profile discontinuities (hollows, waterways, etc…). Also in this case, the two basic requirements, such as strength (related to static or quasi-static loading conditions) and stiffness requirement (related to a transient and steady-state dynamic properties) must be taken into account.

The standard test provides that the vehicle body is constrained at its rear shock towers and two vertical forces, equal in amplitude but opposite in direction, are exerted at the attachment points of the front suspensions. Load and unload cycles, with increasing force amplitude, are applied, until a permanent deformation is observed that significantly affects the performance of the full vehicle.

The static torsion stiffness (K_t) is defined as the ratio between applied torque and torsion angle, determined as the resultant rotation angle between the front and the rear suspension attachment points. Often, its evaluation is repeated at different

assembly stages, from the BIW to the fully assembled vehicle. In this way, the contribution of removable parts, like glass or other components, in the global vehicle stiffness estimation can be assessed (figure 1.7). For common vehicles, target values are usually placed in the range between 7000 and 15000 Nm/deg, while, for torsion strength, the maximum allowed torque is limited in the range 5000 - 9000 Nm [9].
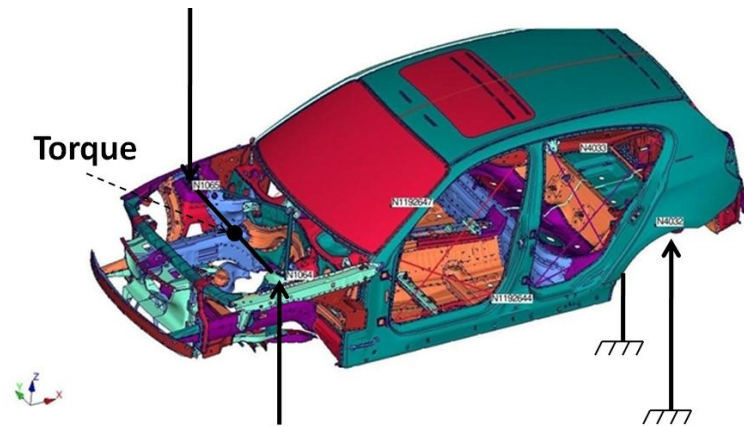
Figure 1.7: Static Torsion Test [14].

The torsion stiffness of the vehicle structure impacts on the system performance in two main ways:

- *in steady-state manoeuvers with high lateral acceleration* (high speed and/or small radius cornering);

- also in this case*, in the subjective feeling of solidness*, which passengers expect from a good vehicle.

For the first case, the transversal weight transferred during a curve from internal to external wheels, causes a reduced grip of the first and, hence, of the overall vehicle handling performance. This situation of low security can be reduced by suspensions with sufficiently high stiffness, or by
providing the vehicle with anti-roll bars. Their operation involves the application of opposite forces to the inertia of the vehicle body; this is generated by the mutual movement between the torsion bars and the suspensions. The body roll motion

causes the lowering of the outside suspension and the extension of the inner one: the reciprocal movement of the two wheels loads the antiroll bar that, while it straightens, tends to recover the equilibrium condition. The effect of the body stiffness on the overall roll stiffness of the vehicle is negligible, if the structure is at least one order of magnitude stiffer than the suspensions.

Regarding the second case, a value for the first torsion frequency must be targeted (usually being in the range of 20 – 30 Hz for most of commercial passenger vehicles) and from it a requirement on the torsion stiffness is derived [9].

A proper body design for torsion is achieved if both the above torsion stiffness requirements are fulfilled; in the design process, this is taken into account by first assessing which requirement is the most restrictive for the current design, and then including that requirement as explicit target in the body design optimization process. Normally, in common vehicles, the solidness requirement is predominant, while, from the very high values of roll stiffness in race cars, the highest values of body torsion stiffness are required to achieve the handling performance targets.

> **Requirements for NVH**

Noise, harshness and vibrations (NVH) are increasingly important in the vehicle dynamic field, because they involve a lot of subsystems related to the quality and the reliability of the vehicle. The vehicle dynamics behaviour concerns two main aspects: the *handling* and the *comfort*.

The first indicates the performance in terms of directional control, stability, road holding, steer ability and manoeuvrability of the vehicle. For simple vehicle characteristics tests, handling analyses can be based on the open-loop model of system, in order to know its behaviour in response to control inputs or disturbances from the road or atmosphere. Instead, closed-loop vehicle system is used to include also the performance of the driver.

The term comfort indicates the perception of the vibrations transmitted by a moving vehicle to the driver, in the frequency range of 0-100 Hz, and is one of the main

aspects in the vehicle quality evaluation. Exposure of the human body to vibration can result in discomfort, interference with activities, disease or injury and motion sickness: any of these effects can reduce the ride quality of a vehicle (figure 1.8).
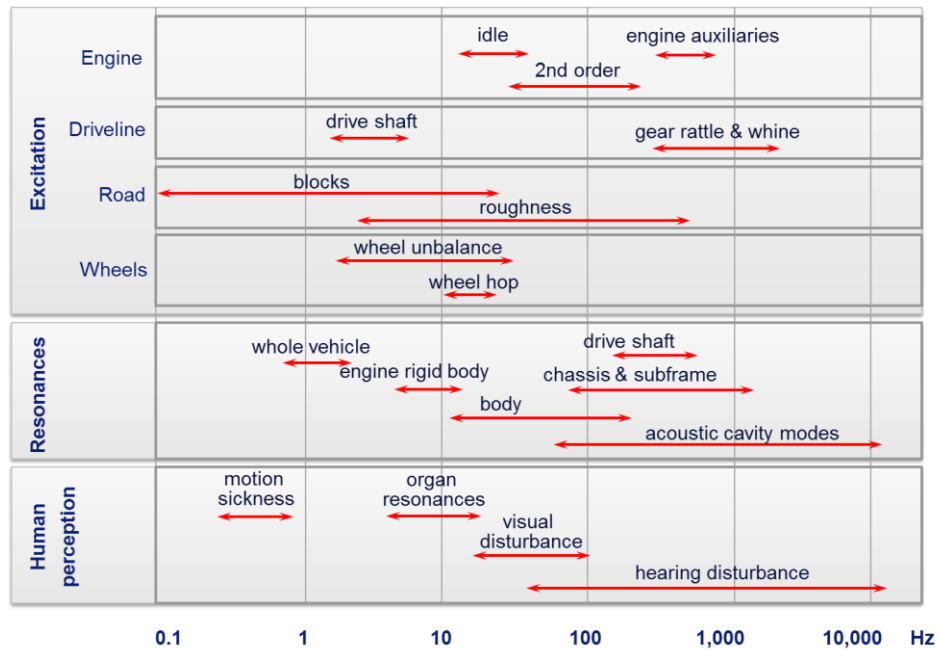
Figure 1.8: Example of NVH mode map [10].

A good vibration comfort is achieved if vehicle resonances are avoided. This can be achieved by making sure that vehicle eigen-frequencies are away from the excitation frequencies present in the normal mode of use (typically, the variation factor is $\sqrt{2}$ [15]).

The vibration modes can be classified into global and local types. The first involves the entire structure, in which the associated energy is uniformly distributed [13]; on the contrary, local modes, much easier to damp, concern only single parts of the body, where most of the elastic energy is concentrated. For this reason, the eigen-frequencies range is fairly wide, covering several tens of Hz for global modes to several KHz for local ones.

However, the dynamic analysis is usually focused on the low frequency range (below 200 Hz), where are between 150 and 250 modes of BIW. Particularly, in the concept

phase, only the first two bending and torsional global modes are considered as benchmarks of the vehicle (figure 1.9).
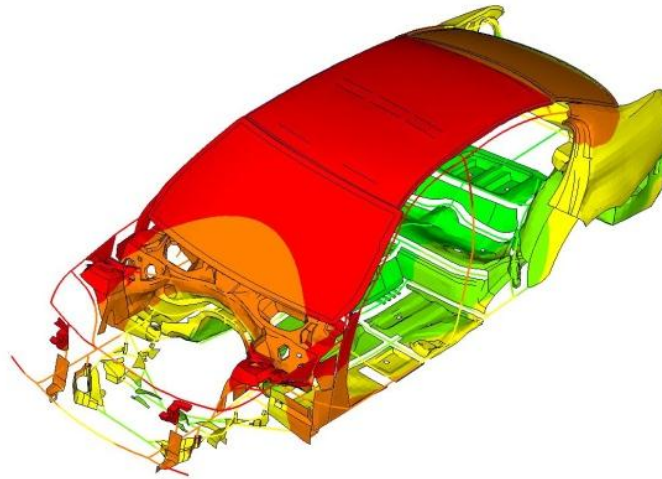
Figure 1.9: First torsional global mode for a concept BIW for passenger car [16].

In order to study input excitations induced to the drivers/passengers, firstly it is necessary to identify the various excitation sources and analyse their main characteristics, i.e. the frequency bandwidth and the maximum amplitude in different modes of use. Typically, the main sources of vehicle vibrations are the wheels, the engine and the driveline [11].

Secondly, a load path analysis is performed, in order to understand how the generated vibrations "change" (amplification or damping phenomena) while going from the source to the receiver (driver and/or passengers).

This very important phase allows to understand how the main subsystems are involved in the filtering process and what is their contribution in the frequency response of the vehicle system [10, 17].

Finally, an analysis of tactile, visual and acoustic sensations that such vibrations generate on the occupants is performed, with the aim of understanding their impact on the subjective feeling of comfortable ride (figure 1.10).

With reference to the human mechanisms of perception (skin receptors, eyes, accelerations and ears), the mechanical vibrations are usually classified in the

frequency domain. All the vibrations with frequencies below 25Hz are perceived as mechanical vibrations, whereas the vibrations higher than 100 Hz are often perceived as noise. From 25 to 100 Hz the vibrations are perceived both as mechanical vibrations and as noise.
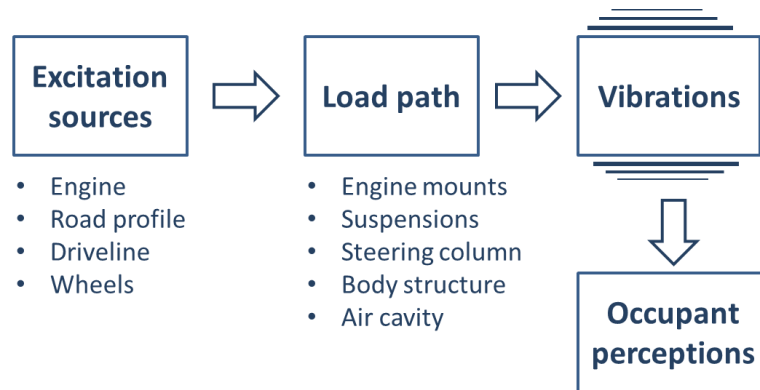
Figure 1.10: Main excitation sources and load paths for vehicle vibrations.

The term *Primary Ride* refers to all the vibrations of the car body at frequencies lower than 5 Hz. In this range the structural vibrations are negligible and the vehicle subsystems can be considered as rigid.

Instead, the term *Shake* indicates the medium frequency range vibrations from 5 to 25 Hz. This range is also named *Secondary Ride*. *Harshness* indicates the higher frequency vibrations, from 25 to 100 Hz. The structural vibrations are considered and usually perceived as *Noise*, which refers to all the vibro-acoustic phenomena above 100 Hz.

1.4. Role of modelling and simulation in the VDP

In recent decades, the VDP is being increasingly driven by complexity and multi-disciplinary nature of its products. Key goal remains the global vehicle performance

for multiple design attributes (passive safety, NVH, ride and handling, fuel economy), but new active and integrated solutions are being introduced, which broadens the design space to further improve the product quality, while meeting the ever increasing demands on safety and ecology.

For this reason, vehicle manufacturers have adopted a development strategy, in which the traditional, experience-driven "trial-and-error" approach has been supported increasingly by "Virtual Prototyping" techniques, based on Computer Aided Engineering (CAE) models. These tools can be used to predict and improve the vehicle (sub-)systems, from the concept phase onwards. CAE simulation and optimization techniques play a crucial role in the industrial development process of modern vehicles [7, 8, 18], due to their ability to manage and optimize efficiently complex and often conflicting sets of design criteria.

Well established 3D modelling techniques are available for structural linear and non-linear analyses (Finite Element Methods, FEM), for vibro-acoustic analyses (FEM + Boundary Element Methods, BEM), for aero- and thermo-dynamic analyses (Computational Fluid Dynamics, CFD), for dynamic simulation (Multi-Body Systems, MBS).

a)   b)   c)
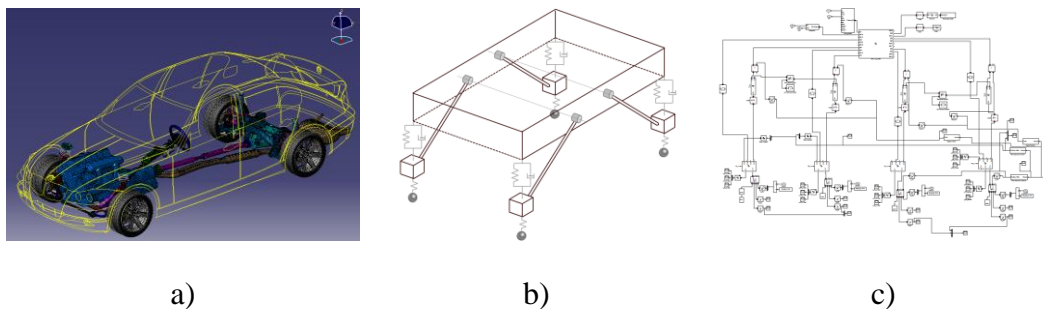
Figure 1.11: Example of vehicle 3D (a), 1D lumped parameters (b) and functional (c) models for vehicle ride and handling simulations.

These high-fidelity virtual models are developed during the detailed and refinement engineering phases, in order to validate the design choices before fixing them in a

physical prototype of the vehicle. An example of detailed MBS model for vehicle ride and handling simulation is shown in figure 1.11-a.

However, the limitation of 3D modelling methodologies is that accurate predictions can be achieved only when highly detailed geometric data become available, which has two main consequences on their applicability in the VDP:

- 3D models are not available in the initial design phases of a new product, when only general information can be derived from predecessor models, while most of the design decisions must still be taken;

- after a detailed model is created, the feasibility of implementing design changes can be prohibitively low, because design constraints become fixed and subsystem designs become frozen; this has important consequences on the development process cost and on time-to-market of the product.

For these reasons, predictive tools and concept 1D simulation models are used during the upfront engineering phase, in order to improve initial CAD models making fast and effective design modifications.

In the field of vehicle engineering, two classes of 1D or *concept modelling techniques* can be mentioned:

- **Physics-based models:** these models have a reduced number of degrees of freedom (DOFs), with the components having a mathematical representation, which incorporates physical characteristics (like inertia, linear and non-linear stiffness, dissipative phenomena, etc.), lumped into a limited number of physical parameters (masses, springs, dampers, …). Bodies can be rigid or flexible; the mutual interaction and constraints is carried out by exchanging power, thus allowing that the behaviour of the system can be predicted with sufficient accuracy. An example is illustrated in figure 1.11-b, which shows a linearized lumped-parameter model of a vehicle for ride and handling simulations;

- **Functional models:** these surrogate models provide a structured representation of functions (activities, actions, processes, operations) within the modelled system or the subject area (figure 1.11-c). Information on the behaviour of the system is derived through virtual or physical tests on predecessor models and

used to create analytical or numerical functional representations (polynomial regression, neural networks, data tables, maps, splines/surfaces matrices). All the functions are then interrelated by a flow block diagram, that graphically represents the system and the direction of information flow. Examples of 1D functional models in vehicle engineering are the kinematics & compliance (K&C) tables for suspension modelling, engine maps, modal reduced models of structural elements.

The availability of upfront engineering techniques is essential in the development of next-generation vehicles, but the applicability of state-of-the-art concept design methodologies must be expanded, by eliminating a number of limiting factors, like [19]:

- a valid method for all problem categories is still missing;
- there is a lack of comparative studies of available methodologies;
- many modelling techniques have not reached maturity or have not yet been tested on industrial cases;
- it is not an easy task to obtain, for each considered case, a good compromise between precision, simplicity, model size and similarity to the reference detailed 3D structure.

Some of these issues will be addressed in this dissertation.

1.5. The vehicle body concept modelling

Concept modelling methodologies are being recognized as an important part of the VDP. Their final objective is to reduce the time-to-market in manufacturing industry and to improve various functional performance attributes, like NVH, safety and energy efficiency of the vehicle. Each of these attributes is hard to improve in the last steps of the development process without raising conflicts with the others. For this

reason, many researchers have developed predictive concept CAE tools, which can be used to predict and improve the vehicle design from the concept phase onwards. A widely used classification divides these methods into three main categories [20]:

- methods concurrent with CAD;
- methods "from scratch";
- methods based on predecessor FE models.

These three groups will be explained in detail in the next sub-sections.

1.5.1. Methods concurrent with CAD

Methods belonging to this category aim at improving components as soon as CAD models become available for the various simulations. There are two main methods belonging to this category: the *associative parametric CAE* and the *isogeometric modelling* methods.

➢ The associative parametric CAE method

This method presents an approach based on an associative parametric modelling [1], which consists in the implementation of a functional architecture, based on the CATIA V5 framework [21]. This diagram is composed by a set of hierarchical levels of design data, with increasing level of detail. So, the designer can create the highest-level architecture in an early design stage and gradually populate the other lower levels when more CAD design knowledge becomes available.

The functional architecture is fully associative, so that at each design stage there is an analysis model with all available knowledge at that time. As shown in figure 1.12, each component is organized according to a "tree" structure. The design specification consists of two types of parameters: the *derived published* and the *internal*

parameters. The first represent a link to the specification parameters defined externally in the super-component, i.e. in the high level component. This ensures that all sub-components meet the basic idea of the super-component. Internal parameters are used for the component-internal use only. When some levels have been frozen, design iterations can then still be performed at the lower levels.
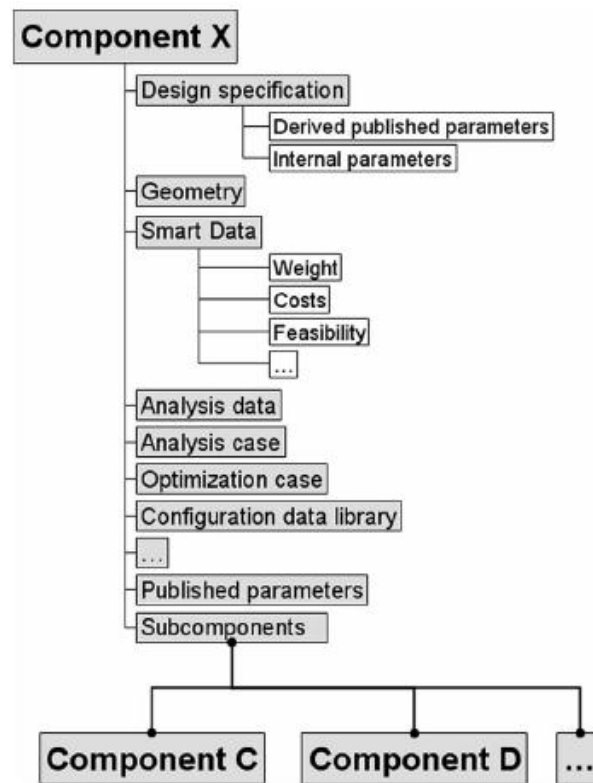
Figure 1.12: The associative parametric CAE method: composition of a single component [1].

➢ **The isogeometric modelling approach**

This approach aims at defining an exact geometric model using basis functions generated from Non-Uniform Rational B-Splines (NURBS) [22].

In order to obtain a particular level of accuracy, it is possible to refine the basis of this kind of geometric curves, useful to define accurately the objects shape, and/or elevate its order, without changing the geometry or its parameterization. Refinements are easily implemented and exact geometry is maintained at all levels, without the necessity of subsequent communication with a CAD description.

It is established that the basic functions are complete with respect to affine transformations, meaning that all rigid body motions and constant strain states are exactly represented.

This promises future analysis capability directly based on the CAD design, thus avoiding the tedious CAD-to-CAE transition. The method can be applied to predict various functional performance attributes, such as statics, normal modes and fluid–structure interaction. The reported cases concern academic structures but also complex real-life structures.

This technique may find future application for concept design purposes. Indeed, it can enable the creation of isogeometric models that incorporate the available design knowledge. Various parameters can be optimized to provide input for the initial CAD formulation.

One disadvantage of this method is that the approach is based on rather exact CAD data, that cannot be available for the entire structure. For this reason, this technique cannot easily provide early simulation predictions.

1.5.2. Methods "from scratch"

This category of concept modelling approaches aims at establishing a functional layout of various BIW components starting from a completely new vehicle structure. For this reason, requirements needed for this category are very complex and intricate. Principal methodologies belonging to this category are: the *topology design optimization* and the *functional layout design* methods.

➤ **The topology design optimization method**

Whit this method, it is possible to determine where material must be present within a predefined space, called admissible design space, in order to optimally satisfy specific design criteria for the structure (for example static stiffness or yield strength) and constraints (supports or joints) [23-24].

The admissible design space consists of a space filled by hexahedral elements, the so-called "voxel" mesh. The methodology provides an initial topology design as first optimization step, after which the algorithm decides for each of the voxels whether material must be removed or not.

The topologically optimized component has, however, rough transition elements, which must be smoothed and modelled to achieve a realistic design.

In the vehicle design process, topology optimization is applied to optimize the load path configuration for statics, NVH and crashworthiness.

➤ **The functional layout design method**

By using this approach, the designer is able to predict the performance of the model, using a simplified concept model, consisting of beams, joints and panels, which represent the functional layout of the structure.

In the most common version [25], the basic project starts from a body topology concept, which consists of three basic parts: beams, joints and panels.

Beams are represented by thin-walled structural metal parts, with simplified shapes of cross-sections. Joints are simple channel profiles located where the beams meet. Panels are represented by coarse four-node quadrilateral shell elements.

The connections between components are modelled with rigid connection elements.

The model is completed by adding lumped and distributed trim masses and defining appropriate boundary conditions and loads. This concept model can be used for size

optimization of vehicle body NVH performance, by changing parameters like shell thicknesses, cross-section beam areas, etc.

Often, beam and joint layout is created and then node locations are optimized, in order to improve the design [26], or other approaches are based on the definition of beam concept FE models, according to new styling lines [27]. Finally, also commercial software are available, like *SFE Concept* software [28], which allow creating concept models, starting from simple geometrical descriptions.

With these tools, designers can define models based on implicit parametrical descriptions of geometry and topology and then assemble various parts at every design stage, by using the built-in FE generator. Firstly, a set of base points and lines must be defined, in order to indicate the position of joints, beams and panel edges. Then, beam cross-sections are defined and assigned to the lines. Parametric joints between the beams are automatically created, the shell components are added, and finally a mesh is created to enable FE analyses. SFE concept model can be modified quickly by moving influence points, stretching or bending base lines and by changing cross-sections.

1.5.3. Methods based on predecessor FE models

This category includes *mesh morphing* and *concept modification* approaches, which are used to design a variant or incremental improvement of an existing vehicle model. They make use of a predecessor FE model to identify issues and to include possible countermeasures already in the initial CAD design of the new vehicle.

➢ **Mesh morphing**

Mesh morphing [29] is a CAE technique that allows to modify an existing mesh, without the need for re-meshing and preserving model integrity and connectivity,

since, during the process, only node coordinates are changed. This method starts from a predecessor FE model to modify the grid locations in the mesh, without changing the element connectivity. When the predecessor mesh has been reshaped, it can be analysed to identify weak spots, so that countermeasures can already be included in the initial CAD design [18].

Two variants are distinguished: the direct or *freedom morphing* and the indirect or *control-box morphing*. In the first, the designer acts directly on the mesh, using the concept of control nodes, deformable nodes and fixed nodes. The drawback is that the morphing operations are not repeatable.

Instead, in control box morphing, it is possible to define control boxes that envelop the existing mesh, and morphing operations are defined on these control boxes.

One can incorporate the feature lines of the predecessor FE model in the control box definition, so that the regularity of feature lines and the element quality are preserved after performing the morphing operations. This is particularly useful for crash models.

In figure 1.13, an application of the two methodologies in the morphing of a vehicle joint structure is shown.

a)   b)
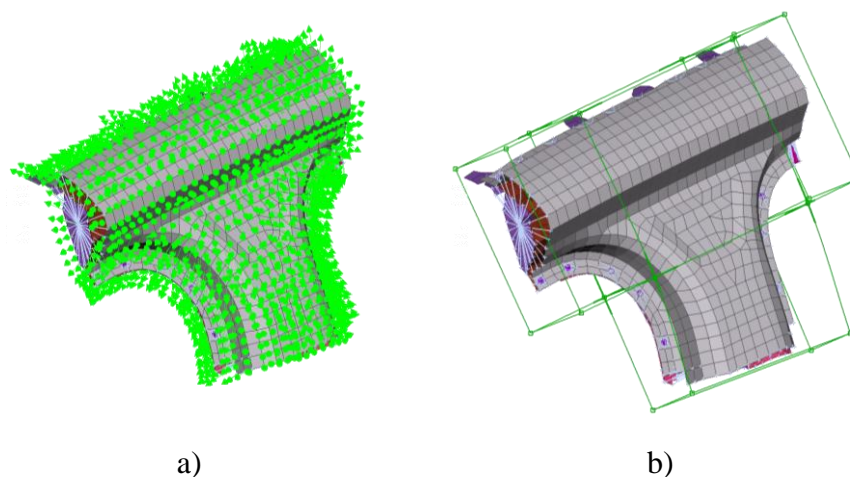
Figure 1.13: Application on a vehicle joint structure: freedom morphing (a) and box morphing approaches (b) [30].

➢ **Concept modification approaches for beam reduction**

Static and dynamic behaviours of the full vehicle mainly influenced by the beams' and joints' stiffness and mass properties. So, Beam&Joint (B&J) concept modelling tools are essential for accurate front-loading engineering of the full vehicle.

Usually, the reduced beam modelling approach consists in replacing detailed 3D FE models of beam members with simplified 1D beam models, also referred to as equivalent 1D concept beams. Along each primary beam-member, a number of intersection planes are defined, corresponding to portions of the beam with almost constant cross-section shape. Mass and stiffness properties of these beams are computed by applying proper analytical or numerical procedures to a set of cross-sections; for each of these, equivalent beam properties are computed.

Once properties of beam segments are determined, equivalent 1D beam elements replace detailed beam-like structures. The entire beam member can be then represented as a series of linear beam elements, using a standard FE library. An example is shown in figure 1.14, where both the original detailed and the simplified FE model of B-pillars of a vehicle BIW are represented.

Several methods can be mentioned, briefly described below.

a)   b)
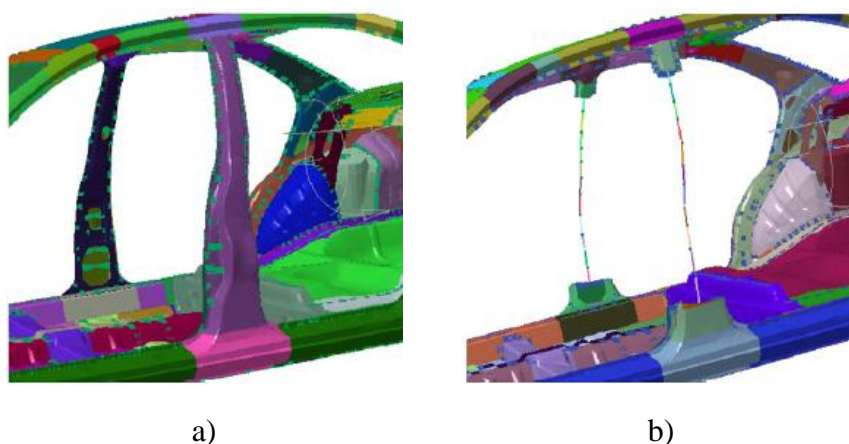
Figure 1.14: Replacement of original (a) with concept model (b) of BIW B-pillars [31].

✓ *The geometric method*

For a typical vehicle BIW, beam-like members are thin-walled structures, formed by two or more curved panels connected to each other by means of spot welds. This procedure, based on a geometric approach, provides that equivalent properties of beam segments are calculated by analysing the mass distribution along each open or closed cross-section. In particular, after defining an intersection plane and a geometric centre point (figure 1.15), geometric properties (e.g. cross-section area, quadratic moments of inertia, etc.) of every shell element at the interface must be calculated, with respect to a local axis system (x_i, y_i, z_i). Subsequently, transformations from all local axis systems to the central reference system (x, y, z) are performed. The sum of all these contributions gives the global geometric properties of the cross-section.
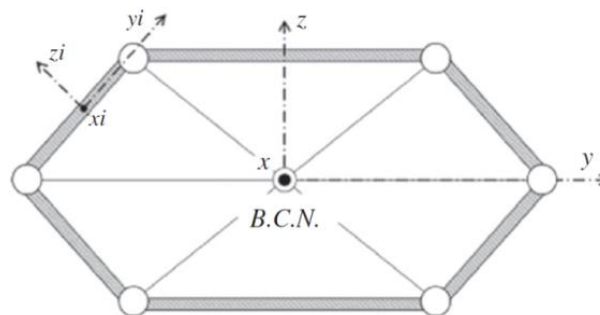
Figure 1.15: Schematic representation of an arbitrary beam cross-section [31].

Typically, the beam-like members of a vehicle have discontinuous structural properties due to holes, spot-welds and stiffeners. In order to take such discontinuities into account, the nominal properties of reduced beam elements (e.g. quadratic moments of inertia, torsional modulus, etc.) must be adjusted by using proper correction factors [61-62]. These corrections are calculated using a model updating procedure. An appropriate optimization algorithm should be chosen, in order to improve the correlation between reference and simplified models. Once the

correction factors of each reduced beam-like members are established, the correct equivalent beam properties can be identified [32].

✓ *The static FE-based method*

Static FE-based concept modelling methods rely on running static FE analyses of the original structure [33-34]. A set of static load cases is generated by applying bending, torsion and axial loads at the end sections of each beam segment. Here, a segment refers to any portion of the beam with constant geometric and structural properties.

Regarding thin-walled beam-structures, central nodes are created for some cross-sections and they are connected to the other nodes of the same cross-sections by means of Multi-Point Constraint (MPC) elements, which are of rigid type for the two end sections and of interpolation type for the intermediate cross-sections.

In this way, external and reaction loads are applied directly to the central node of the end sections, and the rigid elements transfer them to the rest of the structure, while the interpolating elements allow to estimate the linear elastic deformation of the beam central line.

Finally, the stiffness properties of the equivalent 1D beam are estimated by applying the linear elastic load-deformation relationships of the beam structure, starting from the static deformations predicted by analysing the detailed 3D model.

A scheme illustrating the static FE-based method is shown in figure 1.16.

The advantage of this approach is that it can be easily applied to any beam, whatever the shape of its cross-section, always providing results that can be sufficiently accurate to steer the initial design choices.

However, the addition of auxiliary connection elements within the structure prevents the end sections from deforming. Such a modification of the original mesh may result in a significant overestimation of the beam stiffness properties, especially for automotive structures, which are usually formed by spot welded thin-walled panels.
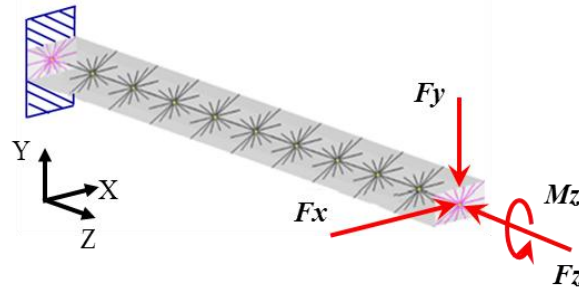
Figure 1.16: Application of static FE-based method: loads, constraint and connection elements applied to the detailed 3D beam model [35].

✓ *The 8-DOF beam theory*

New advanced theories on thin-walled beams, completely describing the cross-section deformation, are available in literature. These theories are important to predict relevant low-frequency vibration modes in interfacing zones, otherwise hardly achievable with conventional beam theories. The most important studies regard a comprehensive theory, named 8-DOF beam theory [36-38], in which warping and distortional effects are added to the classical 6 DOFs (three displacements and three rotations) at each interfacing cross-section.

With regard to 3D thin-walled beams, these cross-sections having 8 DOFs fully represent the general behaviour of the structure; indeed, they consider rigid motions, warping ω (out-of-plane deformations), and distortion χ (in-plane deformations). A good representation of possible deformation of interfacing cross-sections is given by the model depicted in figure 1.17.

By including coupled deformations of torsion, warping and distortion to the extensional and flexural deformations, the same authors developed also a one-dimensional thin-walled box beam theory, in which 8-DOFs are also derived for 1D beam elements.
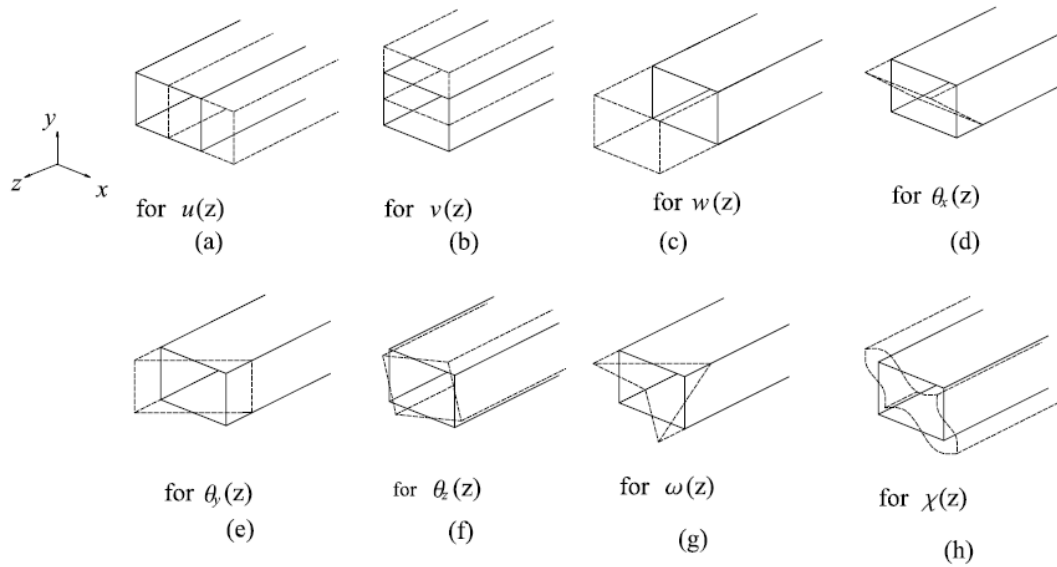
Figure 1.17: Deformation shapes of a box beam cross-section corresponding to 8 DOFs (those represented in a-f images are considered in a standard 6-DOF beam theory) [38].

> ➢ **Concept modification approaches for joint reduction**

Vehicle joints are particular thin metal sheets structures, where three or more beams are connected [39-40]. They govern up to 60% of the global stiffness in self-supporting vehicle body [41]. For this reason, joint structures have to be properly designed, in order to obtain improved static and dynamic characteristics of the vehicle [30, 39, 42-46]. Figure 1.18 shows an example of some principal BIW joints. Two types can be distinguished, the T-type and the Corner-type joints.
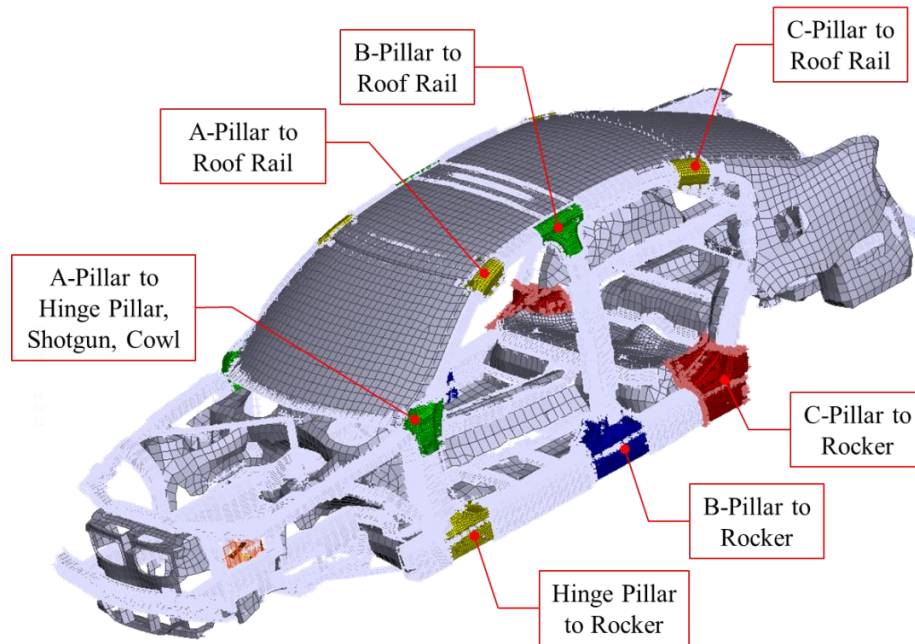
Figure 1.18: Most important joint structures in a FE model of vehicle BIW.

✓ *Static and dynamic reduction*

One of the most important concept modelling approaches is the reduction technique, in which computational efforts of detailed FE model are strongly decreased.

These model condensation methods involve reduction of the number of DOFs of the detailed FE joint model, by representing these with a reduced number of so-called generalized coordinates. In other words, the reduction is a method useful to represent the FE model of a component as a pair of equivalent stiffness and mass matrices.

These matrices are concentrated between central nodes of the beam/joint interfaces, representing the master DOFs, while the DOFs of all other nodes of the detailed joint model are removed (slave DOFs). Usually, joints are simplified after the concept beam layout has been defined. In this way, interpolation elements to the beam centre nodes at the joint ends have to be fully included (figure 1.19).

Static or dynamic reduction techniques are available. The most important method for static condensation is the *Guyan* reduction [47], which returns an exact reduced stiffness matrix, while the mass matrix is approximated.

By reducing the mass matrix, it is assumed for the considered structure that inertia forces on internal DOFs are less important than elastic forces transmitted by the boundary DOFs. This is true for very stiff components, like typical automotive joints. Indeed, the stiffness relations between the end points of the joint have a much stronger influence on the global body behaviour than the exact distribution of mass along the joint. For this reason, a Guyan reduction of the joint structure to its end nodes (coinciding with the beam centre nodes) seems an appropriate choice to create a small-sized representation of the actual joint [20, 43].

Dynamic condensation methods make use of the vibration normal modes of the substructures. They differ from each other for the boundary conditions that are applied to the substructure and for the *enrichment vectors*, that are selected and added to the normal modes. Two well-established examples are:

- the Craig-Bampton fixed interface approach [48], where the normal modes are computed while the substructure is clamped at the connection interfaces, and where the enrichment vectors consist of constraint modes. These latter are the static deformation shapes of the substructure obtained by applying a unit displacement on one interface degree of freedom, while holding the remaining interface DOFs fixed, and repeating this for all the interface DOFs.

- the MacNeal's approach [49], which uses the normal modes of the component in free-free conditions and enrichment vectors that consist of residual flexibility modes. In this case, the enrichment vectors correspond to static deformation shapes obtained by applying a unit force on one of the interface degrees of freedom, with a zero force on the remaining interface DOFs, and repeating this for all the interface DOFs.

In such reduction methods, the component modes are generally computed up to a frequency higher than the frequency range of interest for the assembly. The frequency range considered for the component reduction is typically increased by a factor of 1.5 w.r.t. the frequency range of interest. The enrichment vectors are of vital importance to accurately represent the local flexibility at the connection interface, when the reduced modal model of the substructure is re-assembled to other

substructures. It is clear that the number of enrichment vectors that must be computed strongly depends on the number of interface degrees of freedom [50].

a)   b)
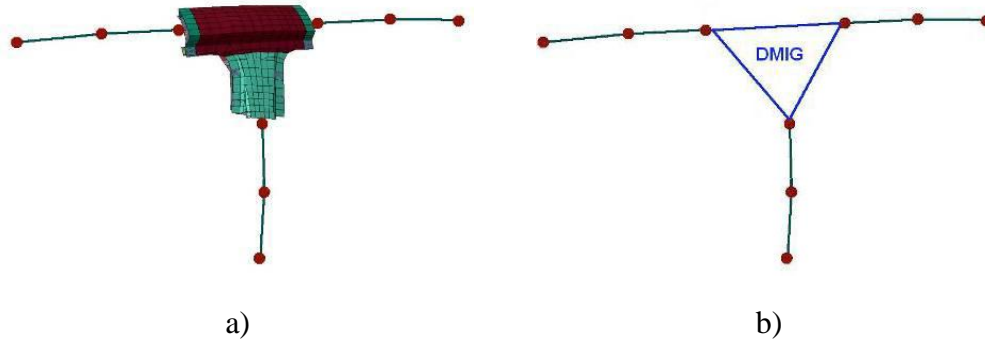
Figure 1.19: Replacement of a detailed joint model (a) with a joint super-element (b) [32].

✓ *Super-element joint approximation method*

Also in this method, the joint structure is replaced by a super-element, which takes into account the rotational and translational flexibility of the terminal beam parts intersecting in the joint [51].

First, the finite-length beams are joined to a small rigid framework formed by the intersection of the beam centroidal paths. Subsequently, the legs are modelled as pin-connected beam elements, with torsional and translational springs in parallel. The joint parameters are then determined through an optimisation procedure that selects spring constants and beam lengths that yield a super-element with mass, stiffness, modal parameters and total strain energy well approximating those of the actual joint (figure 1.20).
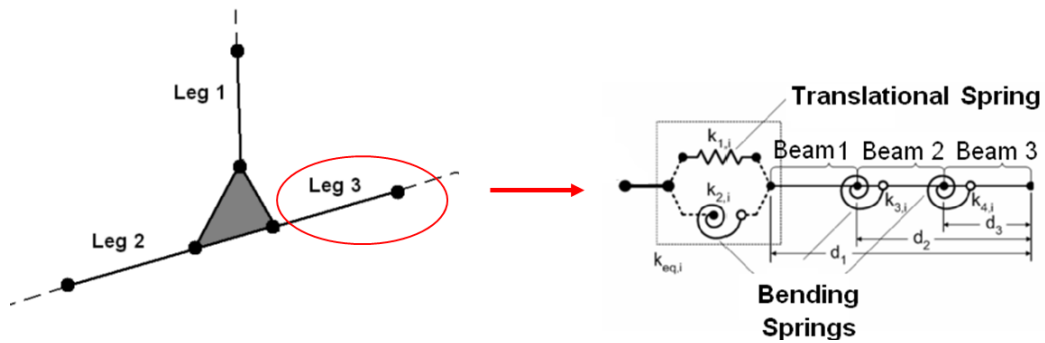
Figure 1.20: Super-element model of one leg [51].

✓ *Dynamic Joint Method*

The joint is defined as inscribed in a sphere with radius r=250 mm, a size fitting most of the joints in a car body [52]. The centre of the sphere is placed in the middle of the various joint centres, and the legs are cut where the sphere intersects them. Finally, a heavy mass is cast onto each leg end, as shown in figure 1.21. Modal analysis is then performed with the joint hanging on soft springs, so that the natural frequency of the assembly is at least one order of magnitude lower than the first natural frequency of the joint, thus creating a free-free set-up.

Figure 1.21: Experimental set-up for the dynamic joint method [52].

The frequencies and the corresponding normal modes are used to visualize the vibration behaviour of the joint. Since the shape and size of the masses are standardized and much heavier than the joint itself, different joints can be compared to each other.

The advantage of using a free-free set-up is that no expensive and stiff tooling is needed. The virtual counterpart of the experimental set-up is easy to reproduce; a CAD geometry is used as a basis to create an FE model. The masses can be added at each leg end as lumped masses with appropriate inertia properties. The final stage is a computational modal analysis, from which the first six modes (rigid body modes) are removed, giving the frequencies and the modes as in the experimental case. The definition of boundary conditions can be easily automated in a software, without the need for manual interaction.

The dynamic method has the advantage of giving a qualitative visualization of weak areas, e.g. where spot-welds are missing, thus suggesting which parts must be made stiffer for potential improvements of the structure behaviour.

Chapter 2: A Dynamic FE-based Method for Concept Modelling of Thin-walled Beam-like Structures

2.1. Overview

As already mentioned in chapter 1, many of vehicle body concept modelling techniques focus on reducing the detailed FE model of the BIW in a simplified model, in order to drastically reduce the required computational resources, as well as the time needed to modify it.

Some of the most widely-used methodologies belong to the category of *concept modification approaches* [34, 51]. In particular, a methodology belonging to such a category, namely the *reduced beam and joint modelling technique* [20, 31, 53], aims reducing the main FE component model of an existing vehicle BIW, such as beams, joints and panels, into simplified models, able to maintain a good accuracy, while strongly reducing the computational time required by simulation.

The primary structural elements that need to be reduced are the beam-like members, which dominate the static and dynamic behaviour of a vehicle BIW, with their stiffness properties. In a typical vehicle body, these load-carrying members are thin-walled structures, formed by two or more curved panels connected to each other by means of spot welds. Classical concept approaches replace these detailed 3D beam models by 1D beam elements, having equivalent stiffness parameters.

In order to overcome limitations of approaches shown in the state-of-art, a new dynamic FE-based method is proposed. This new method allows estimating equivalent stiffness properties of a 1D beam element, using the natural frequencies estimated by means of a modal analysis on the original 3D FE model of the structure. The main advantage of the method is that it takes into account all possible discontinuities and variations, which are due, for instance, to spot welds connections, that are typical in automotive beams.

The method consists of two steps:

1. natural frequencies of the given beam-structure are estimated by means of a modal analysis of the detailed 3D FE model in free-free conditions;

2. flexural and torsional frequencies are expressed as a function of the cross-section stiffness properties, using the ordinary uncoupled differential equations of beam vibrations.

Finally, a numerical procedure estimates equivalent stiffness properties of the 1D concept model, by fitting the analytical formulation derived from differential equations with the targeted values of natural frequencies.

2.2. The dynamic FE-based method

The analysis of dynamic beam model could be a very powerful tool to investigate a possible path of research, in order to correlate the 3D beam characteristics with parameters defining the 1D beam model. In order to achieve this goal, firstly it is necessary to use differential equations of coupled and uncoupled vibrations of a generic prismatic beam.

Subsequently, the solution of these equations should return a valid correlation between the natural frequencies and the stiffness parameters of the beam.

2.2.1. The analytical model

The reference analytical beam model [54] starts from assumptions of Timoshenko model [58], but some assumptions and approximations are considered.

Indeed, shear deflection and warping of the cross-section are taken into account, while the inertia forces due to the torsional rotation and the warping inertia are ignored, since their influence is considered negligible on vibrations. In this way, the total beam deflection is composed by bending deflection and by shear deflection, while the cross-section forces that are considered for displacements equation include the bending moment M, the shear force Q and the inertia load due to bending q_i. Instead, for torsional case, the considered loads are the pure torsional torque T_t, the warping contribution T_w, the warping bi-moment B_w and the inertia load due to torsion μ_i. By defining a Cartesian reference frame (x, y, z), with the origin at the centre of gravity of a generic end section of the beam, where x is the longitudinal axis, y and z are the principal and the secondary bending directions respectively, the equilibrium of bending moments, transverse forces and torques acting on beam differential element yields:

$$\frac{\partial M}{\partial x} = Q \;\; ; \;\; \frac{\partial Q}{\partial x} = -q_i - q \;\; ; \;\; \frac{\partial T}{\partial x} = -\mu_i - \mu \tag{2.1}$$

where q and μ are external lateral and torsional excitation, respectively.

Substituting in this last equation the corresponding cross-section forces and loads expressions and condensing the first two equations, a system of partial differential equations for a generic beam is derived, which governs the dynamic behaviour of the structure. For beams with double-symmetric cross-sections, the centroid is coincident with the shear centre. By setting the external excitations to zero in the flexural and torsional equations of motion, the uncoupled ordinary differential equations governing the modal behaviour of a beam are the following [2]:

$$EI_b \frac{d^4 w_b}{dx^4} + \omega_f^2 m \frac{EI_b}{GA_s} \frac{d^2 w_b}{dx^2} - \omega_f^2 m w_b = 0 \tag{2.2}$$

$$EI_w \frac{d^4\psi}{dx^4} - GI_t \frac{d^2\psi}{dx^2} - \omega_t^2 J_t^o \psi = 0 \tag{2.3}$$

where equations (2.2) and (2.3) refer to the flexural and the torsional vibrations, respectively. The physical meaning of each parameter is given in table 2.1.

For flexural vibrations, by solving the characteristic equation and imposing free-free boundary conditions, the following non-linear frequency equations are obtained [54]:

$$\alpha\,tanh(\alpha \cdot l) + \beta tan(\beta \cdot l) = 0 \tag{2.4}$$

$$\alpha\,tan(\beta \cdot l) - \beta tanh(\alpha \cdot l) = 0 \tag{2.5}$$

where the equation (2.4) refers to symmetric modes and the (2.5) to the anti-symmetric modes. In both equations, the functions α and β are defined as follows:

$$\alpha = \sqrt[4]{p} \cdot \sqrt{\sqrt{1 + q^2} - q} \tag{2.6}$$

$$\beta = \sqrt[4]{p} \cdot \sqrt{\sqrt{1 + q^2} + q} \tag{2.7}$$

Here, the coefficients p and q are defined as:

$$p = \frac{\omega_f^2 m}{EI_b} \tag{2.8}$$

$$q = \frac{\omega_f \sqrt{EI_b m}}{2GA_s} \tag{2.9}$$

Instead, for the torsional vibrations, the characteristic equation leads to the following frequencies:

$$\omega_{t,n} = \frac{n\pi}{L} \sqrt{\frac{GI_t}{J_t^o}} \sqrt{1 + \left(\frac{n\pi}{L}\right)^2 \frac{EI_w}{GI_t}} \qquad n = 0,1,2,\dots \tag{2.10}$$

A_s	Shear area	J_t^o	Polar moment of inertia about gravity centre
l	Half length of the beam	I_t	Torsional modulus
L	Full length of the beam	I_w	Warping modulus
m	Distributed mass	E	Young's modulus
w	Beam deflection	G	Shear modulus
ψ	Twist angle of cross-section	ω_f	Generic flexural natural frequency
I_b	Cross-section moment of inertia	ω_t	Generic torsional natural frequency

Table 2.1: Nomenclature for a generic beam structure.

In the last equation, frequencies for both symmetric and anti-symmetric modes are considered, depending on whether the value of *n* is even or odd, respectively.

The last three equations show the analytical relations between flexural/torsional natural frequencies and bending/torsional stiffness parameters of the beam for symmetric and anti-symmetric modes. Therefore, by using these relations, it is possible to correlate the flexural and torsional natural frequencies of the detailed beam with its stiffness parameters.

2.2.2. The numerical model

Equations (2.4), (2.5) and (2.10) are used as a basis to develop two different numerical methods for the flexural and torsional modes, respectively. In both methods, an unconstrained nonlinear minimization algorithm is used and the first three flexural or first two torsional natural frequencies are used, in order to estimate the beam cross-section properties. For flexural vibrations, I_b and A_s are the design parameters that must be estimated; instead, for torsional vibration, such parameters are I_t and I_w. The optimal values are computed after setting initial guess values and adopting the Nelder-Mead simplex algorithm [55].

The goal is to minimize the squared sum of the differences between the reference frequencies vector, obtained from the initial dynamic simulation on the detailed 3D FE model, and the frequencies vector, iteratively computed by applying equations (2.4) and (2.5) for flexural or (2.10) for torsional modes.

The material properties of the beam are assumed to be known, while the value of the polar moment of inertia is assumed to be given by the sum of the two moments of inertia, estimated in the flexural analysis case, multiplied by the density of the material. Once the optimal values of the shear areas A_{sy} and A_{sz} are computed, the shear factors of the conceptual model in the two bending directions are calculated as:

$$K_y = \frac{A_{sy}}{A_t} \qquad (2.11)$$

$$K_z = \frac{A_{sz}}{A_t} \qquad (2.12)$$

where A_t is the total cross-section area.

By using the same approach, also the problem of coupled torsional/flexural vibrations, occurring in general application cases, can be addressed as shown in [54].

2.3. Dynamic sensitivity analysis with respect to the welding layout

The proposed new dynamic methodology allows defining concept 1D beam models that can reproduce the static and the dynamic behaviour of detailed automotive beam models, usually constituted by spot-welded thin-walled structures. Indeed, the distribution of spot-welds can strongly influence the dynamic behaviour of a beam.

In order to quantify these differences, a sensitivity analysis is carried out, by investigating the dynamic behaviour of four spot-welded beam models, with an increasing distance between two consecutive spot welds of 10, 50, 100 and 200 mm.

Then, simulation results are compared with those relating to a closed box beam, which is considered as the reference case.

The considered model consists of a two meter long beam, defined by two thin-walled panels with C-shaped cross-section, whose geometry and dimensions are shown in figure 2.1-a.

The centre of gravity can be considered coincident with the shear centre; then, the double-symmetry assumption is respected. Since the sheet thickness is much smaller than the two transversal dimensions, the parts are meshed by 4-node shell elements, resulting in a model with 48000 degrees of freedom (DOFs). Subsequently, the two panels are connected by a set of equally spaced spot-welds, along the two open longitudinal walls.

Each of these welding point is created as a small *hexa* solid element, connected to corner nodes of flanges by generic interpolation elements (figure 2.1-c). The Structures environment of LMS Virtual.Lab software [56] is used to create the whole FE model, a part of which is showed in figure 2.1-b.
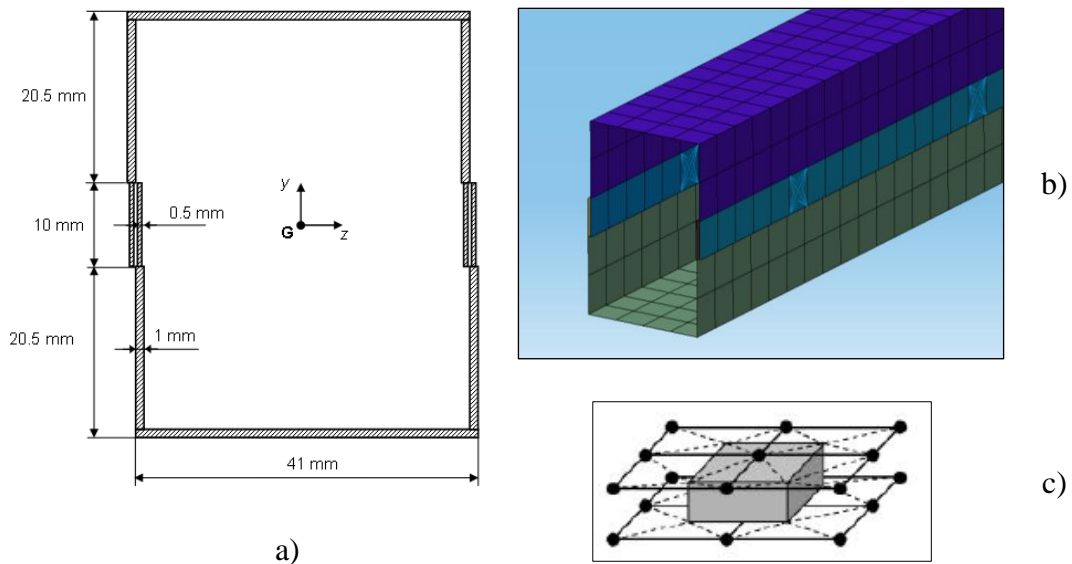
Figure 2.1: Application model: cross-section geometry of beam (a), mesh of detailed 3D beam model with welding zones (b) and a spot weld model, with a central hexa solid element connected to nodes of flanges by interpolation elements (c) [57].

Simulations are carried out under the assumption of homogeneous and isotropic material by using general material properties of steel:

- Young modulus: $E = 210000$ MPa ;
- Poisson ratio: $v = 0.3$;
- Mass density: $\rho = 7.9 \cdot 10^{-9}$ ton/mm^3

The computed natural frequencies are given in table 2.2, whereas figure 2.2 shows the relative variation of each natural frequency of the four models, with respect to the values of the reference case. These results show that, by varying spot-weld distribution, the dynamic behaviour of the beam changes significantly, since natural frequencies increase with the increasing spot weld density. Indeed, for both flexural and torsional modes, the variation of frequencies values increases moving towards higher order modes. In particular, for the bending case, this variation is larger on the vertical (x-y) plane than on the lateral (x-z) plane, because the spot welds have a larger stiffness in their axial direction than in their tangential one.

Mode		Natural freq. of model with closed cross-section (Hz)	Natural freq. of models with different spot-welds distances (Hz)			
			10 mm	*50 mm*	*100 mm*	*200 mm*
Lateral	1st	76.63	76.63	76.54	76.51	76.47
Bending	2nd	208.60	208.17	207.65	207.23	206.38
(x-z plane)	3rd	399.49	396.04	393.24	390.18	383.16
Vertical	1st	90.54	90.37	90.29	89.69	87.99
Bending	2nd	246.54	246.06	243.80	238.01	223.77
(x-y plane)	3rd	473.55	472.54	462.58	440.81	396.51
Torsion	1st	637.34	621.41	530.07	388.00	251.64
	2nd	1392.10	1388.60	1139.30	848.46	575.81

Table 2.2: Natural frequencies estimated for the reference model (beam with closed rectangular cross-section) and for different spot welded beam models [57].
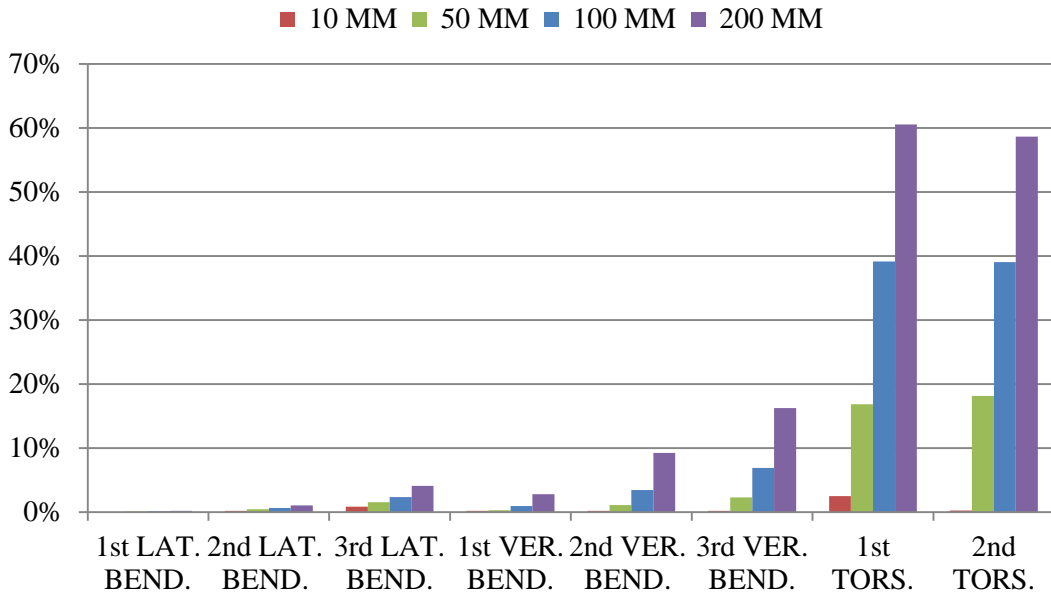
Figure 2.2: Frequency variations between each spot-welded model and the reference model [57].

On the other side, torsion modes show a very high sensitivity, with the frequency variations for the first torsion mode ranging from 2% for the model with higher density of spot-welds, to more than 60% for the model with 200 mm distance between two of these. This is due to the strong decrease of the torsion stiffness, caused by the transition from a closed to a partially open cross-section.

The overall results of this sensitivity analysis suggest that natural frequencies of spot-welded beam-like structures may differ significantly from those of thin-walled beams with closed cross-sections, especially at mid and high frequencies and for torsional modes.

2.4. Method validation

The results, obtained in the previous section, suggest that geometrical methods could be inaccurate for automotive structures. Indeed, for these methods, it is assumed that

the beam has a closed cross-section, such that the spot-weld layout is not taken into account. On the contrary, both the static and the dynamic FE-based approaches take into account the spot-welds influence, by including their impact on the stiffness estimation.

In order to assess the accuracy of the proposed FE-dynamic method, as compared to both the geometrical and the FE-static methods, a comparative analysis is performed. For this purpose, the reference spot-welded model is the third presented in the previous section, i.e. the beam with spot-weld equally spaced by 100 mm. This is a typical layout in automotive beams.

The number of natural frequencies values, used to estimate all the stiffness properties of the equivalent concept model trough the dynamic FE-based method, is chosen equal to eight. In particular, these are the first three in each flexural plane and the first two for torsional vibrations.

Figures 2.3, 2.4 and 2.5 show the corresponding modal shapes. As it can be seen, both torsion modes show significant local deformations in regions of the model around the spot-welds, in opposite to the more regular shape of the flexural modes. This increment of the local flexibility is expected to be responsible for the high differences in torsional performances between the spot-welded and the closed-section beam model.

a)   b)   c)
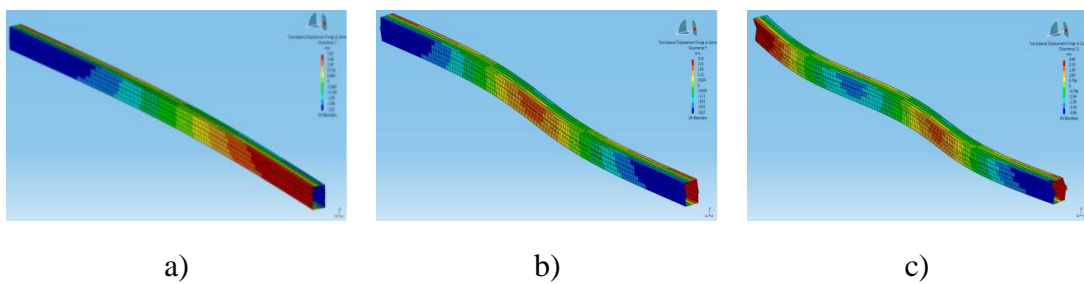
Figure 2.3: First (a), second (b) and third (c) vibration modes in the lateral (x-z) flexural plane [57].
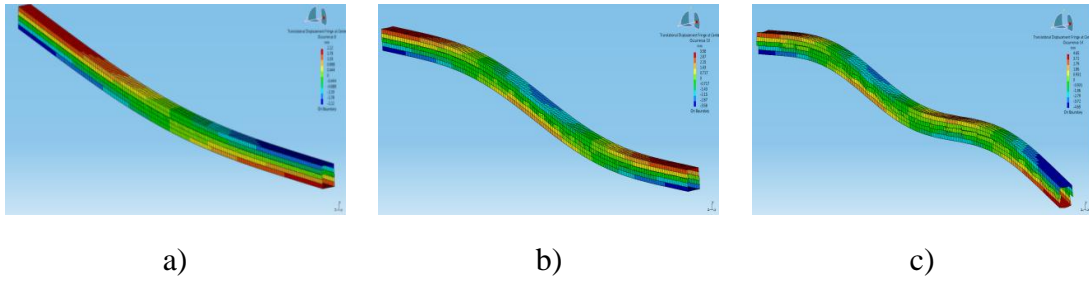
Figure 2.4: First (a), second (b) and third (c) vibration modes in the vertical (x-y) flexural plane [57].
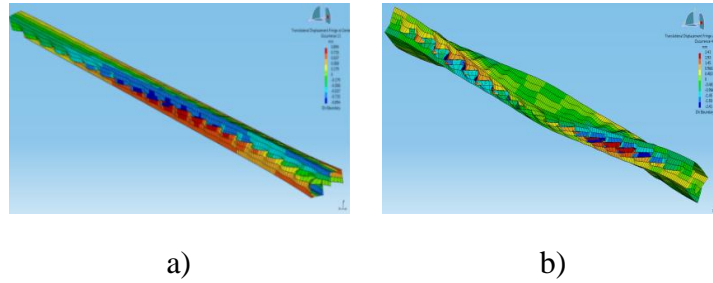
Figure 2.5: First (a) and second (b) torsion modes [57].

Once natural frequencies of the detailed 3D FE model are determined by modal analysis, stiffness properties of the equivalent concept model can be computed, with the numerical procedure described above.

The values estimated for each parameter are listed in table 2.3. For comparison, results obtained with the geometric and static FE-based methods are shown as well.

Regarding the first method, equivalent values are estimated by considering a thin-walled beam with a closed rectangular cross-section. Instead, for the static FE-based method implementation, a proper set of static load cases for the 3D beam model must be previously defined. While one end section is fixed, the other is loaded by applying separately bending, torsion and axial loads. For such purpose, a central node is created and connected to the other nodes of the same cross-section by means a rigid connection element. In this way, external loads are applied directly to the central node of the end cross-section, and the rigid element transfers them to the rest of the

structure. Finally, stiffness properties of the equivalent 1D beam are estimated by applying inverse linear elastic load-deformation relationships of the beam structure, starting from the static deformations predicted by analysing the detailed 3D model [33]. Also in this case, the linear static relations are based on the Timoshenko model [58].

Parameters	Concept modelling methods		
	Geometric	*FE-based static*	*FE-based dynamic*
I_y *(mm^4)*	50695	50746	51177
I_z *(mm^4)*	70865	70828	70920
K_y	0.544	0.126	0.126
K_z	0.433	0.423	0.103
I_t *(mm^4)*	88888	35115	26891
I_w *(mm^6)*	0.00	0.00	2.92e+08

Table 2.3: Equivalent beam properties estimated by different methods.

Note that the larger differences among both static and dynamic FE-based methods and the geometric method regard the shear factors and the torsional parameters.

In particular, the dynamic FE-based method provides an estimate of both the shear factors that is about four times lower than that provided by the geometric method, while the torsional modulus value is more than 3 times lower.

Furthermore, the dynamic method estimates a value for the warping modulus different from zero, as assumed by the other two methods. This proves that the dynamic method estimates the equivalent torsional properties without assuming a constant closed cross-section along the entire beam [59].

All the parameter values listed in table 2.2 can be used to define three different 1D concept beam models, formed by 20 mono-dimensional elements. Each of these elements is 100 mm long, for a total length equal to two meters.

These 1D beam elements have 2 nodes, for a total of 126 DOFs for each concept beam model. This number is almost three orders of magnitude lower than in the

original 3D beam model, which results in a significant reduction of the computational time needed for static or dynamic FE simulations.

2.4.1. Dynamic validation

The dynamic validation involves a modal analysis in free-free conditions, for each of the three different concept 1D beam models. The obtained results are used to assess accuracies of concept 1D beam models for predicting the modal behaviour of the detailed 3D beam structure. The estimated flexural and torsional natural frequencies are listed in table 2.4, together with the relative percentage error, calculated as the percentage difference between the frequencies of each reduced 1D beam model and the values predicted by the detailed 3D beam model.

Modes		Detailed 3D Model	Geometric 1D Beam Model		Static 1D Beam Model		Dynamic 1D Beam Model	
		Natural Freq. (Hz)	*Natural Freq. (Hz)*	*Freq. Diff. (%)*	*Natural Freq. (Hz)*	*Freq. Diff. (%)*	*Natural Freq. (Hz)*	*Freq. Diff. (%)*
Lat. Bend.	1st	76.51	76.83	0.42	76.86	0.46	76.70	0.25
	2nd	207.23	210.31	1.49	210.37	1.52	206.53	-0.34
	3rd	390.18	407.97	4.56	407.98	4.56	391.26	0.28
Vert. Bend.	1st	89.69	90.81	1.25	89.93	0.27	89.74	0.06
	2nd	238.01	248.39	4.36	240.07	0.87	237.96	-0.02
	3rd	440.81	481.29	9.18	449.57	1.99	441.74	0.21
Tors.	1st	388.00	684.26	76.36	430.05	10.84	384.08	-1.01
	2nd	848.46	1372.80	61.80	862.76	1.69	820.53	-3.29

Table 2.4: Natural frequencies of the 3D detailed and three 1D concept beam FE models [57].

As it can be seen, the first bending mode in each flexural direction is accurately predicted by all concept 1D models. On the contrary, the geometric and the static method yield an increasing prediction error for the higher order frequencies, whereas the dynamic model maintains accurate predictions for all of the flexural modes in the evaluated range.

Moreover, the dynamic method returns the most significant improvements with respect to the prediction of torsional frequencies, for which a maximum difference of 3.2% in absolute value is noticed. This result is 3 times and 25 times more accurate than the static and the geometric method, respectively.

2.4.2. Static validation

The second model validation is based on static analyses, in which both the detailed 3D and the dynamic 1D beam model are subjected to a static bending load condition. Every model is clamped at one end section and loaded by a vertical force at the other end section. The concept case is shown in figure 2.6.

Vertical displacements of centre nodes in the two models are estimated and compared. In order to estimate the deformation of the beam centre line for the detailed 3D model, 10 equally-spaced central nodes are created along the beam longitudinal direction and connected to the nodes of each corresponding cross-section by using interpolation spiders [60].

Results show that the concept model provides an excellent estimation of the structure deformation, resulting in an average error on predicted displacements of about 0.44%.
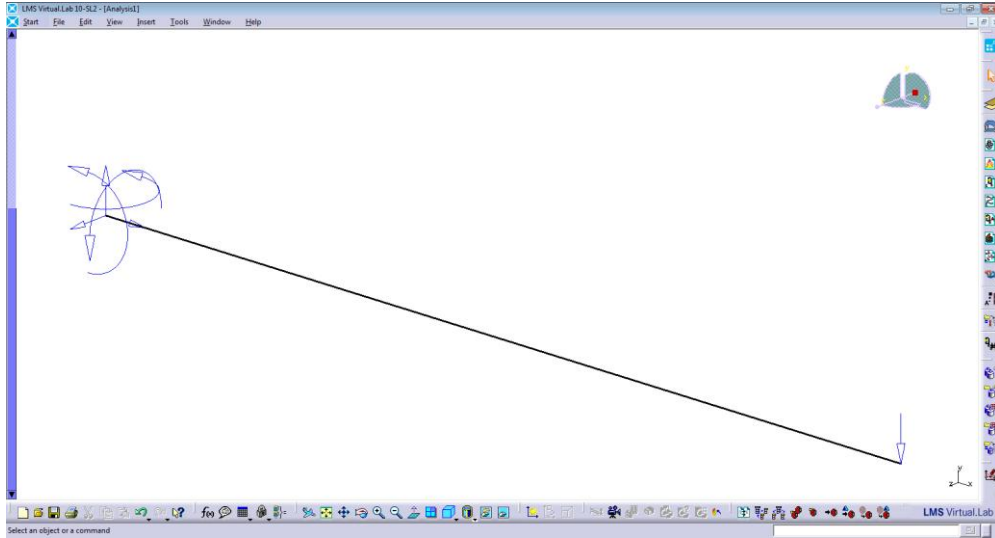
Figure 2.6: Bending load case used for the static validation of the dynamic 1D beam model [57].

2.5. Numerical Modelling of Beams Incorporating Innovative Materials

In the last years, the industrial use of structures incorporating innovative materials, like metal foams or honeycomb sandwich structures, appeared as a promising technology, able to increase the structural lightness, maintaining or often improving static and dynamic performances.

The use of metal foams as fillers of structures is becoming a common practice, in order to obtain a higher energy absorption and a better vibration damping, crucial features for vehicle safety and comfort respectively.

On the other hand, honeycomb structures are being recognized more and more as very important components for applications regarding weight sensitive structures, where good stiffness-weight and strength-weight ratios are required. Their layout consists of two high-rigidity thin-face armours, with inside a low-density honeycomb core.

Many efforts have been carried out to identify the constitutive laws able to characterize the complex behaviour of such materials. As a result, several accurate empirical models have been proposed and validated. Different FE approaches were also used, in order to accurately reproduce in numerical way the experimental behaviours, taking into account the main parameters that affect static and dynamic responses.

2.5.1. Honeycomb sandwich structures

Honeycomb sandwich structures are widely used in many technical applications, due to their lightweight nature, high specific bending stiffness and strength and good energy-absorbing capacity [3, 63-65]. Therefore, these ensure a good compromise between strength and stiffness of the structure, without increasing its weight considerably. The components of honeycomb structures are mainly three: two faces (or skins), a lightweight core and two adhesive layers that are necessary to join the faces to the core (figure 2.7).

By choosing different materials and geometric configurations for face sheets and cores, it is possible to obtain various properties and desired performances; so, optimal designs can be achieved for several applications [66].
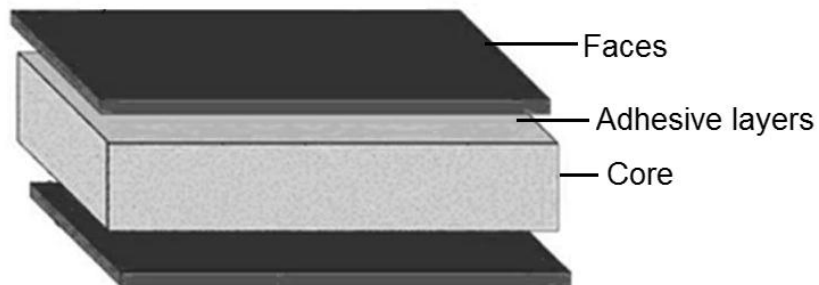
Figure 2.7: Components of a typical honeycomb sandwich structure.

The external faces are expected to react the axial loads and bending moments, while the core mainly contributes to react shear forces.

In case of complex geometrical characteristics and boundary conditions, the analytical methods used to resolve these structures are replaced by numerical methods, based, typically, on the FE approach.

Two main modelling options exist:

- a complex but detailed 3D modelling, accurate in results but quite difficult to define and modify for optimization purposes;

- a simplified modelling approach, based on equivalent methods, which is simpler but less accurate than the first method.

2.5.2. The detailed FE model

A detailed 3D FE model of a generic honeycomb beam-like structure is implemented by considering separately the mesh of the skins and the core; then, the two parts are assembled to create the whole model. Since the components are usually quite thin, it is possible to mesh both the skins and the core by using 2D shell elements, each of them having four corner nodes.

Usually, the two adhesive layers that join the face sheets of skins with the core are not taken into account, because their effect on the structural behaviour can be considered negligible under regular and healthy conditions. Therefore, an ideal contact between the parts is assumed, without the presence of any delamination.

This condition is achieved by placing in the same position the nodes of skins parts and the extreme nodes of the core part. For this purpose, the modelling process starts with the implementation and meshing of a single core cell, as shown in figure 2.8-a. Subsequently, this is replicated along two directions, in order to obtain the final beam (figure 2.8-b). The thickness properties are doubled for each wall in common with two adjacent cells.

a)   b)
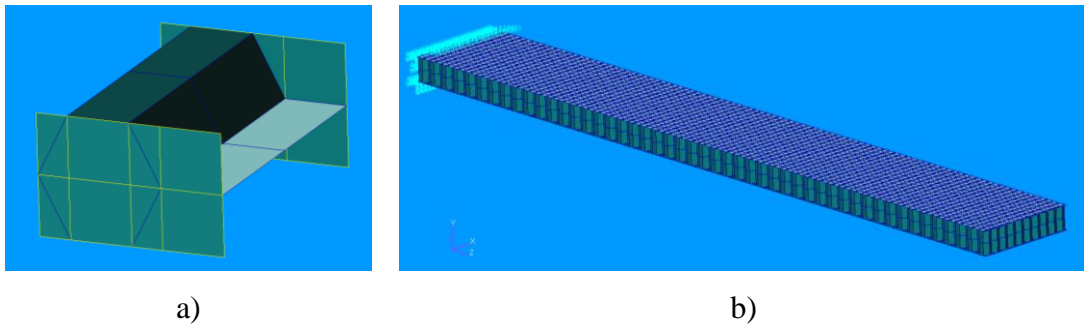
Figure 2.8: Mesh of a single cell (a) and detailed 3D FE model of a clamped honeycomb sandwich beam (b) [67].

Boudjemai et al. [68-69] implemented this 3D detailed FE model, obtaining very accurate dynamic results, related to the estimation of the first three natural frequencies. Indeed, comparing these values with experimental data, the maximum error turned out to be less than 12%.

2.5.3. Equivalent models

Many equivalent methods of honeycomb sandwich structures had been studied and implemented [70-76]. Each of these is based on a particular homogenization approach.

Under this assumption, the complex component is considered as a continuous model with equivalent characteristics to those of the complex model, thus avoiding all the problems caused by the structure's heterogeneity. Figure 2.9 shows a schematic of the equivalent approach. Here, h_c indicates the height of honeycomb core, t_f the face skins thickness, t_{eq} is the thickness of the equivalent skin, a and b parameters are, respectively, the length and the width of both the models; then, it is assumed that these remain unchanged.
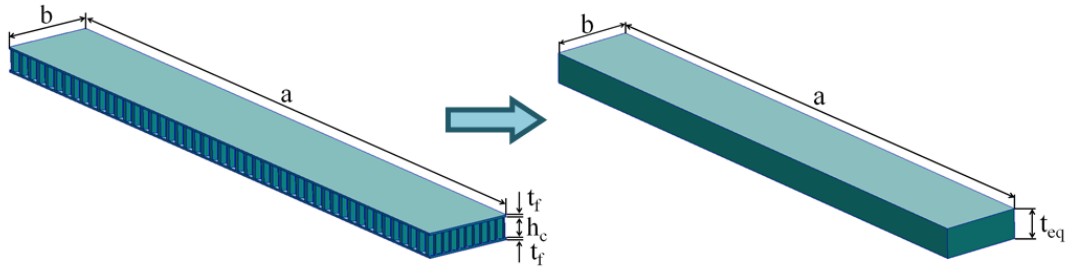
Figure 2.9: Representation of the equivalent approach [67].

Two main equivalent methods have been defined [70], namely the *sandwich theory* and the *equivalent-plate theory*.

By using the first method, only the honeycomb core is homogenized, i.e. replaced by an equivalent homogeneous material. The assumptions consider that only the core can resist to transverse shearing deformations and has a quite considerable axial stiffness, while the top and bottom skins only satisfy the Kirchhoff hypothesis. Then, the honeycomb core is regarded as an orthotropic layer. For an hexagonal honeycomb core, the equivalent elastic parameters are calculated as follows:

$$E_x = E_y = \frac{4}{\sqrt{3}} \left(\frac{t_c}{l}\right)^3 E \tag{2.13}$$

$$G_{xy} = \frac{\sqrt{3}\gamma}{2} \left(\frac{t_c}{l}\right)^3 E \qquad G_{xz} = \frac{\gamma}{\sqrt{3}} \frac{t_c}{l} G \qquad G_{yz} = \frac{\sqrt{3}\gamma}{2} \frac{t_c}{l} G \tag{2.14}$$

$$\nu_{xy} = \frac{1}{3} \tag{2.15}$$

where l and t_c are the length and thickness of the honeycomb cell, while γ is a technology corrected coefficient, with a value included in a range between 0.4 and 0.6.

Instead, in the equivalent-plate theory, the entire honeycomb sandwich structure is converted in an homogenized structure. Equivalent characteristics are determined by equalizing membrane and bending stiffness between complex and equivalent isotropic plates, as shown in the table 2.5 [69].
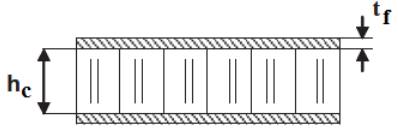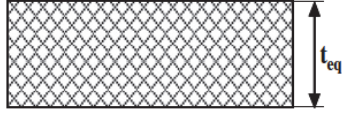
	Honeycomb sandwich plate	**Equivalent isotropic plate**
Membrane stiffness	$\dfrac{2Et_f}{1-\nu^2}$	$\dfrac{E_{eq}t_{eq}}{1-\nu^2}$
Bending stiffness	$\dfrac{Et_f h_c^2}{2(1-\nu^2)}$	$\dfrac{E_{eq}t_{eq}^3}{12(1-\nu^2)}$

Table 2.5: Equivalent parameters of sandwich structure [69].

The t_{eq} and E_{eq} parameters are the equivalent thickness and the equivalent Young modulus of the continuous model, that are obtained from the following equations:

$$t_{eq} = h_c\sqrt{3} \tag{2.16}$$

$$E_{eq} = \frac{2}{\sqrt{3}}\frac{t_f}{h_c}E \tag{2.17}$$

According to the mass equivalence, the equivalent mass density ρ_{eq} can be achieved as:

$$\rho_{eq} = \frac{2\rho_f t_f + 2\rho_c(H-t)}{t_{eq}} \tag{2.18}$$

where ρ_c and ρ_f are the densities of core and face skins materials, while H is the height of sandwich panel, facing skins included.

Two approaches are proposed by Paik et al. [71]: the *equivalent rigidity* method and the *equivalent weight* method.

In the first, plates thickness and elastic moduli are defined such that the rigidity of sandwich panel is equivalent to that of the single skin panel [77]. The rigidity of the panel is considered separately for axial and bending load cases:

$$t_{eq}E_{eq} = 2t_f E_f \tag{2.19}$$

$$\frac{1}{12}t_{eq}^3 E_{eq} = \frac{1}{12}\left[\left(h_c + 2t_f\right)^3 - h_c^3\right]E_f \tag{2.20}$$

Then, equivalent values are obtained by solving the following equations:

$$E_{eq} = \frac{2t_f}{t_{eq}}E_f \tag{2.21}$$

$$t_{eq} = \sqrt{3h_c^2 + 6h_c t_f + 4t_f^2} \tag{2.22}$$

Regarding the material characteristics, the equivalent mass density (ρ_{eq}) is obtained by identifying a unit cell and deriving the volume fraction occupied by the metal:

$$\rho_{eq} = \frac{2t_f\rho_f + h_c\rho_{ca}}{t_{eq}} \tag{2.23}$$

It can be noted that, in this case, ρ_{ca} is not the density of honeycomb core material, but rather its average density, given by:

$$\rho_{ca} \cong \frac{8}{3\sqrt{3}}\frac{t_c}{d}\rho_c \tag{2.24}$$

where d is the standard length of every cell wall.

Instead, for the equivalent weight method, dimensions of the equivalent skin panel are defined so that the weight must be equal to that of the complex structure.

Then, the equivalent plate thickness may be calculated from the following mass equivalence:

$$LWt_{eq}\rho_f = 2LWt_f\rho_f + LWh_c\rho_{ca} \tag{2.25}$$

resulting in:

$$t_{eq} = \frac{2t_f\rho_f + h_c\rho_{ca}}{\rho_f} \tag{2.26}$$

Instead, equivalent elastic moduli are assumed to be equal to those of skin material.

2.6. Concept modelling of innovative beam-like structures

In order to assess the predictive capabilities of the dynamic FE-based method also in case of complex beam-like structures, the concept modelling of an honeycomb sandwich beam is proposed in this section.

2.6.1. The reference FE beam model

Firstly, the detailed 3D FE model of an hexagonal honeycomb sandwich is defined, with the same geometric characteristics of an experimental specimen present in the literature [69], in order to get a reference model useful for comparisons.

Geometric characteristics are indicated in table 2.6, while the three-dimensional geometrical model of the unit honeycomb cell is shown in figure 2.10. The same material is used for both the core and face skins, i.e. a generic aluminium having the following properties:

- Young modulus: $E = 72000$ MPa;
- Poisson ratio: $v = 0.33$;
- Mass density: $\rho = 2.8 \cdot 10^{-9}$ ton/mm^3.

beam length (a)	beam width (b)	thickness of cell (t_c)	cell size (d)	core height (h_c)	thickness of face skins (t_f)	angle of cell (ϑ)
270 mm	40 mm	0.2 mm	2 mm	9 mm	1 mm	60°

Table 2.6: Geometric characteristics of the reference honeycomb sandwich beam.
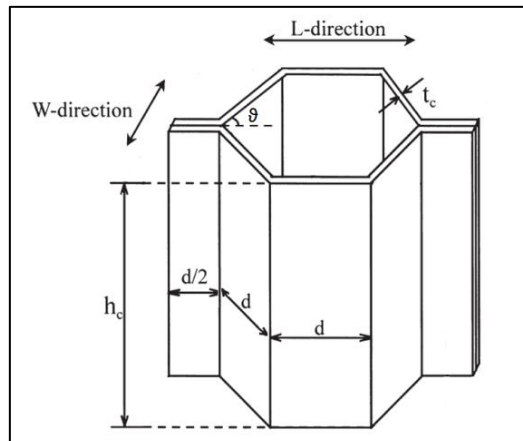
Figure 2.10: Unit cell geometry of honeycomb core [67].

Following the procedure mentioned above, each part is meshed by using 2D shell elements. The mesh of core consists of two elements along the height of each cell unit. The assumption of ideal contact between core and skins is also considered; in this way, the effect of two adhesive layers is assumed negligible. The final model, cantilevered at one extreme end-section, results in approximately 110000 DoFs.

This detailed model is validated by executing a numerical modal analysis and comparing the first three estimated natural frequency values with the experimental data reported in [69]. Table 2.7 shows this comparison between experimental and simulation dynamic results.

A good agreement can be noted, with a relative error of predicted frequencies that remains below the value of 6%. In particular, the third frequency is very accurate, whit a difference less than 0.5%. Higher errors in the first two natural frequencies are

probably due to the different boundary conditions between the modelled and the experimental case, determined by a clamping system.

However, the model with this mesh morphology can be considered reliable and can be used as a reference model for the comparison with the dynamic 1D beam model.

Bending Modes	Natural Freq. of Experimental Model (Hz)	Natural Freq. of Detailed 3D FE Model (Hz)	Frequency Difference (%)
1st vertical	134.50	126.88	-5.67
1st lateral	311.00	323.62	4.06
2nd vertical	711.00	713.02	0.28

Table 2.7: Comparison of dynamic results between experimental data and detailed FE model.

2.6.2. The application case

In the application case, the FE model of an honeycomb sandwich beam is analysed, with the same characteristics of the reference beam model, but with a length equal to one meter, in order to provide the structure with a beam-like behaviour. The detailed 3D model has about 3300 honeycomb cells and over 370000 DoFs. The same aluminium material described above is used for both the skins and the core parts.

In order to get a more detailed comparison, also an equivalent FE model is defined. The considered approach is the equivalent rigidity method, which assumes the top and bottom surface layers resistant to axial and bending deformations, while the core resistant only to shear deformation and satisfying the Bernoulli hypotheses.

Then, equivalent beam thickness (t_{eq}), Young's modulus (E_{eq}) and mass density (ρ_{eq}) are determined by imposing static equalities; only these parameters characterize the skin model of the equivalent honeycomb beam.

The following values are calculated:

- equivalent Young modulus: E_{eq}= 8300 MPa;
- equivalent thickness: t_{eq}= 17.35 mm;
- equivalent mass density: ρ_{eq}= 5.46·10^{-10} ton/mm^3.

The 3D solid elements that are used have a size of 5 x 5 x 4.34 mm, for a total number of DoFs approximately equal to 54000. This mesh size is a compromise between predictive capability and model dimension, chosen after running a convergence test.

Finally, the dynamic 1D beam model is also defined, with geometric and stiffness properties estimated by using the natural frequencies computed by a modal analysis of the detailed FE model and the numerical procedures described in section 2.2.

Note that, in this particular case, the two shear factors are estimated in reference to an equivalent cross-section area, calculated with the following analytical formula:

$$A_{eq} = \frac{V_{real}}{L} \tag{2.27}$$

In this formula, the real volume (V_{real}) is the volume fraction concerning the walls of the core and the skins. It can be calculated as:

$$V_{real} = \frac{M_c}{\rho_c} + \frac{M_f}{\rho_f} \tag{2.28}$$

where M_c and M_f represent respectively the total mass of core and skins parts. Table 2.8 shows the values estimated for each relevant stiffness parameter. It can be noted that, in this case, the warping modulus (I_w) converges to zero, which is consistent with the closed-section nature of the structure under study.

All the parameter values listed in the last table are used to define a concept 1D beam model, constituted by 10 beam elements, each of these having 2 nodes (for a total of only 66 DoFs for the entire concept beam) and a length equal to 100 mm. It is clear that this number of DoFs is much lower than that of the detailed and equivalent 3D beam models.

Parameters	Values of dynamic 1D beam model
A_{eq} (mm^2)	122.05
K_y	0.19
K_z	0.33
I_y (mm^4)	9280.05
I_z (mm^4)	1527.09
I_t (mm^4)	2310.09
I_w (mm^6)	0.00

Table 2.8: Equivalent beam properties for dynamic 1D concept model.

After that the three FE models have been created, a modal analysis in free-free conditions is executed for each of them, in order to assess the accuracy of the two reduced models (equivalent 3D and concept 1D) in predicting the modal behaviour of the detailed 3D beam model.

Modes		Detailed 3D Model	Equivalent 3D Model	Freq. Diff. (%)	Dynamic 1D Model	Freq. Diff. (%)
Vertical Bending	1st	63.80	69.44	8.84	63.80	0.00
	2nd	175.37	191.08	8.96	175.43	0.03
	3rd	342.30	373.67	9.16	342.70	0.12
Lateral Bending	1st	156.88	159.34	1.57	156.88	0.00
	2nd	428.13	434.71	1.54	428.38	0.06
	3rd	827.37	839.78	1.50	828.57	0.15
Torsion	1st	719.01	819.82	14.02	721.71	0.38
	2nd	1437.80	1640.50	14.10	1461.20	1.63
	3rd	2156.00	2462.90	14.23	2236.70	3.74

Table 2.9: Dynamic comparison between the detailed, the 3D equivalent and the 1D concept model, in terms of natural frequencies and percentage differences.

The first flexural and torsional natural frequencies are listed in table 2.9, together with the relative percentage errors, calculated as percentage differences between frequencies of each reduced model and values predicted by the detailed model.

It can be observed that the 3D equivalent model approximates very precisely lateral bending modes, with all error values below 2%. However, differences for vertical bending and especially for torsional vibrations, with values close to 10% and 15% respectively, are not negligible.

Instead, the dynamic 1D model proves to be very accurate also with innovative structures; with all the frequency values very close to those of the reference detailed model. Indeed, the maximum differences are 0.15% and 3.74% for bending and torsional modes, respectively.

2.7. Conclusions

Such proposed method can also be applied for industrial cases, by following a simple procedure. Typically, by using a number of intersection planes, each detailed beam-like member is divided into a series of segments, having almost constant cross-sections. Subsequently, equivalent beam properties are computed and assigned for all of these segments. Finally, the entire beam member can be represented as a series of linear 1D beam elements, taken from a standard FE library.

Chapter 3: A Dedicated MPC Element for Beam-Joint Connection

3.1. Overview

Although the application and thus the positive impact of vehicle concept modelling techniques has increased significantly, some difficulties are still encountered. One of the main challenge lies on the connection between FE dissimilar elements, like detailed 3D shell structures and 1D beam models. Indeed, the detailed 3D FE model of a BIW is composed by 2D shell elements, due to the thin metal sheets realizing the structure. By replacing the 3D beam-like structures models with concept 1D beam elements, it is necessary to design a connection between these concept elements and the detailed 3D shell joints (figure 3.1).

At each beam/joint interface, this connection must ensure an accurate interpolation of motions of the extreme cross-section nodes, in order to obtain a consistent motion of the beam node. To achieve this objective, several connection elements already present in the libraries of the most common commercial FE solvers (such as Nastran, Abaqus, Ansys, etc.) are available, or different mathematical approaches reported in the literature can be used to create new ones.

As a rule, an accurate connection element must transfer the three displacements, the three rotations and the warping related function, from cross-section nodes to the

central node. Moreover, this element should also allow the shell-like cross-section to eventually deform in-plane (distortion). Therefore, the connection element has to be adapted to the various characteristics of cross-section types.

Each standard connection element tries to perform this coupling with a different approximate approach.
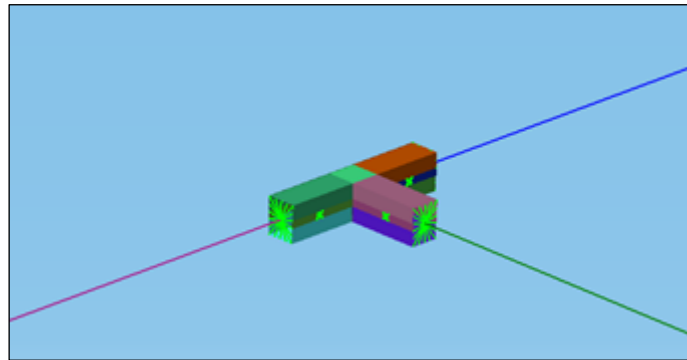
Figure 3.1: Illustration of connections between dissimilar FE models [78].

3.2. Standard connection elements

Connection elements like Nastran RBE2 [60] provide a rigid connection of the same DOFs between one independent node and a set of dependent nodes. In this case, the independent node is represented by the extreme node of the 1D beam element, while the peripheral nodes of the interfacing beam/joint cross-section are the dependent ones. Regarding joints with stiff closed cross-sections, this element gives quite accurate results; this is typically due to the lack of influence of tangential warping and distortion deformations on this type of cross-section.

However, this configuration returns an additional stiffness in the structure, causing significant errors on displacement estimation of nodes, in case of slender structures or with open or spot-welded cross-sections.

On the other hand, general purpose interpolation elements, such as Nastran RBE3 connection element [60], define constraint relations, in which the motion of a single

dependent node is the least square weighted average of the motions of other independent nodes. Therefore, this type of element is able to distribute the loads applied at dependent node to a set of independent DOFs, based on the connection geometry and the local weighting factors. Unlike the RBE2 element, the RBE3 does not increase the stiffness of the structure where it is applied.

Various tests showed that this element accurately describes displacements of the central dependent node in both closed and open cross-sections, but the same accuracy is not achieved on rotation performances, especially in torsional load-cases [79].

Finally, another common connection element is a general Multi-Point Constraint element (MPC) [60], based on linear polynomial constraint equations between DOFs of the dependent and independent nodes. Then, this element describes an imposed linear relationship, expressed in the form:

$$\sum_j R_j u_j = 0 \qquad (3.1)$$

In the equation 3.1, the parameters u_j represent the DOFs of dependent and independent nodes, while R_j are the user-defined scale factors. This means that, before the implementation of this element, it is necessary to set these weighting factors, by using appropriate kinematic or static approaches.

3.2.1. An alternative approach: the RBE2.5 connection element

In order to overcome the limitations described above, alternative approaches have been studied, based on the use of standard connection elements.

For example, Stigliano et al. [32] proposed a new element, called "RBE2.5", which keeps the accuracy of RBE2 on describing cross-section rotations, but avoiding the stiffness variation caused by this type of connection. The name refers to the particular type of configuration; indeed, this element consists of a RBE2 element, which connects the extreme beam node with nodes placed on geometric centres of

peripheral shell elements. In particular, these nodes are connected with the boundary nodes of each corresponding shell element, by means RBE3 connection elements (figure 3.2).

Static and dynamic simulations showed a better accuracy on displacement and rotation estimations at interface nodes, w.r.t. hybrid structures having exclusively RBE2 or RBE3 connection elements. However, this element presents still some limitations, like a high case-sensitiveness. Indeed, an excessive variability of accuracy is showed, in dependence from the type of case study, geometric characteristics and morphologies of cross-sections.
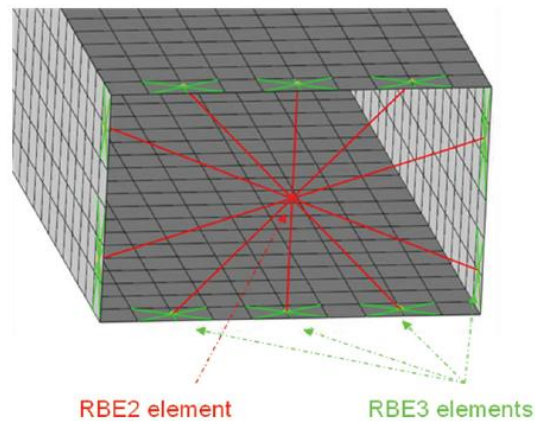
Figure 3.2: The RBE2.5 connection element: a RBE2 element (red element) is connected by spring elements to the central nodes of RBE3 elements (green elements) [32].

3.3. Analytical approaches

In this section, various analytical approaches are examined, implemented for bi- or tri-dimensional problems. Various mathematical formulations are analysed, highlighting positive aspects and limitations for each method.

3.3.1. Bi-dimensional approaches

➢ **The "load continuity" approach**

This approach is based on a 2D linear cross-section analysis, in order to obtain a transformation matrix [*S*], defining a static relationship between the 2D resulting loads, ideally applied to the centroid of the cross-section, and the force distribution generated on corresponding cross-section walls [5].

Theoretical stress fields resulting from the Saint-Venant assumptions for beam-like structures [6] are considered, together with the warping tangential stress for 2D thin-walled beams. Therefore, a fundamental condition for the correct application of the method concerns the location of the beam/joint interface cross-section, that must be placed at a sufficient distance from zones in which loads and boundary conditions are applied.

In the linear elastic field, these load correlations can be inverted, returning a second transformation matrix [*T*], which describes the searched kinematic relationships, between displacements and rotations of extreme node belonging to 1D beam and displacements of 2D shell elements at the interface. Stress distributions caused by the three considered loads (axial force, vertical shear and bending) are shown in figure 3.3.
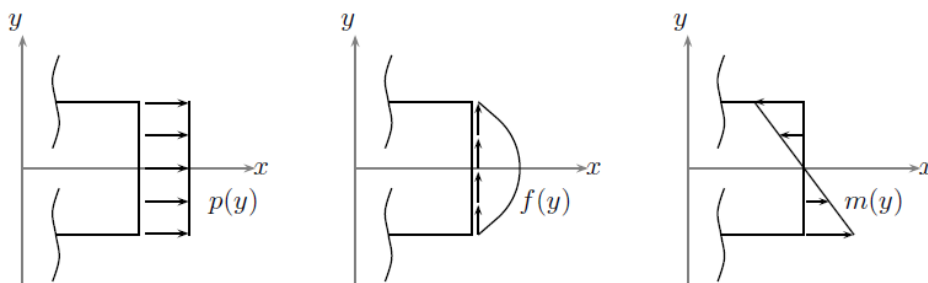
Figure 3.3: Stress distributions on a beam cross-section, due to 2D applied loads [5].

The transformation matrix [S] is composed by the product of three sub-matrices:

- The *Sectional Strain Matrix* [S_1], which correlates the beam deformations with the applied loads;

- The *Stress Recovery Matrix* [S_2], which links the cross-section stresses on 2D shell elements with beam deformations;

- The *Form Nodal Load Matrix* [S_3], which correlates the nodal forces with the nodal stresses of the cross-section.

The size of the first Sectional Strain matrix [S_1] is equal to 3x3. Taking into account the reference system shown in figure 3.3, this matrix can be written, for a generic shell-beam interface, as:

$$
\begin{Bmatrix} \varepsilon_x \\ \gamma_{xy} \\ \kappa_z \end{Bmatrix} = \begin{bmatrix} \dfrac{1}{EA} & 0 & 0 \\ 0 & \dfrac{1}{GK} & 0 \\ 0 & 0 & \dfrac{1}{EI} \end{bmatrix} \begin{Bmatrix} F_x \\ F_y \\ M_z \end{Bmatrix} = [S_1]\{F\} \tag{3.2}
$$

where k_z is the curvature of the middle line of the beam, while K is a factor that takes into account static moment, thickness and inertial moment of the cross-section.

By considering a thin-walled beam, the plane-stress conditions are assumed. Improved warping functions are obtained, by minimizing the second-order approximation of the energy w. r. t. the warping function perturbations.

Finally, through the application of linear constitutive laws, it is possible to get the bi-dimensional stress-deformation relationships at the beam interface:

$$
\sigma_x = E(\varepsilon_x - y\kappa_z) \tag{3.3}
$$

$$
\tau_{xy} = \frac{5E}{8(v+1)}\left[1 - \left(\frac{y}{t}\right)^2\right]\gamma \tag{3.4}
$$

where *t* represents the constant small width of the cross-section. The nodal stresses over the interface cross-section can be obtained by substituting the nodal position coordinates (*y*).

All these relations return the following Stress Recovery matrix $[S_2]$ matrix:

$$
\begin{Bmatrix} \sigma_x^{(1)} \\ \tau_{xy}^{(1)} \\ \sigma_x^{(2)} \\ \tau_{xy}^{(2)} \\ \vdots \\ \sigma_x^{(n)} \\ \tau_{xy}^{(n)} \end{Bmatrix} = E \begin{bmatrix} 1 & 0 & -y^{(1)} \\ 0 & \lambda\left[1-\left(\dfrac{y^{(1)}}{t}\right)^2\right] & 0 \\ 1 & 0 & -y^{(2)} \\ 0 & \lambda\left[1-\left(\dfrac{y^{(2)}}{t}\right)^2\right] & 0 \\ \vdots & \vdots & \vdots \\ 1 & 0 & -y^{(n)} \\ 0 & \lambda\left[1-\left(\dfrac{y^{(n)}}{t}\right)^2\right] & 0 \end{bmatrix} \begin{Bmatrix} \varepsilon_x \\ \gamma_{xy} \\ \kappa_z \end{Bmatrix} = [S_2] \begin{Bmatrix} \varepsilon_x \\ \gamma_{xy} \\ \kappa_z \end{Bmatrix} \qquad (3.5)
$$

where superscripts (*i*) are the global node number, *n* indicates the last node and $\lambda = 5/[8(v+1)]$. The right hand rule is used to define bending stress directions.

Finally, the Form Nodal Load matrix $[S_3]$ provides a relationship between nodal forces and nodal stresses of the 2D beam model. First of all, nodal loads on one generic shell element *k* at the interface are examined. This is a bi-linear 4-node shell element; then, only two nodes (*i* and *j*) are considered for the interface (figure 3.4).
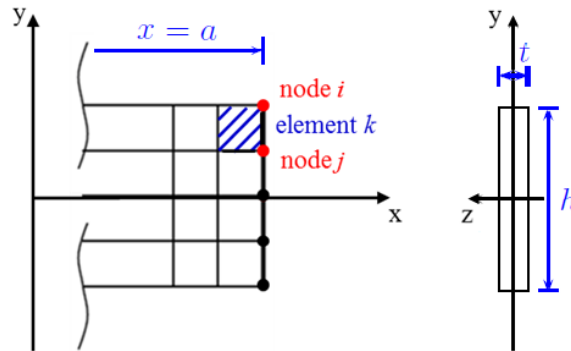
Figure 3.4: Profile of detailed 2D beam model: a generic shell element *k* and the two nodes at interface, *i* and *j*.

The stress distributions at the interface are found by averaging the nodal stresses of nodes i and j. Then, average stresses for k^{th} element in x and y directions can be written as:

$$\tilde{\sigma}_{x(k)} = \frac{\sigma_x^{(i)} + \sigma_x^{(j)}}{2} \tag{3.6}$$

$$\tilde{\tau}_{xy(k)} = \frac{\tau_{xz}^{(i)} + \tau_{xz}^{(j)}}{2} \tag{3.7}$$

Since the average stress at the interface is constant, the nodal loads for i and j nodes can be calculated by using linear shape functions N, yielding:

$$f_x^{(i,j)} = \int_{s_i}^{s_j} N^{(i,j)} \, \tilde{\sigma}_{x(k)} t_{(k)} ds = \frac{A_{(k)}}{4} \left(\sigma_x^{(i)} + \sigma_x^{(j)} \right) \tag{3.8}$$

$$f_y^{(i,j)} = \int_{s_i}^{s_j} N^{(i,j)} \, \tilde{\tau}_{xy(k)} t_{(k)} ds = \frac{A_{(k)}}{4} \left(\tau_{xy}^{(i)} + \tau_{xy}^{(j)} \right) \tag{3.9}$$

where $A_{(k)}$ is the area of kth element and s is a local coordinate, useful to measure the length of element. The same relations are valid for all the other elements along the interface and, then, an assembled matrix relationship can be obtained between nodal forces and nodal stresses:

$$\begin{Bmatrix} f_x^{(1)} \\ f_y^{(1)} \\ f_x^{(2)} \\ f_y^{(2)} \\ \vdots \end{Bmatrix} = \frac{1}{4} \begin{bmatrix} A_{(1)} & 0 & A_{(1)} & 0 & \cdots \\ 0 & A_{(1)} & 0 & A_{(1)} & \cdots \\ A_{(1)} & 0 & A_{(1)} + A_{(2)} & 0 & \cdots \\ 0 & A_{(1)} & 0 & A_{(1)} + A_{(2)} & \cdots \\ \vdots & \vdots & \vdots & \vdots & \vdots \end{bmatrix} \begin{Bmatrix} \sigma_x^{(1)} \\ \tau_{xy}^{(1)} \\ \sigma_x^{(2)} \\ \tau_{xy}^{(2)} \\ \vdots \end{Bmatrix} \tag{3.10}$$

$$= [S_3]\{\sigma^{(i)}\}$$

Note that forces applied to internal nodes (like j node) receive a stress contribution relating to both adjacent elements; instead, external nodes (like i node) receive only the contribution of the element to which they belong.

The relation between forces at the beam central node and nodal forces on the outer contour of the cross-section is obtained by combining equations (3.2), (3.5) and (3.10):

$$\{f\}_{2nx1} = [S_3]_{2nx2n}[S_2]_{2nx3}[S_1]_{3x3}\{F\}_{3x1} = [S]_{2nx3}\{F\}_{3x1} \qquad (3.11)$$

By assuming linear relationships between forces and displacements, it is sufficient to transpose the matrix [S] to obtain a matrix [T], which correlates displacements and rotation of the beam central node with displacements of interface cross-section nodes.

Then, the following kinematic relation is obtained:

$$[T]_{3x2n}\{q\}_{2nx1} = \{Q\}_{3x1} \qquad (3.12)$$

where $\{Q\}_{3x1}$ is the vector of displacements and rotation of the beam central node and $\{q\}_{2nx1}$ is the displacements vector of the cross-section peripheral nodes.

> ➢ **The "deflection continuity" approach**

This second approach is a kinematic method [5], which aims at calculating displacements and rotations of the beam node, through integration of various displacement components of cross-section nodes.

Indeed, the position vector of a generic cross-section point in a final deformed configuration can be expressed in terms of the vector displacement of the central point (that represents the only variable), the direction cosine matrix of the cross-section frame and the warping function with its partial derivatives [80].

Starting from this relation, it is sufficient to set up displacement and rotation continuities, to get correlations between the motion over the 2D interface and that of 1D beam interface.

3.3.2. Tri-dimensional approaches

➢ **The "stress recovery" approach**

In a similar manner to the 2D beam/joint connection, the authors [5] aimed at defining a transformation matrix [S], useful to correlate total loads applied on the beam central node and nodal forces at the interface of a solid beam (figure 3.5). Firstly, under the assumptions of the generalized Timoshenko beam model, the 3D stress components of each solid element are correlated with the resultant loads applied to the beam. To obtain this matrix relation, it is necessary to determine the 3D strain components on each "*Gauss point*" of the interface cross-section, together with derivatives of load resultants, by using the 1D non-linear equilibrium equations. Gauss points are particular mesh points where the solver applies numerical integrations. In this way, the following matrix relation can be written:

$$\{\sigma\} = [D][C_\Gamma]\{F\} \tag{3.13}$$

where $\{\sigma\}$ is the vector of 3D stress components applied on Gauss points, $[D]$ is a matrix defining material parameters, $[C_\Gamma]$ contains derivatives of 3D strains on Gauss points and $\{F\}$ is the vector of resultant forces on the beam interface. In a second step, nodal forces are obtained by means of force extrapolation at Gauss points, using the following second matrix relation:

$$\{\underline{F}\} = [P_A]\{\sigma\} \tag{3.14}$$

where $\{\underline{F}\}$ is the vector of nodal forces and $[P_A]$ is a matrix including the area information and shape function evaluated at the Gauss points.

By using the equation (3.13), the relationship between nodal forces and total loads is obtained, with the transformation matrix [S] defined as:

$$[S] = [P_A][D][C_\Gamma] \tag{3.15}$$
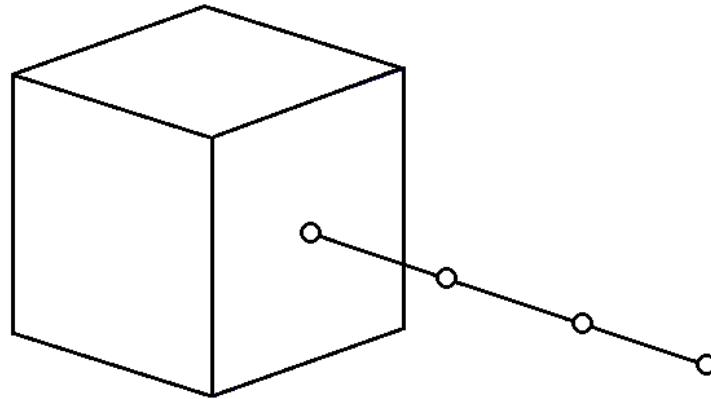
Figure 3.5: Connection between 1D beam element and 3D solid beam.

3.4. A dedicated MPC connection element

Particular structures like vehicle BIW are characterized by various thin-walled panels, connected to each other by means of spot-weld points. In this situation, connection between 3D shell-like joint models and concept 1D beams (substitutes for 3D detailed beam-like structures) is a very important modelling aspect, that requires particular attention in the design phase. Various simulation results showed that the elements used at the interface cross-sections to connect 1D and 3D parts have a significant influence on the static and dynamic accuracies of the full vehicle model.

In particular, it was demonstrated that the use of rigid connection elements can make the entire structure excessively stiff; on the other hand, general purpose interpolation elements can lead to coarse inaccuracies, especially with regard to torsional stiffness [79].

For such reason, a new dedicated MPC connection element is proposed here, in order to overcome limitations of these standard connection elements and achieve more accurate BIW concept models. This new MPC allows to correlate displacements and

rotations of the dependent node (i.e. the central node of the beam/joint interface) with the displacements of peripheral cross-section nodes (figure 3.6).

These kinematic relationships are based on static considerations, derived from the above mentioned "load continuity" approach.

The main characteristic, constituting a breakthrough for the research in this topic, is the extension of the method to the tri-dimensional case.

This fact involves that, for the estimation of displacements and rotations of the dependent central node, also the torsion load-case, together with the axial, bending and shear load-cases, has to be considered while assuming the theoretical stress distributions.
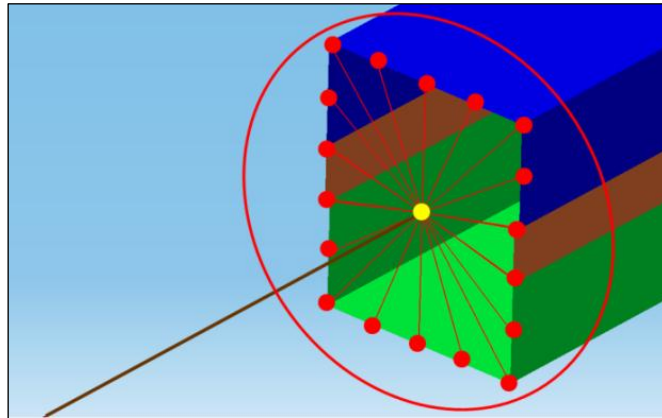
Figure 3.6: The interface element (circled in red) between a concept 1D beam model and a detailed 3D joint model. In yellow the central node, while in red the peripheral cross-section nodes [35].

Unlike the approach available in the literature, in this case the transformation matrix [S] is obtained by calculating the product of only two sub-matrices: the Stress Recovery matrix [S_1] and the Form Nodal Load matrix [S_2].

Regarding the first, the Stress Recovery matrix [S_1] is defined differently, since it correlates the resultant loads applied to the central node directly with the stress components, ideally generated on cross-section nodes.

In order to give an idea of the matrix composition, the simple case of a spot-welded beam with rectangular cross-section is taken into account.

Firstly, it is assumed that the thickness is sufficiently small, with respect to the two cross-section dimensions; this allows using the stress distribution assumptions of thin-walled beams.

Furthermore, for a spot-welded structure, which is open in some cross-sections but closed in those regions where spot-welds are applied, the global static behaviour can be assumed as similar to that of closed cross-section. For this reason, the stress-load equations for this kind of cross-sections are used.

For a 3D beam model, the equilibrium relationship for each considered load case can be written at the beam/joint interface cross-section, w.r.t. a reference system placed on the centre of gravity, with z-axis directed along the longitudinal axis, while x- and y-axis are located along the principal and secondary bending directions, respectively.

The matrix relation between nodal stresses and total loads can be given as:

$$
\begin{Bmatrix}
\tau_{xz}^{(1)} \\
\tau_{yz}^{(1)} \\
\sigma_{z}^{(1)} \\
\tau_{xz}^{(2)} \\
\tau_{yz}^{(2)} \\
\sigma_{z}^{(2)} \\
\vdots
\end{Bmatrix}
=
\begin{bmatrix}
\dfrac{S_y^{*(1)}}{I_y(2t^{(1)})} & 0 & 0 & 0 & 0 & p\left(\dfrac{1}{2\Omega t^{(1)}}\right) \\
0 & \dfrac{S_x^{*(1)}}{I_x(2t^{(1)})} & 0 & 0 & 0 & q\left(\dfrac{1}{2\Omega t^{(1)}}\right) \\
0 & 0 & \dfrac{1}{A_{tot}} & -\dfrac{y^{(1)}}{I_x} & -\dfrac{x^{(1)}}{I_y} & 0 \\
\dfrac{S_y^{*(2)}}{I_y(2t^{(2)})} & 0 & 0 & 0 & 0 & p\left(\dfrac{1}{2\Omega t^{(2)}}\right) \\
0 & \dfrac{S_x^{*(2)}}{I_x(2t^{(2)})} & 0 & 0 & 0 & q\left(\dfrac{1}{2\Omega t^{(2)}}\right) \\
0 & 0 & \dfrac{1}{A_{tot}} & -\dfrac{y^{(2)}}{I_x} & -\dfrac{x^{(2)}}{I_y} & 0 \\
\vdots & \vdots & \vdots & \vdots & \vdots & \vdots
\end{bmatrix}
\begin{Bmatrix}
F_x \\
F_y \\
F_z \\
M_x \\
M_y \\
M_z
\end{Bmatrix}
\qquad (3.16)
$$

The physical meaning of each parameter is given in table 3.1.

The directions of torsion and bending stresses are defined based on the right hand rule. For transition regions between two different thickness values, an average value is set at the node between the two adjacent shell elements.

Note that the stress contribution given by warping is not considered, as well as tangential stresses perpendicular to shear directions, since their global effect on displacements and rotations of the central node can be considered negligible.

Figure 3.7 shows the stress distributions in these two cases. Note also that distortion effects are not taken into account; therefore, pure torsional rotation is assumed.

With regard to the Form Nodal Load matrix $[S_2]$, its definition is not modified, in comparison to that found in the literature [5]. The addition is that the correlation between nodal forces and nodal stresses considers now all the three load directions.

A_{tot} is the total area of the thin-walled cross-section.	Ω is the area encompassed by the middle perimeter line.
$x^{(i)}$ and $y^{(i)}$ are the position coordinates of the ith node, w.r.t. the central reference system.	$t^{(i)}$ is the thickness average value relating to the ith node.
$S_x*^{(i)}$ and $S_y*^{(i)}$ are the cross-section static moments, w.r.t. the x and the y axes, for i^{th} node.	I_x and I_y are the cross-section moments of inertia, w.r.t. the x and the y axes.
p is a factor equal to 1 for the upper horizontal wall, -1 for the lower, 0.5 for nodes at intersections and 0 for vertical walls.	q is a factor equal to 1 for the right vertical wall, -1 for the left, 0.5 for nodes at intersections and 0 for horizontal walls.

Table 3.1: Nomenclature for the $[S_1]$ matrix.

Therefore, in this case, the relation between total loads at the central node and nodal forces on the outer contour of the beam cross-section can be written as:

$$\{f\}_{3nx1} = [S_2]_{3nx3n}[S_1]_{3nx6}\{F\}_{6x1} = [S]_{3nx6}\{F\}_{6x1} \tag{3.17}$$

where $\{f\}_{3nx1}$ is the vector of 3D nodal loads, while $\{F\}_{6x1}$ is the vector of 3D total loads.

a)   b)
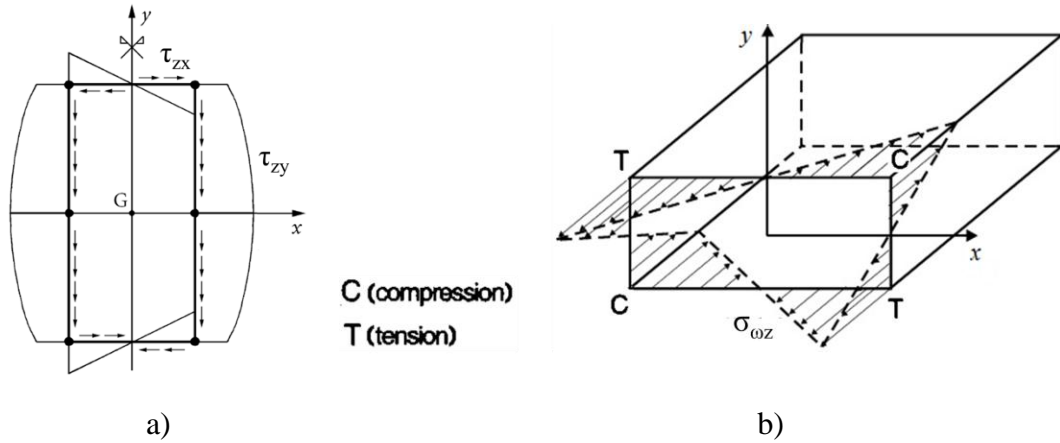
Figure 3.7: Stress distributions along rectangular cross-sections; tangential component due to vertical shear (τ_{zx} and τ_{zy} in a) and normal component of warping (σ_z in b).

As explained in section 3.1, the correlation between displacements and rotations of the beam central node and displacements of the peripheral nodes of the interface cross-section is given in the linear elastic field by transposing the matrix [S]. The new kinematic relationship can be written as:

$$[T]_{6x3n}\{q\}_{3nx1} = \{Q\}_{6x1} \tag{3.18}$$

3.5. A case study

This section describes an application model, on which the proposed new connection element is validated. The geometry of the detailed 3D structure model is described in section 3.5.1. Thereafter, section 3.5.2 describes characteristics of the equivalent 1D concept model. Finally, section 3.5.3 shows a dynamic validation, in order to demonstrate improvements on the predictive accuracy of the concept structure with the proposed MPC elements [35, 78].

3.5.1. Description of the detailed 3D model

The detailed 3D model taken as reference consists of a structure with three spot-welded thin-walled beams, having the same cross-section, and one joint.

Each beam model is one meter long and it is defined by two thin-walled panels with a C-shaped cross-section, whose geometry and dimensions are shown in figure 3.8-a. Panels forming each beam model are connected to each other by a set of equally spaced spot-welds, along each of the two longitudinal walls. Again, the distance between these spot-welds is chosen according to the typical layout in the automotive beams, i.e. equal to 100 mm.

The cross-section has a vertical axis of symmetry and the centre of gravity can be considered coincident with the shear centre. This assumption is very important, because it allows reducing detailed 3D beam model in concept 1D beam models with equivalent stiffness parameters, by applying the concept dynamic FE-based method, already described in chapter 2.

a)   b)
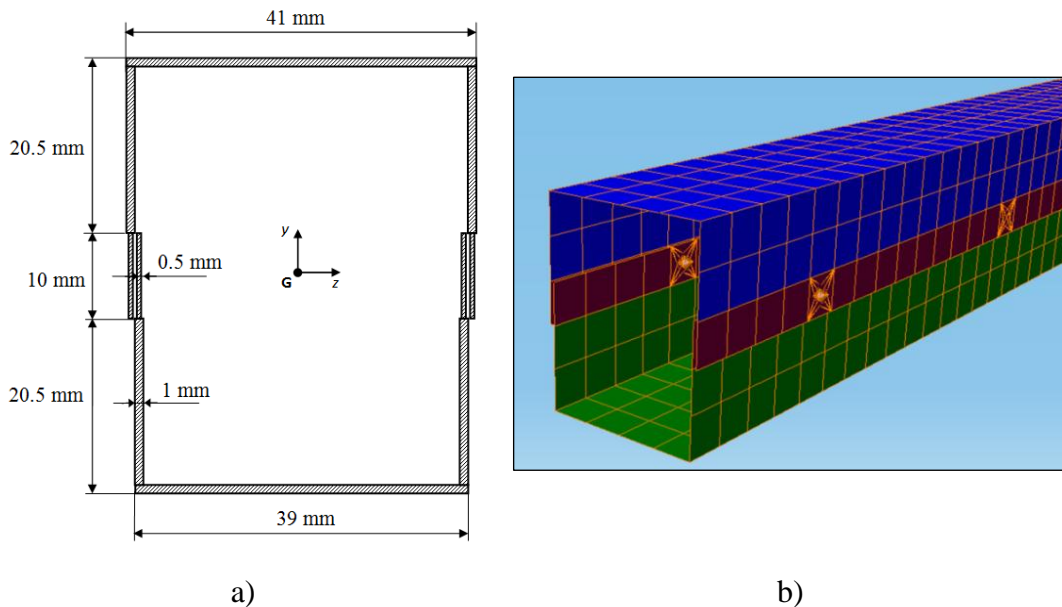
Figure 3.8: Application model: cross-section geometry of beams (a) and shell mesh of detailed 3D beam models (b) [35].

Since the thickness of panels is much smaller than the two transversal cross-section dimensions, it is possible to mesh each beam member by using 4-node shell elements. The three beams intersect in a joint, having the same end sections and also modelled with shell elements.

The Structures environment of LMS Virtual.Lab software [56] is used to create the whole FE model (figure 3.8-b).

The assigned material, assumed as homogeneous and isotropic, is a typical steel, with the following properties:

- Young modulus: $E = 210000$ MPa;
- Poisson ratio: $v = 0.3$;
- Mass density: $\rho = 7.9 \cdot 10^{-9}$ ton/mm^3.

In order to compare the detailed 3D and the 1D concept models also in terms of modal shapes, a beam centre line is created in the first structure, by defining a proper number of central nodes, located at a distance of 100 mm from each other along the longitudinal directions of the beams.

These central nodes are connected with nodes of corresponding cross-sections by interpolation RBE3 elements, so that the modal displacements of each central node are estimated by interpolation of the modal displacements of the cross-section nodes. Figure 3.9 shows the complete detailed 3D model of the structure.
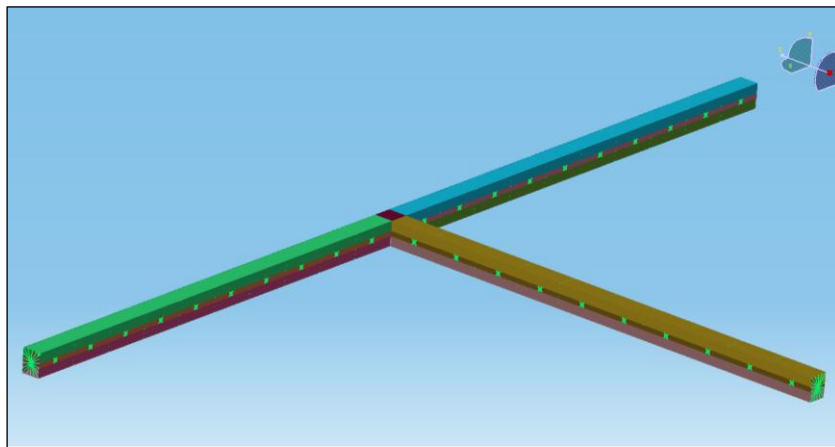
Figure 3.9: The detailed 3D FE model of the structure for the application case [35].

3.5.2. Description of the concept 1D model

The concept model of the structure is composed by concept 1D beam models and a simplified model for the joint.

Regarding the beam members, the dynamic FE-based method, already described in chapter 2, is used as concept modelling approach, in order to estimate the equivalent stiffness parameters. For this type of thin-walled spot-welded beams, the equivalent parameters, useful to define concept 1D beam models, are listed in table 3.2.

Figure 3.11-a shows the concept model, before the joint is reduced.

Parameters	Values for each concept 1D beam model
$A_{eq}\ (mm^2)$	178
K_x	0.144
K_y	0.104
$I_x\ (mm^4)$	69420
$I_y\ (mm^4)$	48164
$I_t\ (mm^4)$	25702.80
$I_w\ (mm^6)$	3.094e+08

Table 3.2: Equivalent beam properties estimated by the concept dynamic FE-based method.

Instead, for the joint reduction, the Craig-Bampton fixed interface technique is applied: in the final concept model, the joint is represented by a super-element, consisting of a stiffness and a mass matrix condensed to a set of master nodes, which includes the central nodes at the three beam/joint interfaces.

This reduction is implemented with Nastran software [81], by keeping the DOFs of these central nodes as masters and the DOFs of the nodes belonging to the detailed

3D joint model as slaves. Figure 3.10 shows the concept structure, before (a) and after (b) the reduction of joint in super-element. The new representation of the joint replaces the detailed 3D model, while guaranteeing the structural continuity of the whole concept model.

Two different concept models of the joint are created: in the first, the Craig-Bampton dynamic reduction is applied to the detailed 3D model by using rigid RBE2 elements at each beam/joint interface; instead, for the second model, the proposed MPC connection element is used to connect the central node to the cross-section nodes, at each beam/joint interface.

a)   b)
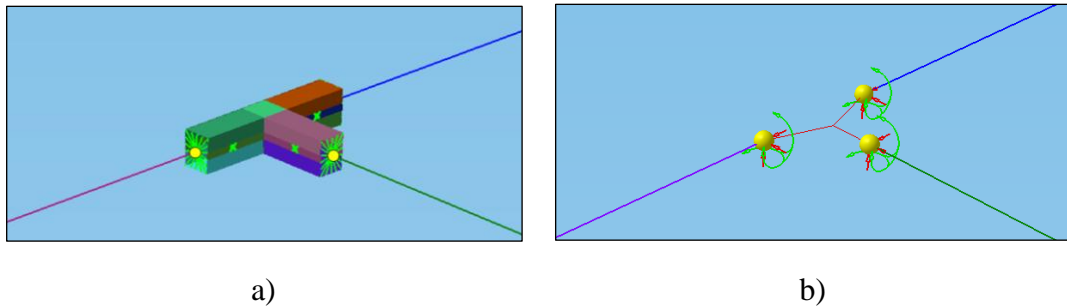
Figure 3.10: Concept model: before (a) and after (b) the reduction of joint in super-element. In yellow, the three master nodes for the super-element [35].

Note that the joint region is defined in such a way that the distance between each interface and the joint centre is sufficiently wide (100 mm in this case) to avoid any violation of Saint-Venant assumptions.

The detailed 3D model of the structure has over 60000 DOFs, while the concept model has only 180 DOFs; this fact results in a strong reduction of the computational time required for simulations.

3.5.3. Dynamic validation

The dynamic validation consists of a modal analysis, performed in free-free boundary conditions by using Nastran software as FE solver. In this way, it is possible to compare the detailed 3D model with the two different concept models, in terms of natural frequencies and mode shapes.

Table 3.3 reports natural frequencies values of the first 12 global modes for all the models, together with percentage differences between the frequencies of each concept model and those of the detailed model.

Furthermore, the diagonal values of the Modal Assurance Criterion (MAC) matrix [82], obtained on *Noise & Vibration* environment of LMS Virtual.Lab software, are reported as well.

With this criterion, a correlation index between two generic modes (*i*) and (*j*), which belong to the modal matrix of the original and the concept model respectively, is evaluated as:

$$MAC_{(i,j)} = \frac{\left(\{V_1\}_i^H \{V_2\}_j\right)^2}{\left(\{V_1\}_i^H \{V_1\}_j\right)\left(\{V_2\}_i^H \{V_2\}_j\right)} \tag{3.19}$$

where superscript *H* denotes the conjugate transpose of the vector. The resulting MAC matrix is evaluated by using all the central nodes that are shared by the detailed and the simplified models (represented by subscripts (1) and (2) in the above formula).

It can be observed that the first concept model with rigid connection elements approximates very precisely the first vibration modes, concerning in particular axial and flexural vibrations; however, for flexural-torsional modes, significant differences between the concept and the detailed model can be appreciated, with a maximum and an average value of 38.73% and 9.09% respectively.

This means that the stiffness of the joint is overestimated, especially when the interfaces are subjected to torsional deformations.

Modes		Detailed model	Concept 1D model with RBE2			Concept 1D model with new MPC		
		Freq. (Hz)	*Freq. (Hz)*	*Freq. Diff.(%)*	*MAC Values*	*Freq. (Hz)*	*Freq. Diff. (%)*	*MAC Values*
	1st	41.63	41.85	0.53	0.99	40.40	-2.97	0.99
	2nd	55.46	55.55	0.17	0.99	54.86	-1.09	0.99
	3rd	79.23	79.44	0.26	0.99	78.77	-0.59	0.99
Flex-Tors	*4th*	188.52	229.57	21.77	0.96	179.99	-4.53	0.99
Flex-Tors	*5th*	196.49	225.76	14.90	0.90	190.38	-3.11	0.96
	6th	197.18	197.55	0.19	0.97	194.60	-1.31	0.98
	7th	256.67	256.90	0.09	0.97	256.01	-0.26	0.99
Flex-Tors	*8th*	266.65	396.93	38.73	0.86	260.47	-2.32	0.98
Flex-Tors	*9th*	285.98	364.37	27.41	0.62	280.23	-2.01	0.90
	10th	293.74	292.37	-0.47	0.95	289.72	-1.37	0.97
	11th	382.43	397.78	4.01	0.93	391.22	2.30	0.84
	12th	410.85	417.10	1.52	0.99	406.66	-1.02	0.99
Average				9.09			1.91	
Max.				38.73			4.53	

Table 3.3: Dynamic comparison between the detailed and two concept models, in terms of natural frequencies, % frequency differences and modal correlation factors [35, 78].

The diagonal MAC values between the 3D detailed model and the 1D concept model with the proposed MPC is reported in figure 3.11.
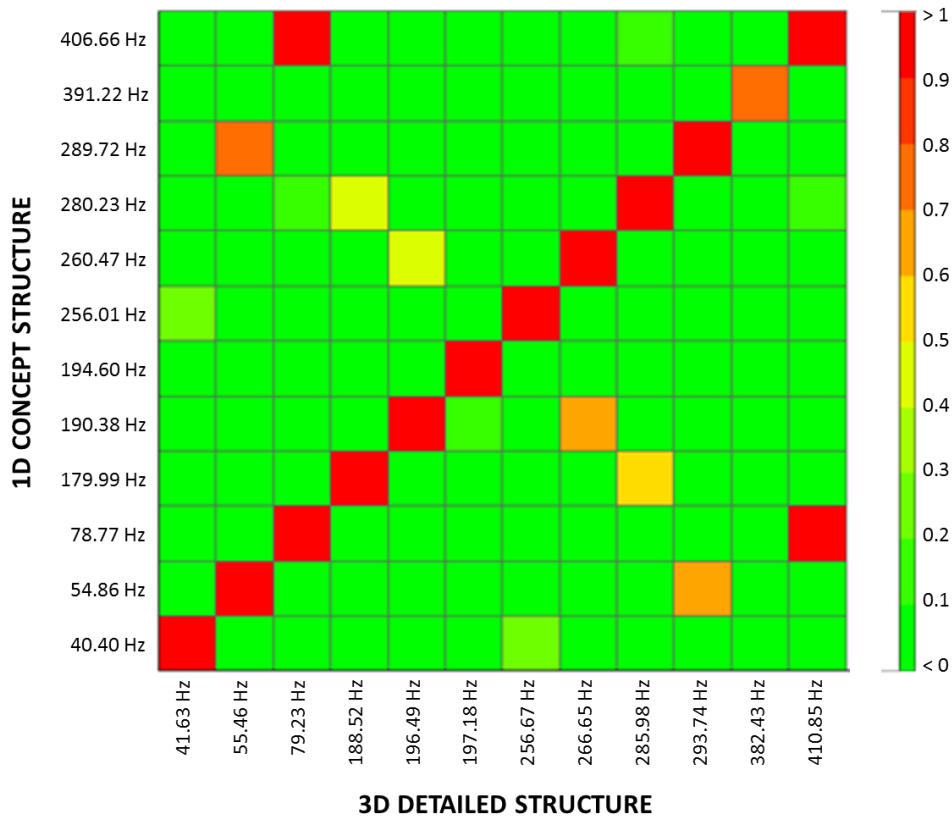
Figure 3.11: MAC matrix between 3D detailed and 1D concept model with the proposed MPC.

Instead, the second concept structure, where the proposed MPC connection elements are used, shows good accuracy for all the types of modes, in terms of both frequencies and MAC values, with a maximum and an average difference value of 4.53% and 1.91%, respectively.

In particular, for modes involving torsional deformations at one or more beam/joint interfaces, the second concept model is up to 16 times more accurate than the first concept model.

Chapter 4: Industrial Applications

4.1. Overview

In this chapter, concept modelling techniques combined with optimization process are applied on the industrial FE model of a vehicle Body-In-White (BIW), in order to prove the effectiveness of approaches described in the previous chapters.

In particular, the MPC connection element, proposed in chapter 3, is here validated, with an application on a partially conceptualized model of the Chrysler Neon car [31]. This model consists of a lower detailed part, while the upper part is reduced, by substituting detailed beam and joint members with ten 1D beam models and four super-elements for joint representation.

The procedure used to achieve this goal followed the "reduced beam and joint modelling" method [20, 31, 53].

Figure 4.1 shows a workflow, describing the steps followed to define the semi-concept model.

Subsequently, the same model with these connection elements is modified by applying a size optimization procedure: by using a Gradient-Based (GB) mathematical programming algorithm [84-85]: the body weight is minimized by modifying the area and inertia properties of concept beams within allowed variation ranges, while keeping unchanged the dynamic functional performance of the model.
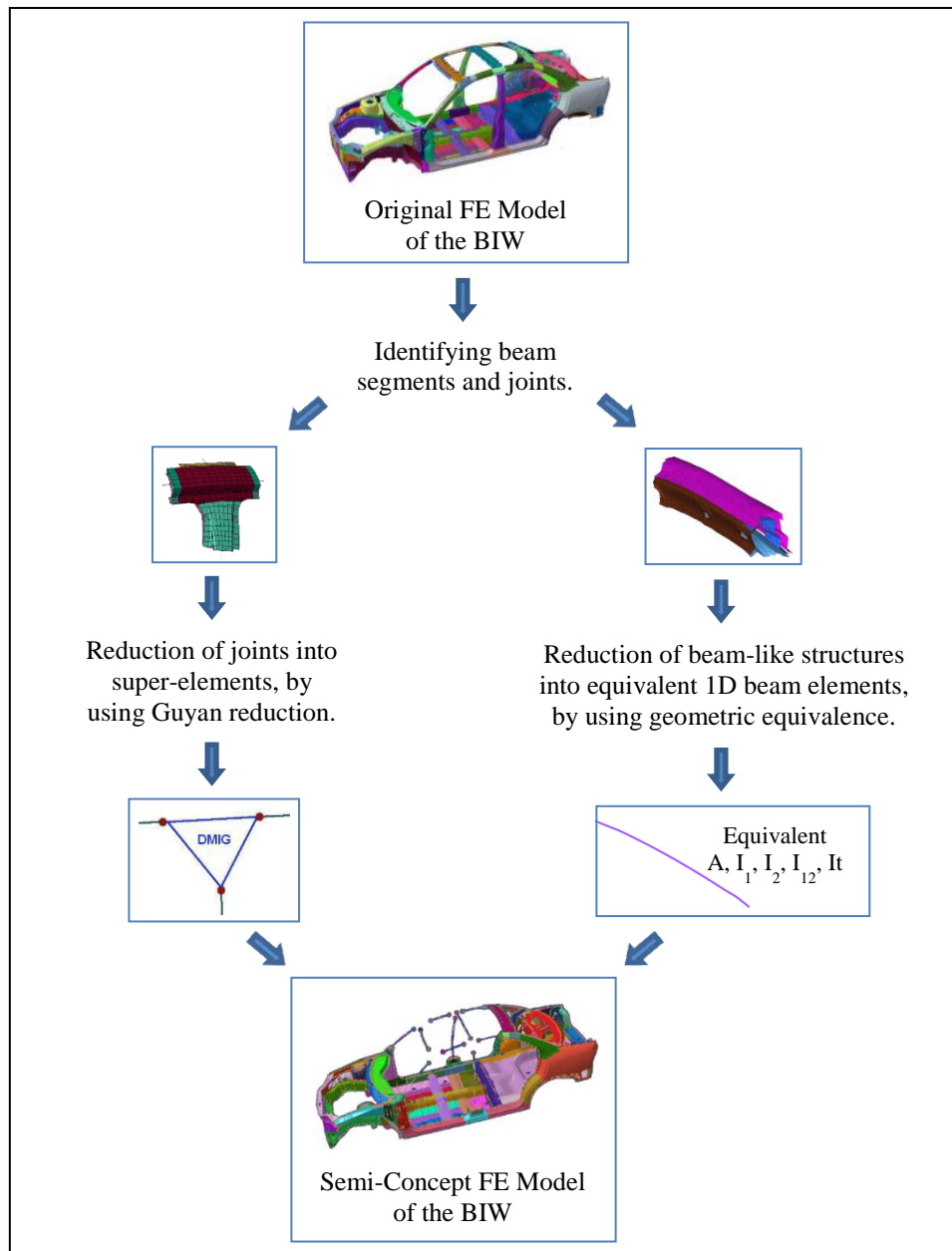
Figure 4.1: Workflow for the definition of beam and joint FE concept models.

4.2. Description of the FE concept model

The considered Chrysler Neon vehicle model consists of 123 panels, meshed using 2D shell elements. The various parts are connected by approximately 3000 spot-weld

connections, defined with small hexa solid elements, linked to corner nodes of flanges by generic interpolation elements. Panels, as the windshield, the roof or various car glasses, have been not included in this model.

A part of this detailed model was reduced. In particular, ten detailed beam-like structures, including A-, B-, C-pillars and transversal roof-rails, have been replaced with 1D beam elements having equivalent stiffness parameters, by means of a method based on a geometrical analysis of each beam cross-section.

At the same time, four joint structures, connecting these concept beams, have been reduced into super-elements, by using Guyan static reduction. In the next two sub-sections, an overview of the concept modelling approaches used for beams and joints reduction is provided. More details can be found in [31].

4.2.1. Concept modelling of beam-like structures

Concept modelling approaches used for beam-like structures aim at replacing detailed 3D FE models of beam members with equivalent beams, also referred to as concept 1D beam models. Mass and stiffness properties of these beams are computed by applying proper analytical or numerical procedures to a set of cross-sections, extracted from the original mesh.
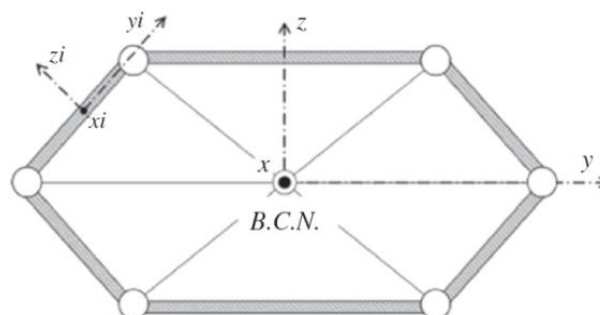
Figure 4.2: Schematic representation of an arbitrary beam cross-section, in which concept geometric method is applied [31].

For this typical vehicle body structure, with discontinuity properties due to holes, spot-welds and stiffeners, the authors preferred to use a procedure based on a geometric approach, in which equivalent properties of beam segments are calculated by analysing the mass distribution along each open or closed cross-section.

Firstly, the number and length of beam elements have been selected, based on the geometry variations of beam cross-sections in the original model.

Then, after defining a set of intersection planes at these boundary zones and the relative geometric centre points, the geometric properties (i. e. the cross-section area, the two quadratic moments of inertia, the polar moment of inertia and the torsional modulus) of shell elements at each cross-section were calculated, with respect to local axis systems (x_i, y_i, z_i in figure 4.2).

Subsequently, transformations from all local axis systems to the central reference system (x, y, z) were performed. The sum of all these contributions returned the global geometric properties of the cross-section.

In order to take into account all discontinuities occurring in a vehicle body, these nominal stiffness properties of beams were corrected through the use of correction factors, found by model updating.

Once equivalent properties of beam segments with almost constant cross-section were determined, equivalent 1D beam elements replaced the various detailed beam-like structures.

4.2.2.   Reduction of joints

For the considered BIW model, static Guyan reduction was used [47]. This method is based on dynamic equations of a model without damping, which provide an exact reduced stiffness matrix between master DOFs, but an approximated mass matrix. However, for typical automotive joints, which are very stiff components, inertia forces on internal DOFs can be considered less important than elastic forces transmitted by the boundary DOFs. For such a reason, the choice of applying this technique for automotive joint reduction can be considered appropriate [20].

In order to implement the reduction procedure to thin-walled structures, four joint groups have been created, by using interpolation RBE3 connection elements between extreme nodes of 1D beam elements and peripheral nodes of joints, at each interface cross-section. Figure 4.3 shows the final semi-concept FE model of the BIW.
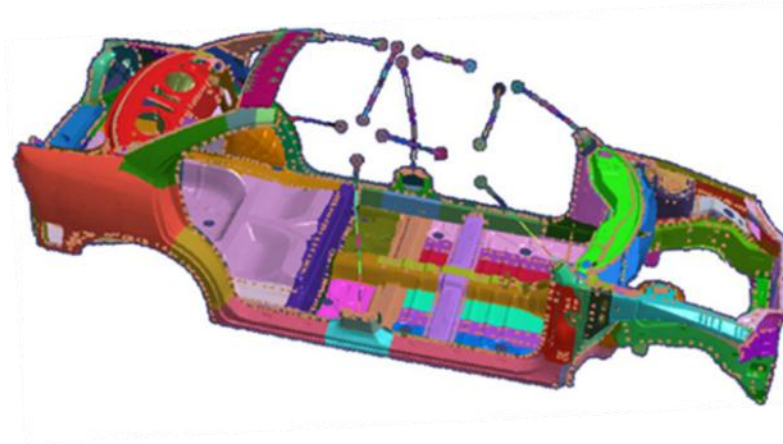
Figure 4.3: The semi-concept model, obtained after beam and joint reductions [31].

4.3. Modifications of MPC implementation

In order to validate the MPC connection element, proposed in this thesis work, also for general industrial cross-sections, some important modifications need to be introduced, concerning the implementation of the stress recovery matrix $[S_1]$.

The latter correlates resultant loads, ideally applied on the central node of the 1D beam element, with component stresses induced on shell elements of the joint cross-section. For thin-walled spot-welded structures, as automotive beam members, the global stress behaviour can be normally assumed as similar to that of closed cross-sections. A typical example is the C-pillar cross-section, showed in figure 4.4. Cases where such assumption is not allowed, i.e. beams with either open or multi-connected cross-sections, will specifically discussed in the next sub-sections.
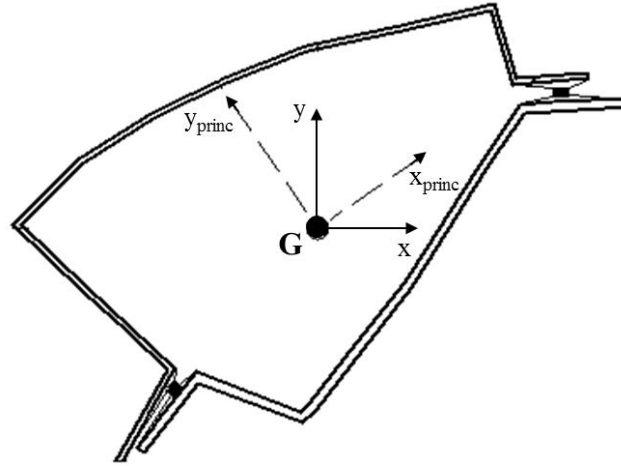
Figure 4.4: The C-pillar cross-section, belonging to the BIW model shown in figure 4.3.

Then, now the correlation between nodal stress components and loads can be written as follows:

$$
\begin{Bmatrix}
\tau_{xz}^{(1)} \\
\tau_{yz}^{(1)} \\
\sigma_{z}^{(1)} \\
\tau_{xz}^{(2)} \\
\tau_{yz}^{(2)} \\
\sigma_{z}^{(2)} \\
\vdots
\end{Bmatrix}
=
\begin{bmatrix}
\dfrac{S_y^{(1)}\cos\vartheta_{(1)}}{I_y(2t^{(1)})} & 0 & 0 & 0 & 0 & \dfrac{\cos\vartheta_{(1)}}{2\Omega t^{(1)}} \\[2ex]
0 & \dfrac{S_x^{(1)}\sin\vartheta_{(1)}}{I_x(2t^{(1)})} & 0 & 0 & 0 & \dfrac{\sin\vartheta_{(1)}}{2\Omega t^{(1)}} \\[2ex]
0 & 0 & \dfrac{1}{A_{tot}} & \dfrac{y^{(1)}}{I_x} & -\dfrac{x^{(1)}}{I_y} & 0 \\[2ex]
\dfrac{S_y^{(2)}A_{(1,2)}^{(2)}}{I_y(2t^{(2)})} & 0 & 0 & 0 & 0 & \dfrac{A_{(1,2)}^{(2)}}{2\Omega t^{(2)}} \\[2ex]
0 & \dfrac{S_x^{(2)}B_{(1,2)}^{(2)}}{I_x(2t^{(2)})} & 0 & 0 & 0 & \dfrac{B_{(1,2)}^{(2)}}{2\Omega t^{(2)}} \\[2ex]
0 & 0 & \dfrac{1}{A_{tot}} & \dfrac{y^{(2)}}{I_x} & -\dfrac{x^{(2)}}{I_y} & 0 \\[2ex]
\vdots & \vdots & \vdots & \vdots & \vdots & \vdots
\end{bmatrix}
\begin{Bmatrix}
F_x \\
F_y \\
F_z \\
M_x \\
M_y \\
M_z
\end{Bmatrix}
\qquad (4.1)
$$

where subscripts (*1*) and (*2*) identify the two nodes of a generic shell element belonging to the cross-section, while the superscript index indicates the global node number. In this example, node 1 is a generic external node of the spot-welded cross-section, while node 2 is internal, i.e. it is located between two adjacent shell

elements. The directions of torsion and bending stresses are defined based on the right hand rule.

It is important to note that all quantities must referred to the main reference system (x_{princ}-y_{princ} in figure 4.4), once identified its orientations.

The physical meaning of each parameter is taken from table 3.1, but now there are some additional geometric parameters. For example, $\vartheta_{(i)}$ represents the orientation of the ith element, with respect to the x-axis, while $A_{(h,k)}$ and $B_{(h,k)}$ are two parameters, considering the orientations of hth and k[th] elements, adjacent to the generic i[th] node.

Indeed, for hybrid cross-sections, such as that examined one, the direction of tangential stress acting on external nodes is determined by the orientation of a single element; instead, the contribution of both adjacent elements must be considered for internal nodes. Therefore, those factors for the generic i[th] node can be defined as follows:

$$A_{(h,k)}^{(i)} = \left(\frac{\cos \vartheta_{(h)} + \cos \vartheta_{(k)}}{2} \right) \tag{4.2}$$

$$B_{(h,k)}^{(i)} = \left(\frac{\sin \vartheta_{(h)} + \sin \vartheta_{(k)}}{2} \right) \tag{4.3}$$

As it can be seen, each shell element contributes 50% to the resultant shear stress acting on the node.

Also in this case, warping and distortion effects, as well as tangential stresses perpendicular to shear directions, are not considered, since their global effect on displacements and rotations of the central dependent node can be considered negligible.

Instead, the "form nodal load" matrix $[S_2]$ assumes the same form described in chapter 3. In case of thin-walled structures, stress distributions due to the torsion load depend on different typologies of the cross-section. In the next sub-sections, appropriate modifications relating to this load case are applied to the $[S_1]$ matrix, with respect to open and multi-connected cross-sections.

4.3.1. Torsion in open cross-sections

In case of beams with open cross-sections, such as the B-pillar cross-section shown in figure 4.5, the distribution of tangential stresses due to torsion loads is drastically different from that expected for closed cross-sections.

Indeed, by considering a generic location along the cross-section, the tangential stress is no longer constant, since it exhibits a linear variation along the thickness of the element, with opposite directions above and below the element middle line, where it is zero. Hence, the resultant stress contribution at each node is zero.

Based on these considerations, the tangential component of warping stress, having a constant trend along the thickness, must be taken into account.
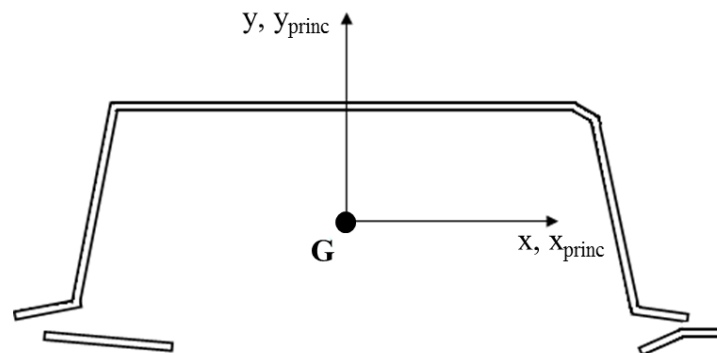
Figure 4.5: The open B-pillar cross-section, belonging to the BIW model shown in figure 4.3 [83].

For a generic open cross-section, the relation between a constant torque and the tangential warping stress at i[th] node can be expressed by the following equation [86]:

$$\tau_\omega^{(i)} = \frac{S_\omega^{(i)}}{t^{(i)} C_\omega} M_z \qquad (4.4)$$

where C_ω indicates the warping constant of the cross-section w.r.t. the shear centre, while $S_\omega{}^{(i)}$ is the warping static moment at generic ith node.

This last function is expressed as:

$$S_\omega = \int_0^S \omega_n \, t ds \qquad (4.5)$$

where (s) is a local axis placed at the middle line of panels, whose orientation is governed by the right-hand rule. Instead, ω_n is the normalized warping, which depends on another quantity, known as double sectorial area (ω_0) [87].

Indeed, the following equation can be written:

$$\omega_n = \frac{1}{A_{tot}} \int_0^S \omega_0 \, t ds - \omega_0 \qquad (4.6)$$

Finally, the double sectorial area is a function of the minimum distance between the shear centre and the tangent line of the generic shell element (ρ_0). Once identified the location of the shear centre, the equation to be applied for each of shell elements is:

$$\omega_0 = \int_0^S \rho_0 \, ds \qquad (4.7)$$

These line integrals along the cross-section can be calculated as sum of contributions of each shell element to the overall functions.

4.3.2. Torsion in multi-connected cross-sections

In a typical vehicle body, not only open or single connected cross-sections may occur, but also multi-connected cross-sections, having three or more panels connected to each other by spot-welds.

Also in this case, some additional considerations should be done on the calculation of the tangential stress due to the torsion load.

For example, as regarding the A-pillar cross-section, having three interconnected panels (figure 4.6), a system of four equations must be implemented, in order to determine direction and magnitude of each tangential nodal stress.
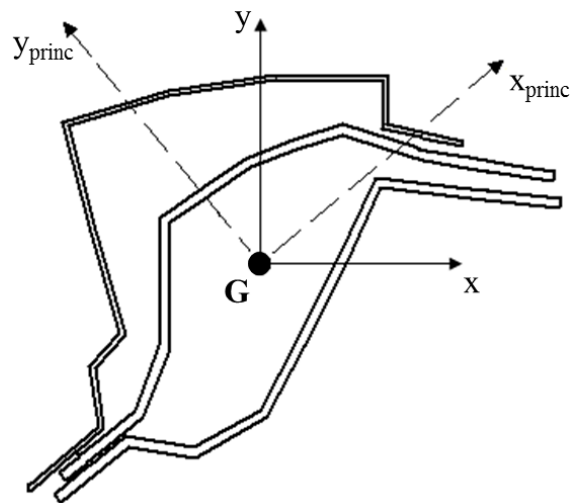
Figure 4.6: The multi-connected A-pillar cross-section, belonging to the BIW model shown in figure 4.3 [83].

The first equation describes the equilibrium condition relative to one of the two connection points (i.e., those points where the three panels ideally intersect). The equation is the following [6]:

$$\sum_{i=1}^{3} \tau_i t_i = 0 \tag{4.8}$$

where the subscript (i) indicates here the ith panel, defining the cross-section. Usually, stresses are considered positive if pointing to the connection point, negative on the contrary.

The second equation is an equivalence condition between the total torsion load applied on the geometric centre and the moment generated by elementary forces applied on the area of the cross-section.

By adding contributions of all the three panels, the equation becomes:

$$\sum_{i=1}^{3} 2\tau_i t_i A_{si} = M_z \tag{4.9}$$

where A_{si} is the sectorial area for each ith panel; namely, the area included between perpendicular distances from geometric centre to tangents of shell elements and the middle line length of considered panel.

Finally, the last two equations are two congruence conditions, that derive from the double application of the following equation, obtained by applying the Stokes' theorem:

$$\oint_{C_i} \tau ds = 2G\Theta\Omega_i \tag{4.10}$$

The parameter Θ indicates the unit torsion angle, Ω_i is the ith semi-area bounded by two panels, G is the shear modulus and C_i denotes the length of the considered panel. Conditions described above define a linear system of four equations with four unknowns, which are the three tangential stresses and the unit torsion angle value.

By assuming a specific direction for each stress, it is possible to obtain a load-stress relationship related to every cross-section node, to be replaced in the matrix $[S_1]$.

4.4. An industrial case study

The proposed MPC connection elements is implemented for each of the six interface cross-sections, between the concept and the detailed parts of the BIW model shown

in figure 4.3. In particular, these interfaces regard the A-, B- and C-pillar cross-sections, discussed in the previous sections.

Since the BIW model is symmetric with respect to the longitudinal plane, each type of MPC is applied twice, for identical but mirrored beam cross-sections.

Before the implementation, it is necessary to configure a set of local axis systems, placed on geometric centres of interface cross-sections. This is useful to identify local principal axes and define DOFs of involved nodes.

For each individual connection, peripheral cross-section nodes are identified as independent nodes, while the central beam node at the same interface represents the dependent node.

Dynamic simulations are carried out, in order to demonstrate improvements on the predictive accuracy of the semi-concept BIW model with proposed MPC connection elements, in comparison to models with other standard connection elements.

In particular, FE modal analyses in free-free conditions are performed using Nastran software [81] as FE solver.

Modes	**Detailed Model**	**Concept Model with RBE3**		**Concept Model with RBE2**		**Concept Model with new MPC**	
	Natural Freq. (Hz)	*Natural Freq. (Hz)*	*Freq. Diff. (%)*	*Natural Freq. (Hz)*	*Freq. Diff. (%)*	*Natural Freq. (Hz)*	*Freq. Diff. (%)*
1st *Tors.*	18.22	16.63	-8.73	18.98	4.17	18.06	-0.88
2nd *Tors.*	26.13	22.16	-15.19	27.13	3.83	26.57	1.68
Lat. Bend.	39.36	36.33	-7.71	40.09	1.85	39.61	0.64
Vert. Bend.	41.73	37.18	-10.90	42.16	1.03	42.18	1.08
Tors+Ben	47.85	43.37	-9.36	48.25	0.83	47.71	-0.29

Table 4.1: Dynamic comparison between the original and the three different concept models of the BIW, in terms of natural frequencies [83].

Table 4.1 shows the first five predicted natural frequencies, estimated for three different semi-concept models of the same BIW. Each of the models is characterized by a different type of connection element (RBE2, RBE3 and MPC type) at all the beam/joint interfaces. The same table shows also the percentage differences between the frequencies, w.r.t. the values related to the detailed model, used as the reference model.

The achieved results indicate that the concept model with general purpose interpolation RBE3 connection elements considerably underestimates natural frequencies of the BIW. Indeed, significant differences between the semi-concept and the detailed model can be appreciated, with a maximum value equal to −15.19% for torsional and −10.90% for flexural frequencies.

On the other hand, the concept model with rigid RBE2 connection elements approximates precisely flexural vibration modes; however, for the torsional ones, the model stiffness is overestimated, with a maximum prediction difference of 4.17%, related to the first torsional frequency.

Instead, the concept model with the proposed MPC connection elements shows very good accuracy for all the considered modes, with a maximum difference value of 1.68%. In particular, for modes involving torsional deformations, the third concept model is approximately up to 2.5 and 9 times more accurate than the first and second concept models, respectively.

4.5. Size optimization of the semi-concept BIW model

Once the accuracy of the proposed beam/joint connection element has been assessed, the concept part of the BIW model (consisting of ten concept beams and four joint super-elements) is subjected to a size optimization process, in order to get in a really short time an optimal concept structure, having the same dynamic performances of the original model (same natural frequencies), but with a minimum weight.

For this purpose, the optimizer available in Nastran solver, known as ''SOL 200'' optimization sequence [60], belonging to GB methods category, is used.

According to this procedure, the optimal solution is found step-by-step in the direction of the steepest descent, identified by evaluating the sensitivities of all response parameters with respect to all design variables.

An important limitation of this method category lies in the local-search strategy, i.e. the possibility that the procedure converges to a local minimum solution.

However, the advantage lies in its high computation speed. Furthermore, it is very suitable to give a first idea on the optimal solution and on possible countermeasures useful to improve the project.

The objective function is defined as to minimize the mass of the concept part of the BIW. Geometric parameters of the beam concept models, namely the cross-section area, the two moment of inertia and the torsional stiffness, are selected as design variables. The full concept structure is composed of 75 2-node beam elements. By considering geometric parameters at both ends of each element, the total number of design variables is equal to 600. A maximum variation of $\pm20\%$ of the value for each of these variables is set to define the design space.

The first five natural frequencies of the detailed model, computed in free-free conditions, are set as target values, covering a frequency range of up to 40 Hz.

For each frequency, an admissible difference is fixed, by setting the upper and the lower bound of value as $\pm5\%$ of the nominal value.

Objective Function/ Target Values	Initial Value	Final Value	Percentage Difference (%)
Total Weight	18.92 (Kg)	16.17 (Kg)	-14.53
1st Frequency	3.16 (Hz)	3.20 (Hz)	1.27
2nd Frequency	6.09 (Hz)	6.39 (Hz)	4.93
3rd Frequency	11.01 (Hz)	11.28 (Hz)	2.45
4th Frequency	29.95 (Hz)	31.37 (Hz)	4.74
5th Frequency	32.55 (Hz)	33.20 (Hz)	2.00

Table 4.2: Summary of optimization results: objective function and frequency target values [83].

The optimization analysis converges to a feasible solution already after only three iterations, with a computational time of only few seconds. The final optimization results are summarized in table 4.2 and table 4.3. In table 4.2, a significant weight reduction, equal to 14.53%, can be observed, while all the natural frequencies remain within the allowed variation ranges.

Instead, table 4.3 shows the average percentage variations of design variables along each of the beam-like members. It is clear that the most significant reduction is achieved on the equivalent cross-section area parameter, for which the optimal values are always found in proximity of the lower bound.

Furthermore, transversal roof-rails exhibit maximum variations for all design variables, which means that their influence on the first five natural frequencies can be considered less relevant, in comparison with other regions of the model.

Design Variables	Percentage Average Variations (%)			
	A-Pillars	*B-Pillars*	*C-Pillars/ Longitudinal Roof-Rails*	*Transversal Roof-Rails*
Cross-section Area	-20	-19	-20	-20
1st Moment of Inertia	-9	-16	-1	-20
2nd Moment of Inertia	-10	-2	-2	-20
Torsional Stiffness	0	-5	-10	-20

Table 4.3: Average differences between optimal and initial value of the design variables per model region [83].

Conclusions

The research work described in this dissertation has presented new concept methodologies, able to reduce beam and joint FE models of the vehicle BIW, with the aim of enabling accurate early predictions of static and dynamic behaviours already in the concept phase of the vehicle development cycle.

Regarding the concept modelling of beam-like structures, a new dynamic FE-based method has been proposed and validated, based on the natural frequencies estimation of a detailed 3D FE beam model, with constant double-symmetric cross-section. Indeed, flexural and torsional frequencies can be expressed as a function of the cross-sectional stiffness properties (e.g. shear areas, quadratic moments of inertia, torsional modulus, etc.), by using the ordinary uncoupled differential equations of beam vibrations.

In particular, the equivalent stiffness properties of the 1D beam concept model have been estimated with a numerical procedure, by fitting the analytical formulation with targeted values of natural frequencies, obtained from a modal analysis of the detailed 3D beam model, in free-free boundary conditions.

This method allows taking into account the discontinuities and variations that may occur along a beam and that affect its stiffness, especially in torsional performances. Therefore, it can be used to define concept 1D beam models of complex structures, like thin-walled spot-welded beams characterizing structures of a typical BIW, or innovative lightweight honeycomb sandwich beams.

As regarding the first typology, a sensitivity analysis has demonstrated that the dynamic behaviour of spot-welded beam-like structures differs significantly from the behaviour of the beam with a closed cross-section.

The case-study, implemented to validate the proposed method, consisted of a spot-welded beam composed by two C-shaped panels, with a typical spot weld layout representative of automotive applications. First eight natural frequencies values of the detailed 3D model have been compared with those predicted by three concept

models. These models have been defined through the proposed dynamic FE-based method and the two main concept methods reported in the state-of-art, that are the geometric and the static FE-based approach. Dynamic results proved that the dynamic FE-based method achieves a higher accuracy in the frequency prediction, compared to that obtained with the other two concept methods. A static validation has been provided as well, showing that, for a cantilever beam subjected to transversal load, the flexural deflection of the concept beam is very close to that of the reference detailed beam model.

Regarding innovative beam structures, dynamic comparisons were made with natural frequencies of a detailed 3D honeycomb sandwich beam model. The latter has been defined by using a 2D shell mesh for both the skins and the core parts. Ideal contact has been assumed between the parts, without the presence of any delamination. Therefore, the adhesive layers, linking skins and core, were not taken into account, considering negligible their effect on the dynamic behaviour of the structure. The validation was carried out by comparing the first three flexural frequencies with experimental data, taken from the literature

Subsequently, two reduced models have been defined: a 1D concept beam model, obtained with the dynamic FE-based method, and a so-called "equivalent" beam model, consisting of a 3D homogeneous single-skin model with equivalent characteristics to those of the detailed model, determined by imposing static equalities.

The predictive dynamic performances of both the 1D and 3D reduced models were compared with the values predicted by the detailed one. The comparison showed a good accuracy, in both the flexural and the torsional frequencies, for the dynamic 1D beam model, while the 3D equivalent model returned a good dynamic behaviour in lateral bending, but a worse accuracy in torsional performances.

By summarizing, it was demonstrated that a very good accuracy can be obtained with the proposed concept method, together with a significant reduction of the number of DoFs and, hence, of computational time demanded to execute FE simulations.

However, some limitations of the method need to be addressed, which define the next steps of this research work. The first is that the method can still be used only for beams with double symmetric cross-sections. The extension to non-symmetric cases

results in a coupling of flexural and torsional vibrations. Therefore, other more complex equations will should to be implemented.

In addition, thin-walled beams structures should have an appropriate stiffness, in such a way that, for low-medium frequency ranges, the influence of local modes on global ones can be considered negligible and the frequency values are reliable for the numerical procedure. This problem mainly affects torsional vibrations.

Not very efficient is the practice of performing dynamic simulations for detailed 3D models of slender beams, in order to validate assumptions for Timoshenko equations. A dedicated routine could be implemented, in order to divide a complex beam-like structure in beam segments with constant cross-sections, and automatically run dynamic simulations for corresponding slender beams. Then, the obtained frequencies can be used to estimate equivalent stiffness parameters for each concept beam member.

The last limitation, related to lightweight structures, is that, at the moment, only homogeneous beams can be taken into account. Other studies should be carried out, in order to consider physical properties of materials, present in composite or in foam-filled beams.

Instead, as regards the concept modelling for vehicle joints, various published studies showed that connection elements used at interfaces between concept beams and detailed joints have a significant influence on the accuracy of the full concept vehicle model. For such a reason, a dedicated MPC connection element has been proposed and validated. This element allows to correlate displacements and rotations of the central node of the joint end-section with the displacements of peripheral cross-section nodes, by applying a static approach based on "load continuity" conditions. These conditions require to implement relationships between resulting loads ideally applied to the centroid of the cross-section and the force distribution generated on interface walls. Therefore, theoretical stress fields are considered, resulting from Saint-Venant assumptions for beam-like structures, with respect to axial, bending, shear and torsion load-cases.

In order to assess the accuracy of the proposed method, a first case-study was considered, consisting of a structure with three spot-welded beams with the same cross-section, connected by a joint. Two different concept models have been

implemented, one using rigid RBE2 and another using the dedicated MPC connection elements for the reduction of joint into super-element.

Then, their natural frequencies and MAC values were compared with values of the detailed 3D model taken as reference, proving that the proposed MPC connection element permits to estimate mass and stiffness characteristics between master nodes at each joint end-section more accurately than the rigid connection spiders.

Also and industrial case-study has been tested, by applying MPC elements on a semi-conceptualized industrial BIW. In particular, connections were implemented for six interface cross-sections, belonging to A-, B- and C-pillars, which divided detailed and concept parts. The latter consisted of ten concept 1D beam members and four super-elements, replacing the joints.

Dynamic modal analyses showed good accuracy in the prediction of natural frequencies, returning estimated values very close to those of the detailed BIW model. In particular, for modes involving torsional deformations, the concept BIW model with MPC achieved an accuracy approximately 2.5 and 9 times better than that related to the concept model with rigid RBE2 and general purpose interpolation RBE3 connection elements, respectively.

The main limitation of this approach regards the location of the beam/joint interface cross-section, that must be placed in zones where Saint-Venant assumptions can be verified. Other extensive studies should be done, in order to consider, in the MPC formulation, all the stress components that can be present on thin-walled structures, such as those due to cross-section distortion. Indeed, for compliant components, these effects can influence their mechanical behaviour in a non-negligible way.

List of Publications

International peer-reviewed journal articles:

G. De Gaetano, D. Mundo, F. I. Cosco, C. Maletta, S. Donders, *Concept Modelling of Vehicle Joints and Beam-like Structures through Dynamic FE-based Methods*, Shock and Vibration, Volume 2014 (2014), Article ID. 303567.

Full papers in proceedings of International Conferences:

G. De Gaetano, F.I. Cosco, C. Maletta, D. Mundo, S. Donders, *Dynamic FE-based Method for Concept Modelling of Vehicle Beam-like Structures*, Proceedings of: International Conference on Noise and Vibration Engineering – ISMA 2012, Leuven (Belgium), Sept. 2012.

G. De Gaetano, F. I. Cosco, C. Maletta, S. Donders, D. Mundo, *Concept Modelling of Vehicle Joints and Beam-like Structures through Dynamic FE-based Methods*, Proceedings of: International Conference on Structural Engineering Dynamics – ICEDyn 2013, Sesimbra (Portugal), Jun. 2013.

G. De Gaetano, F. I. Cosco, C. Grarre, C. Maletta, S. Donders, D. Mundo, *Innovative Concept Modelling of Sandwich Beam-like Structures*, Proceedings of: International Conference On Vibration Problems – ICOVP 2013, Lisbon (Portugal), Sept. 2013.

G. De Gaetano, D. Mundo, G. Vena, M. Kroiss, L. Cremers, *A Study on Vehicle Body Concept Modelling: Beam to Joint Connection and Size Optimization of Beam-like Structures*, Proceedings of: International Conference on Noise and Vibration Engineering – ISMA 2014, Leuven (Belgium), Sept. 2014.

Bibliography

[1] C. Ledermann, C. Hanske, J. Wenzel, P. Ermanni, R. Kelm, *Associative parametric CAE methods in the aircraft pre-design*, Aerospace Science and Technology, Vol. 9, No. 7, (2005), pp. 641–651.

[2] I. Senjanović, *Ship vibrations, Part 2*, University of Zagreb (Zagreb), 1990.

[3] M. He, W. Hu, *A study on composite honeycomb sandwich panel structure*, Materials and Design, Vol. 29, No. 3, (2008), pp. 709–713.

[4] D. Hui, T. J. Kozik, O. Ochoa, *Composite material technology, 1993: presented at the 16th annual Energy-Sources Technology Conference and Exhibition, Houston, Texas*, ASME, New York, (1993).

[5] H. Song, *Rigorous joining of advanced reduced-dimensional beam models to 3D finite element models*, Ph.D. Thesis, Institute of Technology, Georgia (USA), 2010.

[6] E. Viola, *Scienza delle Costruzioni - Teoria della Trave*, Pitagora Editrice, Bologna, 1992.

[7] R. Hadjit, M. Brughmans, H. Shiozaki, *Application of fast body optimization procedures to shorten car development cycles*, Proceedings of: JSAE Annual Congress, Yokohama (Japan), May 2005.

[8] H. Shiozaki, Y. Kamada, S. Kurita, S. Goossens, J. Van Herbruggen, V. Cibrario, L. Poppelaars, *CAE based vehicle development to reduce development time*, Proceedings of: JSAE Annual Congress, Yokohama (Japan), May 2005.

[9] D. E. Malen, *Fundamentals of Automobile Body Structure Design*, Published by SAE, 2011.

[10] T. D. Gillespie, *Fundamental of vehicle dynamics*, Published by SAE, 1992.

[11] G. Genta, L. Morello, *The automotive chassis: Volume 2: system design*, Springer, 1st edition, 2009.

[12] G. Genta, L. Morello, *The automotive chassis: Volume 1: component design*, Springer, 2009.

[13] L. Morello, L. R. Rossini, G. Pia, A. Tonoli, *The automotive body: Volume II: system design*, Springer, 1st edition, 2010.

[14] J. Helsen, L. Cremers, P. Mas, P. Sas, *Global static and dynamic car body stiffness based on a single experimental modal analysis test*, Proceedings of: International Conference on Noise and Vibration Engineering − ISMA 2010, Leuven (Belgium), Sept. 2010.

[15] J. Weber, *Automotive development processes: processes for successful customer oriented vehicle development*, Springer, 2009.

[16] M. Kroiss, L. Cremers, V. Evangelou, *Conceptual car design at BMW with focus on NVH performance*, Proceedings of: 5th ANSA & μETA International Conference, Thessaloniki (Greece), Jun. 2013.

[17] R. V. Dukkipati, J. Pang, M. S. Qatu, G. Sheng, Z. Shuguang, *Road vehicle dynamics*, Published by SAE, 2008.

[18] H. Van der Auweraer, T. Van Langenhove, M. Brughmans, I. Bosmans, N. El Masri, S. Donders: *Application of Mesh Morphing Technology in the Concept Phase of Vehicle Development*, International Journal of Vehicle Design, Vol. 43, No. 1-4, (2007), pp. 281-305.

[19] P. Mihaylova, *Concept modeling techniques for the design of automotive structures*, Ph. D. Thesis, Università degli Studi di Firenze, Firenze (Italy), 2012.

[20] S. Donders , Y. Takahashi, R. Hadjit, T. Van Langenhove, M. Brughmans, B. Van Genechten, W. Desmet, *A Reduced Beam and Joint Concept Modelling Approach to Optimize Global Vehicle Body Dynamics*, Finite Elements in Analysis and Design, Vol.45, No. 6-7, (2009), pp. 439-455.

[21] Dassault Systèmes, CATIA V5R17, August 2006.

[22] T. Hughes, J. Cottrell, Y. Bazilevs, *Isogeometric analysis: CAD, finite elements, NURBS, exact geometry and mesh refinement*, Computer Methods in Applied Mechanics and Engineering, Vol. 194, No. 39–41, (2005), pp. 4135–4195.

[23] M. Bendsoe, N. Olhoff, O. Sigmund, *Topology optimization — theory, methods, and applications*, 2nd edition, Berlin (Germany), Springer, 2004.

[24] M. Bendsoe, N. Olhoff, O. Sigmund (Eds.), *Machines and Materials: Status and Perspectives*, Proceedings of: Symposium on Topological Design Optimization of Structures – IUTAM 2005, Copenhagen (Denmark), Oct. 2005.

[25] I. Raasch, *Sizing in conceptual design at BMW*, Proceedings of: SAE Noise and Vibration Conference, Traverse City, Michigan (USA), May 2005.

[26] Y. You, H. Yim, C. Kim, K. Kim, *Development of an optimal design program for vehicle side body considering the B.I.W. stiffness and light weight*, Proceedings of: SAE Noise and Vibration Conference, St. Charles, Illinois (USA), May 2007.

[27] C. Chapman, M. Pinfold, *The application of a knowledge based engineering approach to the rapid design and analysis of an automotive structure*, Advances in Engineering Software, Vol. 32, No. 12, (2001), pp. 903–912.

[28] SFE, SFE Concept (http://sfe1.extern.tu-berlin.de/concept/concept.html).

[29] M. Alexa, *State-of-the-art reviews: recent advances in mesh morphing*, Computer Graphics Forum, Vol. 21, No. 2, (2002), pp. 173–197.

[30] A. Moroncini, L. Cremers, N. Baldanzini, *Car body concept modeling for NVH optimization in the early design phase at BMW: a critical review and new advanced solutions*, Proceedings of: International Conference on Noise and Vibration Engineering – ISMA 2012, Leuven (Belgium), Sept. 2012.

[31] D. Mundo, R. Hadjit, S. Donders, M. Brughmans, P. Mas, W. Desmet, *Simplified modeling of joints and beam-like structures for BIW optimization in a concept phase of the vehicle design process*, Finite Elements in Analysis and Design, Vol. 45, No. 6-7, (2009), pp. 456-462.

[32] G. Stigliano, D. Mundo, S. Donders, T. Tamarozzi, *Advanced vehicle body concept modeling approach using reduced models of beams and joints*, Proceedings of: International Conference on Noise and Vibration Engineering - ISMA 2010, Leuven (Belgium), Sept. 2010.

[33] S. Corn. J. Piranda, N. Bouhaddi, *Simplification of Finite Element Models for Structures having a Beam-like Behaviour*, Journal of Sound and Vibration, Vol. 232, No. 2, (2000), pp. 331-354.

[34] J. Pirada, S. Huang, S. Corn, C. Stawicki, X. Bohineust, *Improvement of Dynamic Models in Car Industry*, Proceedings of: 15th International Modal Analysis Conference - IMAC XV, Orlando, Florida (USA), Feb. 1997.

[35] G. De Gaetano, D. Mundo, F. I. Cosco, C. Maletta, S. Donders, *Concept Modelling of Vehicle Joints and Beam-like Structures through Dynamic FE-based Methods*, Shock and Vibration, Volume 2014 (2014), Article ID. 303567.

[36] J. H. Kim, Y. Y. Kim, *Analysis of thin-walled closed beams with general quadrilateral cross sections*, ASME Journal of applied mechanics, Vol. 66, No. 4, (1999), pp. 904–912.

[37] Y. Y. Kim, J. H. Kim, *Thin-walled closed box beam element for static and dynamic analysis*, International Journal for Numerical Methods in Engineering, Vol. 45, No. 4 (1999), pp. 473–490.

[38] J. H. Kim, Y. Y. Kim, *New accurate efficient modeling techniques for the vibration analysis of T-joint thin-walled box structures*, International Journal of Solids and Structures, Vol. 39, No. 11, (2002), pp. 2893– 2909.

[39] G. Osborne, G. Prater, R. Lesiv, D. Lamb, M. Catanier, *Vehicle concept model abstractions for integrated geometric, inertial, rigid body, powertrain, and FE analysis*, Proceedings of: ASME 2011 International Mechanical Engineering Congress & Exposition, Denver, Colorado (USA), Nov. 2011.

[40] A. M. Shahhosseini, G. Prater, G. M. Osborne, E. Y. Kuo, *Major compliance joint modelling survey for automotive body structures*, International Journal of Vehicle Systems Modelling and Testing, Vol. 5, No. 1, (2010), pp. 1-17.

[41] Y. -M. Moon, T. -H. Jee, Y. -P. Park*, Development of an automotive joint model using an analytically based formulation*, Journal of Sound and Vibration, Vol. 220, No. 4, (1999), pp. 625-640.

[42] S. Donders, *Computer-aided engineering methodologies for robust automotive NVH design*, Ph.D. Thesis, K. U. Leuven, Leuven (Belgium), 2008.

[43] N. Bylund, *Simulation driven product development applied to car body design*, Ph.D. Thesis, University of Technology, Lulea (Sweden), 2004.

[44] L. Long, *Design-oriented translators for automotive joints*, Ph.D. Thesis, Polytechnic Institute and State University, Virginia (USA), 1998.

[45] E. Nikolaidis, M. Zhu, *Design of automotive joints: using neural networks and optimization to translate performance requirements to physical design parameters*, Computers & Structures, Vol. 60, No. 6, (1996), pp. 989-1001.

[46] E. Nikolaidis, L. Long, Q. Ling, *Neural networks and response surface polynomials for design of vehicle joints*, Computers & Structures, Vol. 75, No. 6, (2000), pp. 593-607.

[47] R. Guyan, *Reduction of stiffness and mass matrices*, AIAA Journal, Vol. 3, No. 2, (1965), pp. 380–387.

[48] K. Volz, *Car body design in the concept stage of vehicle development*, Proceedings of: Second European LS-DYNA Conference, Gothenburg (Sweden), Jun. 1999.

[49] R. MacNeal, *A hybrid method of component mode synthesis*, Computers & Structures, Vol. 1, No. 4, (1971), pp. 581–601.

[50] S. Donders, R. Hadjit, L. Hermans, M. Brughmans, W. Desmet, *A Wave-Based Substructuring Approach for Fast Modification Predictions and Industrial Vehicle Optimization*, Proceedings of: International Conference on Noise and Vibration Engineering – ISMA 2006, Leuven (Belgium), Sept. 2006.

[51] G. Prater, A. M. Shahhosseini, E. Y. Kuo, P. R. Metha, V. T. Furman, *Finite Element Concept Models for Vehicles Architecture Assessment and Optimization*, Published by SAE, 2005.

[52] N. Bylund, *ADRIAN: A software for computing the stiffness of automotive joints and its application in the product development process*, Journal of Computing and Information Science in Engineering, Vol. 5, No. 4, (2005), pp. 388-393.

[53] D. Mundo, G. Stigliano, S. Donders, H. Van Der Auweraer, *Concept design of vehicle bodies using reduced models of beams, joints and panels*, International Journal of Vehicle Design, Vol. 57, No. 1, (2011), pp. 71-83.

[54] I. Senjanović, I. Ćatipović, S. Tomašević, *Coupled Flexural and Torsional Vibrations of Ship-like Girders*, Thin-Walled Structures, Vol. 45, No.12, (2007), pp. 1002-1021.

[55] J. C. Lagarias, J. A. Reeds, M. H. Wright, and P. E. Wright, *Convergence Properties of the Nelder-Mead Simplex Method in Low Dimensions*, SIAM Journal of Optimization, Vol. 9, No. 1, (1998), pp. 112–147.

[56] LMS International, LMS Virtual.Lab Rev 10-SL2, (October 2011), http://www.lmsintl.com/virtuallab.

[57] G. De Gaetano, F.I. Cosco, C. Maletta, D. Mundo, S. Donders, *Dynamic FE-based Method for Concept Modelling of Vehicle Beam-like Structures*, Proceedings of: International Conference on Noise and Vibration Engineering – ISMA 2012, Leuven (Belgium), Sept. 2012.

[58] S. P. Timoshenko, *On the transverse vibrations of bars of uniform cross sections*, Philosophical Magazine, Vol. 43, No. 253, (1922), pp. 125-131.

[59] I. Senjanović, S. Tomašević, N. Vladimir, *An advanced Theory of thin-walled Girders with Application to Ship Vibrations*, Marine Structures, Vol. 22, No. 3, (2009), pp. 387-437.

[60] MSC Software Corporation, *Nastran 2013 Quick Reference Guide*, Santa Ana, California (USA), 2013.

[61] S. B. Lee, J. R. Park, H. J. Yim, *Numerical approximation of vehicle joint stiffness by using response surface method*, International Journal of Automotive Technology, Vol. 3, No. 3, (2002), pp. 117–122.

[62] P. Vinot, S. Cogan, J. Piranda, *Shape optimization of thin-walled beam-like structures*, Thin-Walled Structures, Vol. 39, No. 7, (2001), pp. 611–630.

[63] B. Wang, M. Yang, *Damping of honeycomb sandwich beams*, Journal of Materials Processing Technology, Vol. 105, No. 1-2, (2000), pp. 67–72.

[64] K. Hyeung-Yun, H. Woonbong, *Effect of debonding on natural frequencies and frequency response functions of honeycomb sandwich beams*, Composite Structures, Vol. 55, No. 1, (2002), pp. 51–62.

[65] S. D. Yu, W. L. Cleghorn, *Free flexural vibration analysis of symmetric honeycomb panels*, Journal of Sound and Vibration, Vol. 284, No. 1-2, (2005), pp. 189–204.

[66] A. Petras, M. P. F. Sutcliffe, *Failure mode maps for honeycomb sandwich panels*, Composite Structures, Vol. 44, No. 4, (1999), pp. 237–252.

[67] G. De Gaetano, F. I. Cosco, C. Grarre, C. Maletta, S. Donders, D. Mundo, *Innovative Concept Modelling of Sandwich Beam-like Structures*, Proceedings of: International Conference On Vibration Problems – ICOVP 2013, Lisbon (Portugal), Sept. 2013.

[68] A. Boudjemai, R. Amri, A. Mankour, H. Salem, M. H. Bouanane, D. Boutchicha, *Modal analysis and testing of hexagonal honeycomb plates used for satellite structural design*, Materials and Design, Vol. 35, (2012), pp. 266–275.

[69] A. Boudjemai , M. H. Bouanane, Mankour, R. Amri, H. Salem, B. Chouchaoui, *MDA of Hexagonal Honeycomb Plates used for Space Applications*, World Academy of Science, Engineering and Technology, Vol. 66, No. 6, (2012), pp. 221–229.

[70] X. Li-juan, J. Xian-Ding, W. Yang-Bao, *Equivalent analysis of honeycomb sandwich plates for satellite structure*, Journal of Shanghai Jiao Tong University, Vol. 37, No. 7, (2003), pp. 999–1001.

[71] J. K. Paik, A. K. Thayamballi, G. S. Kim, *The strength characteristics of aluminium honeycomb sandwich panels*, Thin-Walled Structures, Vol. 35, (1999), pp. 205–231.

[72] A. Noor, W. Burton, C. Bert, *Computational models for sandwich panels and shells*, Applied Mechanics Reviews, Vol. 49, No. 3, (1996), pp. 155–199.

[73] N. Buannic, P. Cartraud, T. Quesnel, *Homogenization of corrugated core sandwich panels. Composite Structures*, Composite Structures, Vol. 59, No. 3, (2003), pp. 299–312.

[74] X. Sheng-jin, K. Xian-ren, W. Ben-li, M. Xing-rui, Z. Xiao-chao, *Method of equivalent analysis for statistics and dynamics behavior of orthotropic honeycomb sandwich plates*, Acta Materiae Compositae Sinica; Vol. 17, No. 3, (2000), pp. 92–95.

[75] M. H. Fu, J. R. Yin, *Equivalent elastic parameters of the honeycomb core*, Acta Mechanica Sinica, Vol. 31, No. 1, (1999), pp. 113–118.

[76] B. Hassani, E. Hinton, *A review of homogenization and topology optimization II–analytical and numerical solution of homogenization equations*, Computers and Structures, Vol. 69, No. 6, (1998), pp. 719–738.

[77] Y. Kaneko, K. Takeuchi, *Design and construction of a seawater survey ship built using aluminium honeycomb panels*, Proceedings of: Second International Conference on Fast Sea Transportation, Yokohama (Japan), Dec. 1993.

[78] G. De Gaetano, F. I. Cosco, C. Maletta, S. Donders, D. Mundo, *Concept Modelling of Vehicle Joints and Beam-like Structures through Dynamic FE-based Methods*, Proceedings of: International Conference on Structural Engineering Dynamics – ICEDyn 2013, Sesimbra (Portugal), Jun. 2013.

[79] A. Maressa, D. Mundo, S. Donders, W. Desmet, *A wave-based substructuring approach for concept modeling of vehicle joints*, Computers & Structures, Vol. 89, No. 23-24, (2011), pp. 2369-2376.

[80] V. L. Berdichevskii, *Variational-asymptotic method of constructing a theory of shells: PMM*, Journal of Applied Mathematics and Mechanics, Vol. 43, No. 4, (1979), pp. 711–736.

[81] MSC Software, Nastran 2011.1 Version (2013).

[82] W. Heylen, S. Lammens, P. Sas, *Modal Analysis Theory and Testing*, 2nd edition, K. U. Leuven, Leuven (Belgium), 1997.

[83] G. De Gaetano, D. Mundo, G. Vena, M. Kroiss, L. Cremers, *A Study on Vehicle Body Concept Modelling: Beam to Joint Connection and Size Optimization of Beam-like Structures*, Proceedings of: International Conference on Noise and Vibration Engineering – ISMA 2014, Leuven (Belgium), Sept. 2014.

[84] M. Ohsaki, *Optimization of Finite Dimensional Structures*, CRC Press, 2010.

[85] A. Moroncini, L. Cremers, M. Kroiss, *NVH structural optimization using beams and shells FE concept models in the early car development phase at BMW*, Proceedings of: International Conference on Noise and Vibration Engineering – ISMA 2010, Leuven (Belgium), Sept. 2010.

[86] P. A. Seaburg, C. J. Carter, *Torsional Analysis of Structural Steel Members*, American Institute of Steel Construction, Chicago, 1997.

[87] W. Chen, T. Atsuta, *Theory of Beam-Columns, Volume 2: Space Behavior and Design*, McGraw-Hill, New York, 1977.